“Structure and Vibrational Dynamics of Hydrated Proton-rich Water-Air Interface”

Dissertation

Zur Erlangung des Grades

“Doktor der Naturwissenschaften”

im Promotionsfach Chemie

am Fachbereich 09
Chemie, Pharmazie, Geographie und Geowissenschaften
der Johannes Gutenberg-Universität Mainz

Sudipta Das

geboren in Kalkutta, Indien

Mainz, 2019

1. Berichterstatter: Prof. Dr. Mischa Bonn
2. Berichterstatter: Prof. Dr. Carsten Sönnichsen

Tag der mündlichen Prüfung: 08.11.2019

Statutory Declaration

I hereby declare that I wrote this dissertation submitted without any unauthorized external assistance and used sources acknowledged in this work. All textual passages, which are appropriated verbatim or paraphrased from published and unpublished texts, as well as all information obtained from oral sources are duly indicated and listed in accordance with bibliographical rules. In carrying out this research, I complied with the rules of standard scientific practice as formulated in the statues of the Johannes Gutenberg-University Mainz to ensure standard scientific practice. I shall write in first person plural instead of singular (we instead of I) to make the text more readable.

Sudipta Das

Abstract:

Hydrated protons are critical in a wide variety of industrial, biological and environmental processes. Therefore, a large number of studies have focused on understanding the molecular scale structure and dynamics of hydrated protons in water. Despite extensive efforts, acquiring molecular scale information has been challenging, partly because structure and dynamics of protons are intricately linked to the vibrational dynamics of the solvating water molecules. Massive improvements in computational and experimental techniques have resulted a deeper understanding of physicochemical behavior of hydrated protons inside bulk water. However, in nature, the exposed surface of water is equally common as the bulk. Understanding how the exposed surface of the water is affected by the presence of hydrated protons is of paramount importance given the ubiquity of such surfaces.

The work described in this dissertation addresses the effect of adsorbed protons on the structure and dynamics of the water-air interface using a surface sensitive vibrational spectroscopy named Sum Frequency Generation (SFG). The water molecules at the aqueous surface, unlike inside the bulk have a non-centrosymmetric alignment and thus can be probed separately without any interferences from the bulk using SFG spectroscopy. SFG, thus, effectively probes the vibration of the water molecules in the first few monolayers of the aqueous surface.

In the first part, we study the relative surface affinity of proton (hydronium) and sodium ions at both a water surface covered with a negatively charged surfactant and the bare water surface by measuring the extent of disorder amongst the interfacial water molecules caused by the hydronium and/or sodium. We find that at the negatively charged surfactant-covered interface, sodium has marginally higher surface affinity than hydronium. In contrast to it, at the nominally neutral water-air interface hydronium has much higher surface affinity than sodium, implying that the surface affinity of ions depends both on the type of cation and interface.

In the second part, we quantify the onset of surface adsorption of protons (hydronium) and its conjugate base, i.e. hydroxide ion at the bare water-air interface by determining the bulk concentration at which hydronium/hydroxide significantly perturbs the interfacial water organization monitored with SFG. We find that hydronium causes the perturbation of the interfacial water alignment already at a few mM concentration, while several 100s mM of hydroxide is needed to cause similar perturbation. Thus, the hydronium ion is orders of magnitude more surface active than the hydroxide ion at the water-air interface.

In the following section, we explore the nature of the proton at the aqueous surface and specifically unveil the interfacial proton continuum. Combining ab initio molecular dynamics simulation and ‘phase sensitive’ SFG spectroscopy, we find that both ‘Eigen’ and ‘Zundel’ types of hydronium moieties are present at the surface. Moreover, we also experimentally determine the adsorption

Gibbs free energy of hydronium at the aqueous surface to be -1.3 kcal/mol, which reasonably agrees with the theoretical predictions from literature.

In the final part of this thesis, we unveil the effect of the protons on the vibrational dynamics of water at the water-air interface, which can be probed using 'time resolved' SFG spectroscopy in "pump-probe" scheme. We have observed a substantially slow dynamics of the SFG intensities on a hundred ps time scale that follows the vibrational excitation and relaxation process. This effect scales with the concentration of hydrated protons in water and totally absent in pure water. We attribute such slow temporal changes to establishment of a new quasi- equilibrium state between surface and bulk protons, which follows the temperature jump after vibrational relaxation process. Evidently, dynamics in acidic water is different from that of pure water.

Zussammenfassung:

Hydrierte Protonen sind in einer Vielzahl von industriellen, biologischen und ökologischen Prozessen entscheidend. Daher haben sich viele Studien auf das Verständnis der molekularen Struktur und Dynamik von Hydrierprotonen im Wasser konzentriert. Trotz intensiver Bemühungen war der Erwerb von Informationen im molekularen Maßstab eine Herausforderung, teilweise weil Struktur und Dynamik von Protonen eng mit der Schwingungsdynamik der lösenden Wassermoleküle verbunden sind. Massive Verbesserungen in der Theory und experimentellen Technik haben zu einem tieferen Verständnis des physikalisch-chemischen Verhaltens von hydrierten Protonen im Volumenwasser geführt. In der Natur jedoch ist die exponierte Wasseroberfläche ebenso häufig wie das Volumenwasser . Es ist von größter Bedeutung, zu verstehen, wie die freigelegte Oberfläche des Wassers durch das Vorhandensein von Hydrierprotonen beeinflusst wird, da diese Flächen allgegenwärtig sind.

Die in dieser Dissertation beschriebenen Arbeiten befassen sich mit der Wirkung von adsorbierten Protonen auf die Struktur und Dynamik der Wasser-Luft-Schnittstelle unter Verwendung einer oberflächlich empfindlichen Schwingungsspektroskopie namens Sumum Frequency Generation (SFG). Die Wassermoleküle an der wässrigen Oberfläche haben, anders als im Volumen, eine nicht-zentrosymmetrische Ausrichtung und können daher separat ohne Interferenzen mit dem Volumen mittels SFG-Spektroskopie projiziert werden. SFG untersucht so effektiv die Vibration der Wassermoleküle in den ersten paar Atomlagen der wässrigen Oberfläche.

Im ersten Teil erforschen wir die relative Oberflächenaffinität von Protonen (Hydronium) und Natriumionen auf einer Wasseroberfläche, die mit einem negativ geladenen Tensid bedeckt ist, und der Oberfläche des reinen Wassers, indem wir das Ausmaß der Störung auf das Wasser, verursacht durch Hydronium und/oder Natrium, messen. Wir stellen fest, dass Natrium an der negativ geladenen, Grenzschicht eine geringfügig höhere Oberflächenaffinität hat als Hydronium. Im Gegensatz dazu hat Hydronium an der nominell neutralen Wasser-Luft-Schnittstelle eine viel höhere Oberflächenaffinität als Natrium, dies bedeutet, dass die Oberflächenaffinität der Ionen sowohl von der Art der Kation als auch von der Grenzschicht selbst abhängt.

Im zweiten Teil wird der Beginn der Oberflächenadsorption von Protonen (Hydronium) und seiner konjugierten Basis, d. h. Hydroxid-Ion an der Schnittstelle zwischen Wasser und Luft, quantifiziert, indem die Massenkonzentration bestimmt wird, bei der Hydronium/Hydroxid die mit SFG überwachte Gewässer signifikant beeinträchtigt. Wir stellen fest, dass Hydronium bereits bei wenigen mM-Konzentrationen die Orientierung des Wassers an der Grenzschicht stört, während mehrere 100s mM Hydroxid benötigt werden, um eine ähnliche Störung zu verursachen. Somit ist das Hydronium-Ion um mehrere Größenordnung aktiver als das Hydroxid-Ion an der Wasser-Luft Schnittstelle.

Im folgenden Abschnitt erforschen wir die Beschaffenheit des Protons auf die wässrige Oberfläche und enthüllen speziell das Protonenkontinuum an der Grenzfläche. Durch die Kombination von ab initio molekularer Dynamiksimulation und "phasenauflösender"SFG-Spektroskopie stellen wir fest, dass sowohl Eigen- als auch Zundel-Sorten an der Oberfläche vorhanden sind. Darüber hinaus bestimmen wir experimentell auch die Adsorption Gibbs freie Energie von Hydronium an der wässrigen Oberfläche auf -1,3 kcal/mol, was mit den theoretischen Vorhersagen aus der Literatur im Rahmen des Fehlers übereinstimmt.

Im letzten Teil dieser Arbeit enthüllen wir die Auswirkungen der Protonen auf die Schwingungsdynamik des Wassers an derWasser-Luft Schnittstelle, die durch "zeitauflösende"SFG-Spektroskopie untersucht werden kann. Wir haben eine langsame Dynamik der SFG-Intensitäten auf einer 100-ps-Zeitskala beobachtet, die dem Vibrationserregungs- und Entspannungsprozess folgt. Dieser Effekt skaliert mit der Konzentration von hydrierten Protonen in Wasser und fehlt völlig in reinem Wasser. Wir schreiben die langsame zeitliche Veränderungen einem neuen quasi-Gleichgewichtszustand zwischen Oberflächen- und Volumenprotonen zu, der auf den Temperatursprung nach dem vibrationellen Relaxationsprozess folgt. Offensichtlich unterscheidet sich die Dynamik im sauren Wasser von der des reinen Wassers.

Publications covered in this thesis

Chapter 4

Das, S.; Bonn, M.; Backus, E. H. G. The surface affinity of cations depends both on the cations and the nature of the surface; J. Chem. Phys. 2018, 150, 044706

Chapter 5

Das, S.; Bonn, M.; Backus, E. H. G. The surface activity of the hydrated proton is substantially higher than that of hydroxide; Angew. Chem. Int. Ed. 10.1002/anie.201908420

Chapter 6

Das, S*.; Imoto, S*.; Sun, S.; Nagata, Y.; Backus, E. H. G.; Bonn, M. Nature of hydrated proton at the water-air interface; Manuscript in preparation (* Equal contributions)

Chapter 7

Das, S.; Bonn, M.; Backus, E. H. G. Acid influences the vibrational dynamics of the water-air interface; Manuscript in preparation

Contents

Chapter 1

Introduction:

Surface:

"God made the bulk; the surface was invented by the devil..."
-Wolfgang Pauli

…and the devil's invention is omnipresent. The exposed part of every object around us is surface. A surface defines the boundary of an object from its surroundings. Therefore, the atoms/molecules present at the surface experience different molecular-scale interactions compared to the molecules inside the bulk. It leads the physiochemical properties of an object to differ at its surface compared to that inside its bulk; as such, these properties can be categorized as 'surface properties'.

The study of 'surface properties', *surface science*, has covered a vast range until now: from very well-defined single-crystal metal surfaces to complex surfaces of biological cell membranes. However, from the dawn of the development, the efforts to characterize surfaces have suffered the challenge of finding an appropriate noninvasive measurement/characterization technique. Therefore, techniques, such as scanning tunneling microscopy, atomic force microscopy, neutron scattering, and reflectometry and X-ray diffraction, have remained limited to study primarily the sample-surfaces that can withstand ultrahigh vacuum (UHV) conditions, and therefore, mainly the solid surfaces. Liquid surfaces can hardly be studied well with these techniques.

Vibrational spectroscopy:

On the contrary, the bulk properties of liquids have been well studied with vibrational spectroscopic techniques, such as Raman and IR spectroscopy. Vibrational motion is a characteristic motion of any molecule or chemical moiety. The energy of this motion reflects the bonding strength between two atoms. Classically, under the assumption of an harmonic energy potential, vibrational energy is expressed as follows:

$$E_i = \frac{h}{2\pi}\sqrt{\frac{k_i}{\mu_i}} \qquad (1)$$

Where, k_i is the force constant of the harmonic oscillator *i* and μ_i is its reduced mass, where the chemical bond is considered as an analog of a spring holding two atoms. The force constant provides a measure for the curvature of the potential energy surface of the bond dissociation along its dissociation axis. Since both the force constant and the reduced mass depend on the atoms involved in the chemical bond, vibrational energy is often the fingerprint of a specific chemical moiety. For example, the O-H stretch motion of H_2O vibrates at ~ 3500±500 cm^{-1}, but the equivalent O-D mode of D_2O vibrates at ~2500±500 cm^{-1}. The intensity, phase or frequency of a vibration may change upon changing the chemical environment. For example, in the gas phase, H_2O molecules vibrate at 3756, 3657 and 1595 cm^{-1} (symmetric and asymmetric stretch, and bend vibrations respectively)[1]. The vibrational features appear to be very sharp as well. In the liquid phase, the symmetric and asymmetric features appear around 3400 cm^{-1} and the bend appears at 1650 cm^{-1}. The features are also broader in the liquid phase, mainly due to a network of hydrogen bonds widely varying in strength and a substantial homogeneous broadening[2]. The hydrogen-bonding network changes and new vibrational modes appear in the presence of ions in the water. For example, a broad continuous region (~2000-3000 cm^{-1}) of OH vibration arises in both IR and Raman intensity in the presence of HCl[3]. Thus, molecular vibrations can be used as a probe to investigate different molecular structures influenced by varying chemical environment. Based on this principle, surface-specific nonlinear spectroscopic techniques, such as non-resonant second harmonic generation (SHG) and vibrationally resonant sum-frequency generation (SFG) spectroscopy were developed that eventually turned into very useful tools to investigate liquid surfaces and indeed have been widely used to understand the structure and dynamics of the aqueous surfaces in detail.

Water:

Water is ubiquitous and perhaps, the most peculiar liquid on earth. Several of the properties of water are different from those of other liquids, such as water's maximum density at 4^o C instead of being at 0^o C, its high surface tension, and large heat capacity. This unique behavior is largely caused by the hydrogen (H-) bonds[1] present in the condensed phase. In the bulk of water, the H-bonds are continuous and directional in all three dimensions (3D), causing four immediate neighbors to surround each water molecule in a tetrahedral arrangement and plays a substantial role in determining bulk water's typical physicochemical properties and vibrational dynamics. The surface disrupts this 3D continuity, and the water molecules no longer stay in a tetrahedral arrangement leading to different physicochemical properties of interfacial water.

Water surface:

Since the surface (interface) of water separates the liquid aqueous phase from the gas (e.g., air)

[1] A hydrogen-bond is primarily an electrostatic force between a H atom of one H_2O molecule with the O-atom of its neighboring molecule.

and/or solid (e.g., ice, mineral, metal) phase, the role of water molecules has a paramount importance on interfacial chemistry covering a wide variety of disciplines, such as atmospheric science, geochemistry, electrochemistry, and corrosion. However, our knowledge of the fundamental physical chemistry of aqueous interfaces, especially pertaining to excess ions, such as salts and/or acids, is very limited compared to that of solid-air surfaces. The understanding of such aqueous interfaces containing dissolved ions, especially dissolved and dissociated acid is particularly important and relevant for atmospheric chemistry and biochemistry.

Acidic water interface:

A different chemical environment at a surface compared to inside the bulk may lead to different chemical reactivity. Since hydronium is involved in many (bio-/geo-) chemical reactions, such as the production of the Cl_2 in the liquid aerosol particles[4] that requires a pH< 2, it is useful to understand the interfacial structure and dynamics of the hydronium ion. Despite the significance of the interfacial structure of acidic solutions, quite a few aspects of the interfacial structure and dynamics have remained poorly understood. In the following, I briefly review the experimental and theoretical studies that have tried to determine if at all, hydronium has any surface affinity.

Macroscopic measurements:

A macroscopic measurement technique to investigate liquid surfaces is to monitor the change in surface tension, which is supposed to be sensitive to the changes in the surface structure of water. The surface tension of the neat water surface is 72.7 mN/m at 293 K. In between pH 3-10, it varies minimally. Only below pH 1, the surface tension reduces[5] to 71.4 mN/m. If water is approximated as a combination of surface water and a bulk water region, then a partition coefficient, i.e. the relative surface-to-bulk concentration, of 1.5 is obtained for the hydronium ion at the water-air interface[6], implying a surface excess of protons at sufficiently low pH.

A surface in excess of hydronium, in principle, should result in a positively charged aqueous surface. Electrokinetic studies[7], however, report the opposite. The electrostatic (zeta) potential calculated from the mobility of the air bubbles in an electric field vanishes around pH 4-5. At higher, yet below neutral pH, the zeta potential is already negative, implying that the surface is negatively charged; in other words, hydroxide ions reside predominantly at the surface.

The apparent disparity in the outcome of two different measurement techniques possibly stems from the interpretation of molecular-scale phenomenon from the macroscopic observables. Application of the techniques that can extract the molecular scale observables can be helpful to resolve the disparity; given the technique has the ability to distinguish the response of the surface moieties from that of the overwhelmingly large

number of bulk moieties.

Molecular-scale experimental measurements:

The experimental challenge to distinguish hydronium ions at the surface from those in the bulk of water can be achieved using laser-based nonlinear spectroscopic techniques, such as second harmonic generation (SHG) and sum-frequency generation (SFG). Petersen and Saykally have performed resonant SHG studies on surfaces of strongly acidic solutions[8]. Their results agree with the notion of surface adsorption of hydronium ions at very low pH.

A handful but significant efforts have been made to characterize the acidic water surface by directly probing the resonances of water containing hydronium in the subphase[9-14]. These studies have looked at the vibrational resonances of OH bond at ~3300, ~3500 and ~3700 cm^{-1}. In the presence of acid, the low-frequency side of the spectrum increases in intensity; suggesting an enhanced alignment of water molecules consistent with the notion of adsorbed hydronium ion at the surface.

Although not truly surface specific, synchrotron-based X-ray photoemission spectroscopy (XPS) has also provided valuable information about the surface affinity of the hydronium ion. Since this type of measurement relies on the mean free path of the electrons from micro-jet of liquid water, it can distinguish between "surface" and "bulk" water by tuning the incident photon energy. XPS spectra reveal that formic and acetic acid stay predominantly in their protonated forms at the surface of water, suggesting that the surface of neat water is acidic[15]. A similar XPS study on iodine solution has shown an enhanced concentration of iodide at pH 1 but not at neutral pH. These results can only be explained based on the surface activity of hydronium[16]. However, X-ray fluorescence measurements on RbBr have found no enhancement of fluorescence intensity at pH 4 compared to that at pH 6, which indicates no surface activity of protons[17] within the range pH=4-6.

Molecular-scale calculations:

Although modeling hydronium using full atomistic simulation is very difficult for the water-air interface, several trials have already been made to theoretically rationalize the experimental evidence. But, the outcome has largely varied depending on the way the proton is treated: as a point charge or a polarizable moiety, in both or either of Eigen ($H_9O_4^+$) and Zundel ($H_5O_2^+$) forms (details about Eigen and Zundel are presented in *section 1.6*). Conclusions have also varied depending on the type of theory used, namely dielectric continuum theory or density functional theory based ab-initio molecular dynamics (AIMD)/multi state-electron valence bond molecular dynamics (MS-EVB MD). In an early work, Dang found that the Eigen form does not favorably adsorb at the

surface[18]. Later works using EVB and classical MD resulted in an appreciable affinity of the hydronium ion towards the water-air interface[10, 19-21]. A simplified explanation is based on the fact that the protons of the H_3O^+ cation are excellent H-bond donors and that the oxygen atom, given the overall positive charge of the hydronium ion, makes for a poor H-bond acceptor. This causes the H_3O^+ cation at the interface to orient its oxygen atom to the air and its hydrogen atoms towards the bulk making strong hydrogen bonds with water molecules. The free energy of adsorption, however, has been found to vary amongst different calculations. A meticulous calculation at quantum mechanical level, which samples all possible interconvertible structures of hydronium, in principle, can give the precise value of the free energy of adsorption, but it requires unattainable computing power. Nevertheless, the work from Levin and coworkers using the dielectric continuum theory and treating the proton as a point charge inside a square well potential resulted in an adsorption free energy of 7.5 kJ/mol[22, 23]. However, other polarizable force fields suggest that the Gibbs free energy of adsorption can be as high as ~12.6 kJ/mol[24]. Simultaneously, it has also been pointed out that the absolute value of the adsorption free energy depends on whether or not the interactions between the oxygen of hydronium and other water molecules are considered [25]. Therefore, in essence, there is a consensus that hydronium has a considerable surface affinity towards the water-air interface. However, a precise quantification of that is yet to be accomplished.

Structure of hydronium in liquid water -Eigen vs Zundel:

In this regard, an important question is the molecular structure of the proton in water. Attempts to answer this question so far have revolved around two structural motifs, namely Eigen and Zundel.

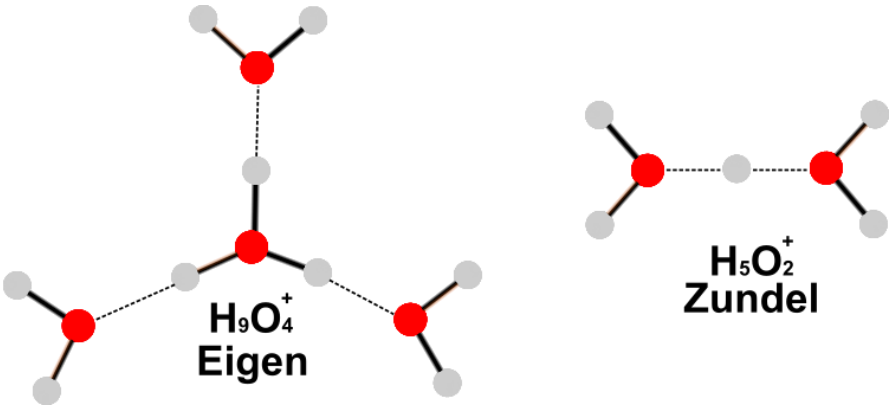

Figure 1: Structures of Eigen and Zundel motifs

As shown in figure 1, an Eigen (E) motif is a proton (H^+) solvated by a water molecule as H_3O^+ that is further solvated by three other water molecules yielding $H_3O^+(H_2O)_3$ or $H_9O_4^+$. A Zundel (Z) motif is a proton equally shared between two neighboring water molecules yielding $H_5O_2^+$.

In the gas phase, both Z and E motifs give rise to characteristic vibrational features. The Z complex vibrates at 1050 and 1760 cm^{-1}. The former corresponds to the motion of proton rattling between two neighboring water molecules, and the latter corresponds to the Fermi resonance of the motion of the proton with the bending motion of the OH groups of the flanking water molecules. The proton shuttling motion occurs at ~2600 cm^{-1} in the E complex[26]. The absorption spectra of acid in the liquid phase, unlike the gas phase, are rather broad and featureless, making the interpretation very challenging[3, 27]. An interesting difference of IR spectra of proton in liquid phase from that in the gas phase is the growth of a continuum-like absorption in the mid-IR region. Besides that, the Z complex shows its characteristic absorption features at ~3200-3400 cm^{-1} (OH stretch vibration of the flanking water molecules), 1760 and 1150 cm^{-1}. The E complex shows absorption at 2700 cm^{1}. Studies have indicated that in the liquid phase both Z and E motifs coexist and interconvert. A two-color transient infrared absorption experiment has indicated that the interconversion occurs within 50 fs[28]. However, a broadband 2D-IR study has reported that a Z motif is stable for at least 480 fs in liquid water[27]. As such, these two results contradict each other. However, it is also possible that the transient absorption and the 2D-IR experiments report on different short and long term proton transfer mechanisms, respectively. In essence, there is a consensus that both Z and E motifs exist in liquid water (bulk), but their interconversion timescale is yet to be determined quantitatively. Investigation of the structural forms of protons and their interconversion at the water-air interface is more challenging and yet to be done.

Lipid/Membrane/Surfactant- acidic water interface:

At the bare water-air interface, the surface affinity of protons is of the order of thermal energy (~-3kJ/mol) at room temperature[19, 29, 30]. At the lipid/membrane-water interface, however, it can be substantially higher[31, 32] (~-13kJ/mol) implying a greater surface propensity of protons. This increased affinity can be one of the consequences of the significantly altered arrangement of interfacial water molecules at already charged aqueous interfaces like lipid/membrane/surfactant-water interface[33, 34]. Compared to the neat water-air interface, interfacial water molecules next to a charged surface, such as a monolayer of lipid/surfactant, remain strongly aligned. Not only that, at aqueous electrolyte solution-air interfaces covered with lipids/surfactants, even the composition of the electrolytes can also be significantly different, e.g., next to a negatively charged surface, cations with larger charge density are more abundant than smaller charge density[35, 36]. An interesting question, therefore, is how (dis-)similar is the arrangement of water molecules in the presence of a proton compared to other monovalent cations at such charged interface.

Vibrational dynamics of acidic water:

The vibrational spectral features of water/ aqueous solutions are broad due to both inhomogeneous broadening and homogeneous broadening. Inhomogeneous broadening of vibrational spectra of liquid water has been attributed to different factors such as the

inhomogeneity of hydrogen bond configurations[37], intermolecular vibrations[38, 39], coupling amongst delocalized symmetric and asymmetric modes[40-42], and Fermi resonance caused by coupling with bend overtones[43]. Homogeneous broadening is caused by the different amplitude decay times of the different OH oscillators (frequently expressed as T_1) and a loss of phase coherence amongst the OH oscillators. The time scale of the latter is frequently expressed as T_2^*. T_1 and T_2^* provide information about the dynamic changes of the vibrations which are nearly impossible to decipher only from an intensity (vs. frequency) spectrum, especially if an inhomogeneous broadening mechanism is co-existing. Therefore, one needs a time-resolved spectroscopic technique that can probe the dynamics on a timescale of a few tens of femtoseconds and separate the different timescales of vibrational de-coherence/relaxation leading to spectral broadening. Monitoring such dynamics can lead to an understanding of the ways the water molecules dissipate vibrational energy.

One such time-resolved techniques is "pump-probe" spectroscopy, in which a pair of pulses are used to 'excite' the sample and 'probe' the transient modifications of the optical response induced by the excitation. In bulk H_2O, the vibrational lifetime and spectral diffusion lifetime are found to be 0.23±0.3 ps[44] and 0.18 ps,[45] respectively, but at the interface, these are 0.84[46, 47] and 0.24 ps[48] respectively. Thus, the vibrational and diffusion dynamics are slower at the interface than inside the bulk. One explanation for the slower dynamics at the interface is the reduced average number of hydrogen bonding partners around a water molecule to dissipate the energy. In bulk liquid H_2O, the lifetime of the stretch mode of the proton ($H_9O_4^+$) has been found to be 0.12 ps and a lifetime of interconversion between Eigen and Zundel forms ($H_9O_4^+ \leftrightarrow H_5O_2^+ + 2H_2O$) was found to be sub-0.1ps[28]. However, in another study, the lifetime of the Zundel complex has been determined to be at least 0.48 ps[27], creating an apparent contradiction with the previously mentioned study. The effect of protons on the vibrational dynamics of bulk H_2O is yet to be completely explored, but the effect of protons on the dynamics of aqueous acidic water interface is totally unknown. An important next step, therefore, is to monitor such dynamics at the interfaces. Harnessing such knowledge may help to explore potential implications of energy flow pathways in biochemical reactions.

Overview:

Through all the studies done so far, we know that excess hydronium adsorbs at the air-water interface. Yet, there are significant gaps in our understanding of the effects of excess hydronium at the water-air interface, such as:

- What is the relative surface adsorption of excess proton in the presence of an already negatively charged water-air interface;
- At which bulk concentrations do the surface adsorption of excess hydronium and its conjugate base hydroxide start;

- Is there any difference in surface affinities of hydronium and hydroxide ion at the water-air interface,

- Does the hydrated proton at the water-air interface remain as either or both Zundel ($H_9O_4^+$) and/or Eigen ($H_5O_2^+$) form(s),

- What is the absorption Gibbs free energy of hydrated proton at the water-air interface,

- Does the angular distribution of "free OH" (explained later) change in the presence of an acid, and

- Do the dynamics of the acidic interface differ from that of pure water? What is the molecular mechanism causing such changes, if it does change?

In this thesis, I present my efforts to unravel the modulation of structure and dynamics of water at a water-air interface in the presence of acid in the subphase using vibrationally resonant sum-frequency generation (SFG) spectroscopy. In the following section, I first discuss the fundamentals of SFG.

Chapter 2

Theory:

A rigorous description of the theory of light-matter interaction can be found in books from Boyd[49] and Shen[50] and review from Lambert and Davies[51]. In the following, I summarize the essentials of nonlinear optics and SFG.

Polarization:

Light-matter interactions are generally used to understand the properties of matter. In classical terms, light being an electromagnetic wave exerts a force on the electron cloud of the matter (atom/molecule), i.e. induces an electric dipole, μ, that depends on the driving electric field $E(t)$ strength as:

$$\mu_i(r,t) = \alpha_i E(r,t) \tag{2}$$

Where α_i is the polarizability of the *i*-th electron. In a condensed phase, such as liquid water, the individual electric dipoles can be summed up and represented as a macroscopic dipole moment per unit volume, also known as polarization, P:

$$P(r,t) = \epsilon_0 \chi^{(1)} E(r,t) = \sum_i \alpha_i E(r,t) \tag{3}$$

Where ϵ_0 is the vacuum permittivity, and $\chi^{(1)}$ is the macroscopic average of α_i.[2] The induced dipole oscillates at the same frequency as the driving electric field and radiates another light at the same frequency as the incident field. This causes linear optical effects like reflection and refraction.

In cases with low intensity or incoherent light sources, linear optical effects are predominant. As the field strength of the incident light becomes comparable to that of intra/inter-atomic field strength, light-matter interactions become nonlinearly dependent on the incident electric field. The induced dipole then must be represented as:

[2] Assuming the static dipole to be zero.

$$\mu(r,t) = \alpha E(r,t) + \beta E^2(r,t) + \gamma E^3(r,t) + \cdots \quad (4)$$

Where β and γ are first and second-order hyperpolarizabilities, respectively. The polarizabilities can now be expressed as:

$$\begin{aligned} P(r,t) &= \chi^{(1)}E(r,t) + \chi^{(2)}E^2(r,t) + \chi^{(3)}E^3(r,t) + \cdots \\ &= P^{(1)}(r,t) + P^{(2)}(r,t) + P^{(3)}(r,t) + \cdots \\ &= P^{(1)}(r,t) + P^{NL}(r,t) \end{aligned} \quad (5)$$

Where $\chi^{(k)}$ represent the *k*-th order susceptibility of the material, and P^{NL} represents the nonlinear polarization, driving all the nonlinear phenomena in the material.
There are a number of different nonlinear light-matter interactions possible. In this introduction, I briefly discuss one type of it, namely sum-frequency generation, that I have used to probe aqueous acidic interfaces.

Sum Frequency Generation (Conventional/Direct/Homodyne):

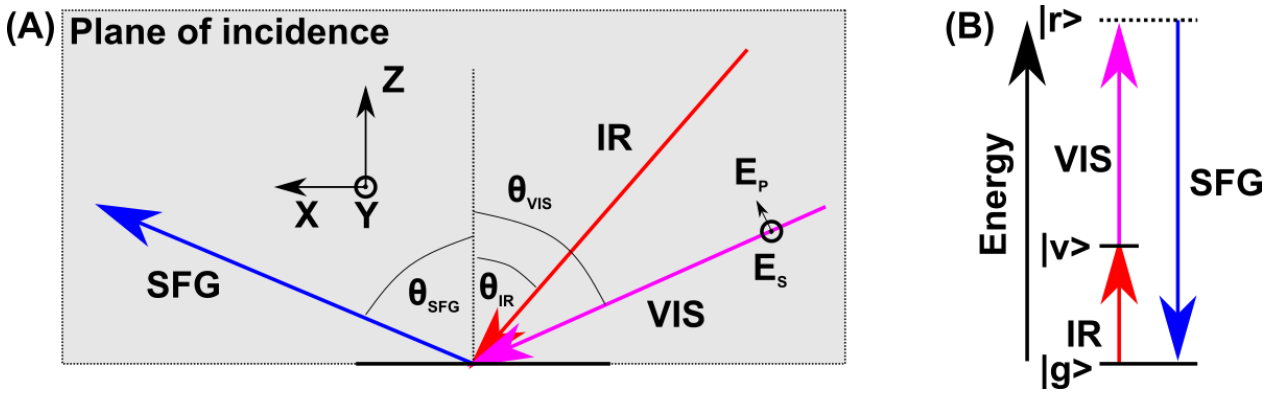

Figure 2. Schematics of (A) the SFG process and (B) the energetics of vibrational SFG, where $E_{p/s}$ represents the p/s polarized electric field and |g>,|v>, and |r> are ground, excited, and virtual states, respectively.

Figure 2 shows the schematics of the SFG process (A) and the energy level diagram of vibrational SFG (B). When two electric fields with frequencies $\omega_1$and ω_2 propagating in the direction r are overlapped in time and space, the resulting electric field can be written as:

$$\begin{aligned} E(r,t) &= \frac{1}{2}(E_1(r,t) + E_2(r,t)) \\ &= \frac{1}{2}\left(E_1(r)e^{-i\omega_1 t} + E_2(r)e^{-i\omega_2 t} + c.c.\right) \\ &= E_1(r)\cos(\omega_1 t) + E_2(r)\cos(\omega_2 t) \end{aligned} \tag{6}$$

The second-order nonlinear polarization created in the material due to the two fields E_1 and E_2 is:

$$\begin{aligned} P^{(2)}(\omega,t) &= \epsilon_0\chi^{(2)}E^2(t) \\ &= \epsilon_0\chi^{(2)}[E_1\,cos(\omega_1 t) + E_2\cos(\omega_2 t)]^2 \\ &= \frac{\epsilon_0\chi^{(2)}}{2}[(E_1^2 + E_2^2) + E_1^2\cos(2\omega_1 t) + E_2^2\cos(2\omega_2 t) \\ &\quad + 2E_1E_2\cos((\omega_1 - \omega_2)\,t) + 2E_1E_2\cos((\omega_1 + \omega_2)t)] \end{aligned} \tag{7}$$

The first term in equation (7) is frequency independent direct current (DC) field, the second and third terms represent second harmonic generation (SHG) at frequencies $2\omega_1$ and $2\omega_2$ respectively, the fourth term represents difference frequency generation (DFG), and the final term represents sum-frequency generation (SFG):

$$\omega_3 = \omega_1 + \omega_2 \tag{8}$$

Although, four different nonzero frequency components are present in the nonlinear polarization (eq 7), typically one of these frequency components is present with any appreciable intensity in the radiation resulted by the nonlinear optical interactions since the required phase-matching condition of only one of the aforementioned interaction can be met at a time by properly selecting the input radiation and the orientation of the nonlinear crystal. Commonly, in experimental conditions, one of these two incoming frequencies, say, ω_1 is tunable in the mid-IR frequency range ($\lambda_{IR} = 4000\ nm$) that is resonant with vibrational transitions in the system. The other, i.e. ω_2 is fixed at near-IR (visible) frequency ($\lambda_{VIS} = 800\ nm$). Therefore,

$$\omega_{SFG} = \omega_{IR} + \omega_{VIS} \tag{8a}$$

At the interface, the necessary phase matching condition[49] results in the energy and momentum conservation of both the incoming and outgoing photons involved in the SFG process:

$$\hbar\omega_{SFG} = \hbar\omega_{IR} + \hbar\omega_{VIS} \tag{8b}$$

$$k_{\parallel}^{SFG} = k_{\parallel}^{IR} + k_{\parallel}^{VIS} \tag{9a}$$

$$k_{SFG} sin\theta_{SFG} = k_{IR} sin\theta_{IR} + k_{VIS} sin\theta_{VIS} \tag{9b}$$

Where, $k_{\parallel}^{i}$ is the surface-parallel component of the wave-vector of the corresponding photon i.

In a Cartesian coordinate system with the unit vectors *i, j, k,* the SFG polarization is:

$$P_{SFG}^{(2)}(\omega_{SFG}, \omega_{VIS}, \omega_{IR}) = \epsilon_0 \sum_{i}^{x,y,z} \sum_{j}^{x,y,z} \sum_{k}^{x,y,z} \chi_{ijk}^{(2)}(\omega_{SFG}, \omega_{VIS}, \omega_{IR})\, E_{j,VIS}^{int}(\omega_{VIS}) E_{k,IR}^{int}(\omega_{IR}) \tag{10}$$

Where E_j^{int} is the interfacial field in the Cartesian coordinate system. $P_{SFG}^{(2)}, \chi_{ijk}^{(2)}$, and E_j^{int} are strictly functions of frequency (ω), but for further discussions, we omit the frequency

dependence for simplicity.

The individual components of $P_{i,SFG}^{(2)}$ can be written as:

$$P_{x,SFG}^{(2)} = \epsilon_0 \sum_{j}^{x,y,z} \sum_{k}^{x,y,z} \chi_{xjk}^{(2)} E_{j,VIS}^{int} E_{k,IR}^{int} \tag{11a}$$

$$P_{y,SFG}^{(2)} = \epsilon_0 \sum_{j}^{x,y,z} \sum_{k}^{x,y,z} \chi_{yjk}^{(2)} E_{j,VIS}^{int} E_{k,IR}^{int} \tag{11b}$$

$$P_{z,SFG}^{(2)} = \epsilon_0 \sum_{j}^{x,y,z} \sum_{k}^{x,y,z} \chi_{zjk}^{(2)} E_{j,VIS}^{int} E_{k,IR}^{int} \tag{11c}$$

E_j^{int}, the interfacial field in the Cartesian coordinate system is related to the incident field, E_j^I in the following ways:

$$E_{(x|z)}^{int} = \left(1 - r_p\right) E_{(x|z)}^{I} \tag{12a}$$

$$E_y^{int} = (1 + r_s) E_y^I \tag{12b}$$

Where, r_p and r_s are Fresnel factors in *p* and *s* polarizations of the incident light, respectively.

For an electromagnetic wave propagating along the *X*-*Z*-plane in interface bound Cartesian coordinate system (Fig. 2), the electric field vector of the *p*-polarized light can be resolved along both the *X* and *Z*-axes (eq 13 a,c), while the electric field vector of the *s*-polarized light only has an electric field component along the *Y*-axis (eq 13b). In an experimental non-colinear beam geometry (as shown in Fig 1), the absolute orientation of the polarization of the electric field of the light is related to the Cartesian coordinate system in the following ways:

$$E_x^I = E_p^I sin\theta \tag{13a}$$

$$E_y^I = E_s^I \tag{13b}$$

$$E_z^I = E_p^I cos\theta \tag{13c}$$

Therefore, the interfacial fields can now be written in relation to the absolute orientation of the

polarization of the incoming light field as:

$$E_x^{int} = \left(1 - r_p\right) sin\theta E_p^I = K_x E_p^I \tag{14a}$$

$$E_y^{int} = (1 + r_s) E_s^I = K_y E_s^I \tag{14b}$$

$$E_z^{int} = \left(1 + r_p\right) cos\theta E_p^I = K_z E_p^I \tag{14c}$$

Now, the intensity of the *s/p*-polarized SFG light emitted from the surface and eventually detected can be expressed as the sum of the squares of the component SFG electric fields, viz.,

$$I_{s,SFG} \propto \left|E_{y,SFG}^I\right|^2 \propto \left|L_y P_{y,SFG}^{(2)}\right|^2 \tag{15a}$$

$$I_{s,SFG} \propto \left|L_y \sum_j^{x,y,z} \sum_k^{x,y,z} \epsilon_0 \chi_{yjk}^{(2)} K_{j,VIS} E_{(p|s),VIS}^I K_{k,IR} E_{(p|s),IR}^I\right|^2 \tag{15b}$$

and,

$$I_{p,SFG} \propto \left|E_{x,SFG}^I\right|^2 + \left|E_{z,SFG}^I\right|^2 \propto \left|L_x P_{x,SFG}^{(2)}\right|^2 + \left|L_z P_{z,SFG}^{(2)}\right|^2 \tag{16a}$$

$$I_{p,SFG} \propto \left|L_x \sum_j^{x,y,z} \sum_k^{x,y,z} \epsilon_0 \chi_{xjk}^{(2)} K_{j,VIS} E_{(p|s),VIS}^I K_{k,IR} E_{(p|s),IR}^I\right|^2 + \left|L_z \sum_j^{x,y,z} \sum_k^{x,y,z} \epsilon_0 \chi_{zjk}^{(2)} K_{j,VIS} E_{(p|s),VIS}^I K_{k,IR} E_{(p|s),IR}^I\right|^2 \tag{16b}$$

for, $j,k = x,z; E_{(p|s)}^I = E_p^I$ and for $j,k = y; E_{(p|s)}^I = E_s^I$

Where, L_i is the Fresnel factor of the SFG light generated at the interface.

The abovementioned explanation of SFG is true in the frequency domain. There is an equivalent explanation for SFG process in the time domain. Although we do not do SFG experiments in the time domain, it is important to have a basic understanding of the process in the time domain, which in turn helps to better understand the phase-resolved SFG measurements (explained later).

Time Domain Picture of SFG:

A detailed discussion on this topic is available in refs.[49, 52-54]. A very brief description is given here. A sub-picosecond broadband IR pulse arriving at the sample creates a coherence between the ground and first vibrational excited state resulting in a first-order non-resonant polarization ($P_{NR}^{(1)}(t)$) and resonant polarization ($P_{R}^{(1)}(t)$). The $P_{NR}^{(1)}(t)$ vanishes soon after the *IR* pulse disappears. The $P_{R}^{(1)}(t)$ undergoes free induction decays (FIDs) for finite duration, as shown in Fig 3. The coherence then further interacts with the VIS pulse and undergoes a coherent anti-stokes Raman type transitions. Therefore, out of these IR active vibrations, only those that are also Raman active can contribute to the SFG signal.

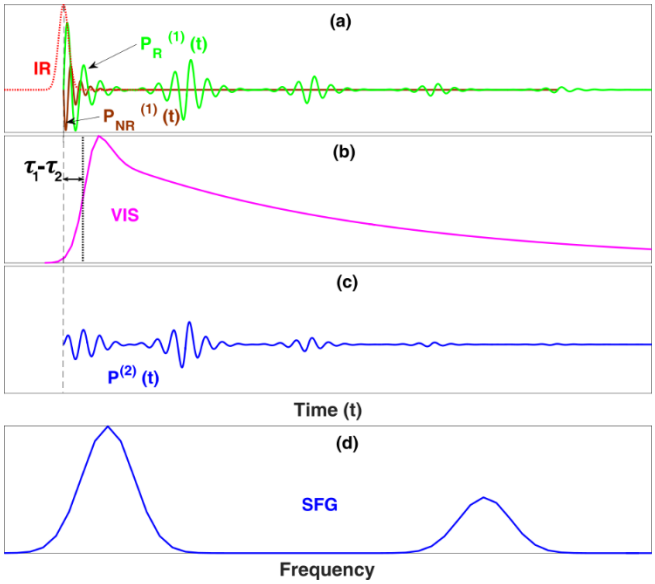

Figure 3: ***A schematic time domain representation of the SFG process:*** *(a) The red dotted line represents the IR pulse profile. The IR pulse initiates the coherent nonresonant ($P_{NR}^{(1)}(t)$) and resonant ($P_{R}^{(1)}(t)$) polarization that undergoes free induction decay (FID) shown in dark red and green, respectively. The nonresonant polarization and the IR pulse have comparable duration. The resonant polarization has finite duration. (b) The VIS pulse (after transmitted from the etalon) profile in time domain. The VIS pulse upconverts the total 1st order polarization.$(\tau_1 - \tau_2)$ is the time delay between the IR and the VIS pulse, measured from the halfway of the rising edge of the VIS pulse. (c) The resulting coherent 2nd order polarization is due to the upconversion process. (d) A schematic SFG spectrum in frequency domain.*

The SFG signal, in the time domain, can be described by a second-order response

function $R^{(2)}(t)$ that contains the information of the molecular vibrations:

$$P_{SFG}^{(2)}(t) = \epsilon_0 \int_0^{\infty} \int_0^{\infty} R^{(2)}(\tau_1, \tau_2) E_{VIS}(t-\tau_2) E_{IR}(t-\tau_1) d\tau_1 d\tau_2 \quad (17a)$$

Here $R^{(2)}(\tau_1, \tau_2)$ is the second-order response function, which contributes to the polarization produced at time t by the electric fields applied at earlier times $t-\tau_1$ and $t-\tau_2$. In eq 17a, it is assumed that the $R^{(2)}(\tau_1, \tau_2)$ obeys the causality condition $R^{(2)}(\tau_1, \tau_2) = 0$ for either $\tau_1$or $\tau_2 < 0$, meaning that the polarization value depends only on the past and not on the future values of the incoming electric fields, hence the lower limits of integration are zeros.

The SFG response thus emitted is transformed into the frequency domain by the spectrograph through Fourier transformation in the following manner:

$$P_{SFG}^{(2)}(t) = \epsilon_0 \int_{-\infty}^{\infty} \frac{d\omega_{VIS}}{2\pi} \int_{-\infty}^{\infty} \frac{d\omega_{IR}}{2\pi} \int_0^{\infty} d\tau_1 \int_0^{\infty} d\tau_2 \, R^{(2)}(\tau_1, \tau_2) \times E_{IR}(\omega_{IR}) e^{-i\omega_1(t-\tau_1)} E_{VIS}(\omega_{VIS}) e^{-i\omega_2(t-\tau_2)} \quad (17b)$$

$$P_{SFG}^{(2)}(t) = \epsilon_0 \int_{-\infty}^{\infty} \frac{d\omega_{VIS}}{2\pi} \int_{-\infty}^{\infty} \frac{d\omega_{IR}}{2\pi} \chi^{(2)}(\omega_{SFG}, \omega_{VIS}, \omega_{IR}) E_{VIS}(\omega_{VIS}) E_{IR}(\omega_{IR}) e^{-i\omega_{SFG}t} \quad (17c)$$

Where, $\omega_{SFG} = \omega_{VIS} + \omega_{IR}$ and the second-order susceptibility:

$$\chi^{(2)}(\omega_{SFG}; \omega_{VIS}, \omega_{IR}) = \int_0^{\infty} d\tau_1 \int_0^{\infty} d\tau_2 \, R^{(2)}(\tau_1, \tau_2) e^{i(\omega_1\tau_1 + \omega_2\tau_2)} \quad (17d)$$

By replacing the left hand side of the above equation with $\int_{-\infty}^{\infty} \frac{d\omega_{VIS}}{2\pi} \int_{-\infty}^{\infty} \frac{d\omega_{IR}}{2\pi} P^{(2)}(\omega) e^{-i\omega_{SFG}t}$, we recover the usual frequency domain response of the polarization:

$$P_{SFG}^{(2)}(\omega) = \epsilon_0 \chi^{(2)}(\omega_{SFG}; \omega_{VIS}, \omega_{IR}) E_{VIS}(\omega_{VIS}) E_{IR}(\omega_{IR}) \quad (18)$$

Properties of $\chi^{(2)}$:

The nonlinear susceptibility $\chi_{ijk}^{(2)}$ is a third rank tensor having 27 elements. The number of elements out of these 27 having nonzero contributions is dependent on the presence/ absence of centrosymmetry in the medium. In a centrosymmetric medium, all directions are equivalent. Therefore, after an inversion operation, $\chi_{ijk}^{(2)}$ should not change sign, i.e.

$$\chi_{ijk}^{(2)} = \chi_{-i-j-k}^{(2)} \tag{19}$$

However, since a third rank tensor must change its sign after inversion operation, the following is also true:

$$\chi_{ijk}^{(2)} = -\chi_{-i-j-k}^{(2)} \tag{20}$$

In order for both eq. 19 and 20 to be simultaneously correct, $\chi_{ijk}^{(2)}$ must be 0. Therefore, in a centrosymmetric medium, SF is not generated. In many cases (eg. water) the bulk medium is centrosymmetric. However, at the boundary between two materials (interfaces), the centrosymmetry is necessarily broken giving rise to a SFG signal.

For an interface which is isotropic in the *X*-*Y* plane, but not along the *Z*-axis, only those components of $\chi_{ijk}^{(2)}$ that have quadratic combinations of *X* and/or *Y* are unique and generate SFG signal*:*

$$\chi_{zxx}^{(2)}\left(\equiv \chi_{zyy}^{(2)}\right) \tag{21a}$$

$$\chi_{xzx}^{(2)}\left(\equiv \chi_{yzy}^{(2)}\right) \tag{21b}$$

$$\chi_{xxz}^{(2)}\left(\equiv \chi_{yyz}^{(2)}\right) \tag{21c}$$

$$\chi_{zzz}^{(2)} \tag{21d}$$

As discussed earlier, for an electromagnetic wave propagating along the *X*-*Z*-plane in interface bound Cartesian coordinate system (Fig. 2), the electric field vector of the *p*-polarized light can be resolved along both the X- and Z-axes (eq 13 a,c), while the electric field vector of the *s*-polarized light has only a component along the Y-axis (eq 13b). Therefore, by correctly choosing

the appropriate combination of polarization of the incoming and outgoing light waves specific tensor elements can be probed:

$$\chi^{(2)}_{yyz}: \text{ssp} \tag{22a}$$
$$\chi^{(2)}_{yzy}: \text{sps} \tag{22b}$$
$$\chi^{(2)}_{zyy}: \text{pss} \tag{22c}$$
$$\chi^{(2)}_{zzz} + \chi^{(2)}_{xxz} + \chi^{(2)}_{xzx} + \chi^{(2)}_{zxx}: \text{ppp} \tag{22d}$$

where ssp/ppp represents s/p-polarized ***SFG***, s/p-polarized ***VIS*** and p-polarized ***IR***, respectively.

Resonant and Non-resonant susceptibilities:

The surface susceptibilities associated with the non-resonant and resonant SFG responses are termed as non-resonant susceptibility, $\chi^{(2)}_{NR}$, and resonant susceptibility, $\chi^{(2)}_{R}$, respectively. Hence, the SF activity of the adsorbed molecules can be fully described as:

$$\chi^{(2)} = \chi^{(2)}_{NR} + \chi^{(2)}_{R} \tag{23}$$

For dielectric materials, $\chi^{(2)}_{NR}$ is typically very small. However, for transition metal surfaces, $\chi^{(2)}_{NR}$ may have a significant magnitude since the *d*-electrons can be (partially) excited by the 800 nm pulse. Strictly speaking, in such case, the so-called non-resonant response is actually an off-resonant response.

A $\chi^{(2)}$ is the macroscopic average of all the individual molecular hyperpolarizabilities, β, of the molecules at the surface:

$$\chi^{(2)} = N\langle\beta\rangle, \tag{24}$$

where N is the number density of the molecules, and $\langle\ \ \rangle$ indicates the orientational average.

If ω_{IR}, the frequency of the tunable IR beam, is near a vibrational resonance, ω_{υ}, and ω_{VIS} is far away from any electronic resonances, then the molecular hyperpolarizability can be expressed as:

$$\beta = \left(\frac{2\pi}{h}\right)\left(\frac{\alpha\mu}{\omega_{IR} - \omega_{\upsilon} + i\Gamma}\right) \tag{25}$$

where, α and μ are Raman transition polarizability and IR transition dipole moment, respectively, and Γ is the full width at half maximum (FWHM) of the vibrational linewidth. Thus, a resonance must be both Raman and IR active to be SFG active.

Therefore, a single non-zero component of $\chi_R^{(2)}$ can be expressed as:

$$\chi_R^{(2)} = \left(\frac{2\pi N}{h}\right)\langle\left(\frac{\alpha\mu}{\omega_{IR} - \omega_{\upsilon} + i\Gamma}\right)\rangle \tag{26a}$$

$$\chi_R^{(2)} = \frac{A}{\omega_{IR} - \omega_{\upsilon} + i\Gamma} \tag{26b}$$

$$I_R \propto \left|\chi_R^{(2)}\right|^2 \propto \left|\frac{A}{\omega_{IR} - \omega_{\upsilon} + i\Gamma}\right|^2 \tag{27}$$

where A is the strength or amplitude of the vibrational mode.

Thus, as ω_{IR} approaches the frequency of a vibrational mode, ω_{ν}, $\omega_{\upsilon} - \omega_{IR} \rightarrow 0$, and $\chi_R^{(2)}$ increases and results in an enhanced SFG signal.

The SFG spectrum, i.e. the SFG intensity as a function of frequency, can provide a plethora of information. However, the SFG intensity scales with the square of the $\chi_R^{(2)}$, where $\chi^{(2)}$is a complex number. The sign of its imaginary part (±) holds information about the absolute orientation of the dipole moment with respect to the surface plane. In the intensity spectrum, the information about the absolute orientation of the transition dipole moment (up vs. down) with respect to the surface plane is lost. Therefore, it is necessary to know the actual imaginary and real $\chi^{(2)}$ in order to determine the absolute orientation of the molecules. Experimentally these can be measured using a phase-resolved (heterodyne) SFG approach.

Phase-Resolved (Heterodyne) SFG:

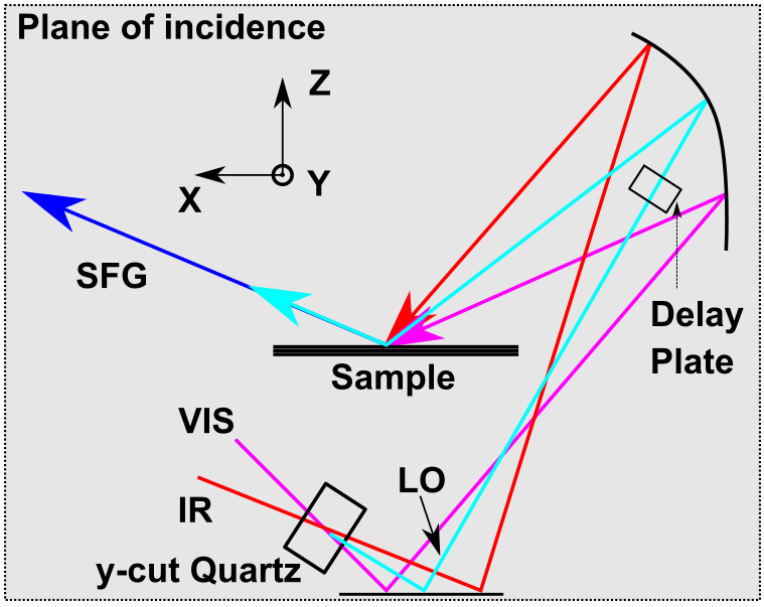

Figure 4: ***Schematic of phase-resolved SFG experimental technique:*** *The incoming IR (red) and VIS (magenta) transmit through a y-cut quartz crystal and generate an SFG response called local oscillator (LO, in cyan). The IR and VIS beams are refocused onto the sample surface to produce a resonant SFG response (blue). Both SFG responses travel the same optical path from the sample to the detector. The delay plate in the optical path of the LO-SFG response introduces a time delay.*

In a phase-resolved SFG experiment, an SFG signal from the sample surface interferes with another SFG signal that is called local oscillator (LO), and the interference is detected (Fig 4):

$$E_{det} = E_{sample} + E_{LO} \tag{28}$$

$$E_{sample} = \epsilon_0 F_{sample} \chi^{(2)}_{sample} E_{VIS} E_{IR} \tag{29a}$$

$$E_{LO} = \epsilon_0 F_{LO} \chi^{(2)}_{LO} E_{VIS} E_{IR} \tag{29b}$$

Where, ϵ_0 is the vacuum permittivity and F_k is the Fresnel factor of sample/LO. Here, E_{sample} and E_{LO} denote the SF electric field from the sample and the LO, respectively. $\chi^{(2)}_{sample}$ is the quantity of interest and the goal is to extract its spectral shape. The spectrum of IR pulse can be obtained by replacing the sample with quartz:

$$E_{sample=quartz} = \epsilon_0 F_{quartz} \chi^{(2)}_{quartz} E_{VIS} E_{IR} \tag{29c}$$

We retrieve the phase of the sample relative to the phase of the LO, by introducing a time delay between the sample SFG response and the LO pulse. It is equivalent to delay the LO in time with respect to the sample SFG while arriving at the spectrograph:

$$\begin{aligned} E_{det}(t) &= E_{sample}(t) + E_{LO}(t-T) \rightarrow \\ E_{det}(\omega) &= E_{sample}(\omega) + E_{LO}(\omega) e^{i\omega T} \end{aligned} \tag{30}$$

The T represents the time delay between the SFG from the sample and the LO introduced using a delay plate (details in the experimental setup section).

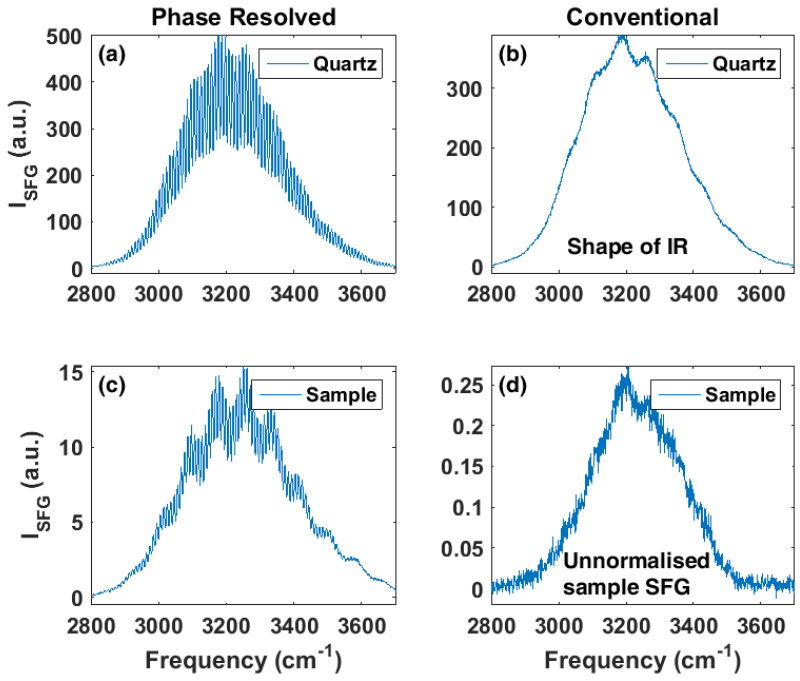

Figure 5: (a & c) Detected phase-resolved intensity spectra for quartz and sample (H_2O) respectively, (b & d) Detected conventional intensity spectra for quartz and sample.

Figure 5 (a & c) represent the detected phase-resolved intensity spectra of quartz and sample, respectively. Due to the introduction of the delay, the total detected intensity is represented as:

$$I_{SFG} \propto |E_{det}|^2 \tag{31a}$$

$$I_{SFG} \propto \left|E_{sample}\right|^2 + |E_{LO}|^2 + E_{sample}E_{LO}^{*}e^{(-i\omega T)} + E_{sample}^{*}E_{LO}e^{(i\omega T)} \tag{31b}$$

The two complex cross-terms contain the phase information and give rise to an interference pattern as shown in panel (a) and (c).

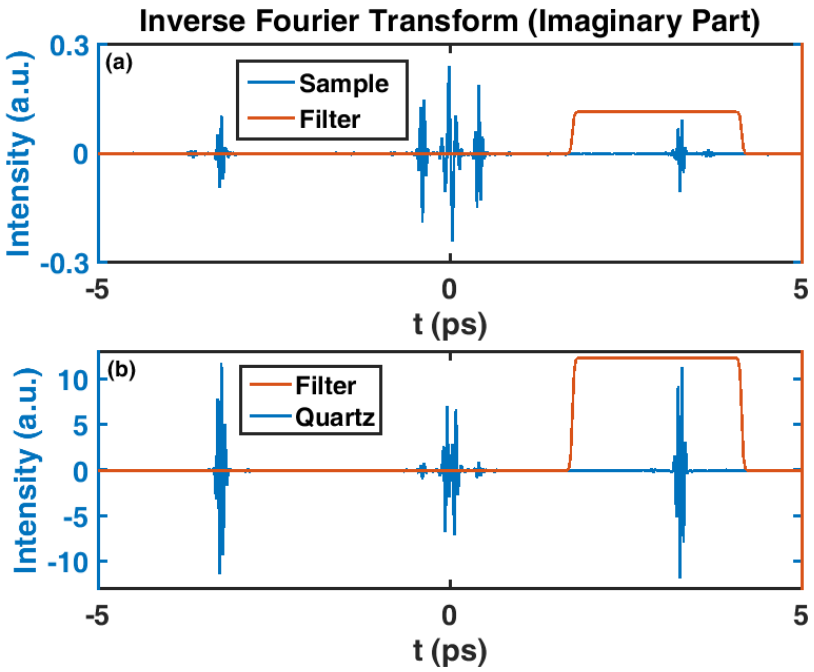

Figure 6: Imaginary part of the inverse Fourier transform of the interference pattern of the intensity spectra detected in phase-resolved measurement. The red curve represents the filter function used to isolate one of the cross-terms.

The intensity detected in the frequency domain is first inverse Fourier transformed into the time domain. The resultant imaginary parts of the transformed functions for both quartz and sample are shown in figure 6. The term $\left|E_{sample}\right|^2 + |E_{LO}|^2$ appears at time zero. The cross-terms appear at certain time delays $(\mp T)$ equal to the time-delay introduced by the delay plate**.** One of the cross terms is filtered by multiplying this time-domain interferogram with a filter-function**.** The resulting filtered interferogram is Fourier transformed into the frequency domain (Fig 7) to produce the complex spectrum $E_{sample}E_{LO}^{*}e^{(-i\omega T)}$. The intensity spectrum detected for z-cut quartz is treated in the same way to produce $E_{quartz}E_{LO}^{*}e^{(-i\omega T)}$.

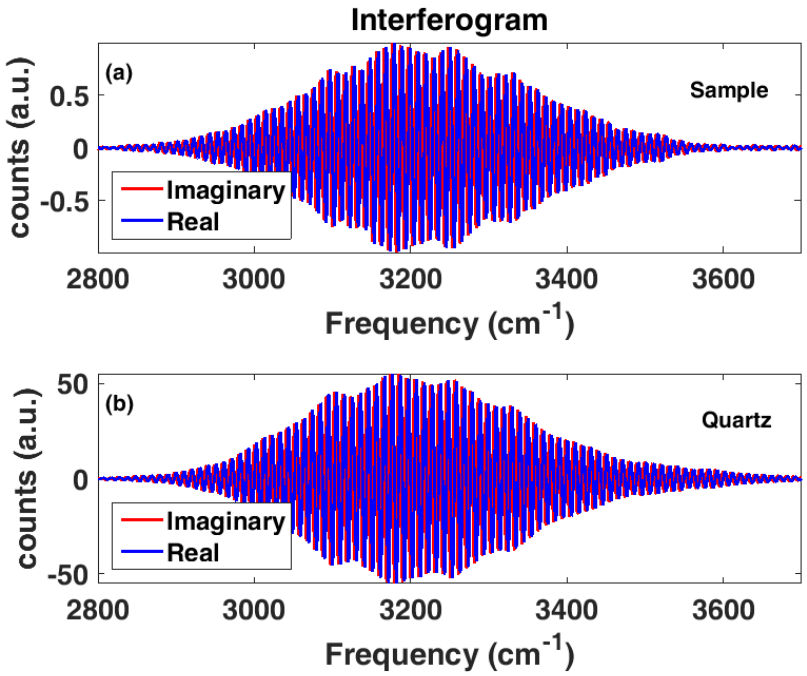

Figure 7: The complex interferogram in the frequency domain for both Sample (panel a) and quartz (panel b)

The real and imaginary $\chi^{(2)}$ spectra Fig. 8 (a)) are obtained by dividing the sample interferogram by the quartz interferogram:

$$\chi^{(2)} = \frac{E_{sample}E_{LO}^{*}e^{(-i\omega T)}}{E_{quartz}E_{LO}^{*}e^{(-i\omega T)}} \tag{32a}$$

$$\chi^{(2)} = \frac{\epsilon_0 F_{sample}\chi_{sample}^{(2)}E_{VIS}E_{IR}}{\epsilon_0 F_{quartz}\chi_{quartz}^{(2)}E_{VIS}E_{IR}} \tag{32b}$$

$$\chi^{(2)} = F_{eff}\left(\frac{\chi_{sample}^{(2)}}{\chi_{quartz}^{(2)}}\right) \tag{32c}$$

Where, $F_{eff} = \frac{F_{sample}}{F_{quartz}}$ is the effective Fresnel factor.

The $\left|\chi^{(2)}\right|^2$ returns the intensity spectrum as shown in figure 8(b):

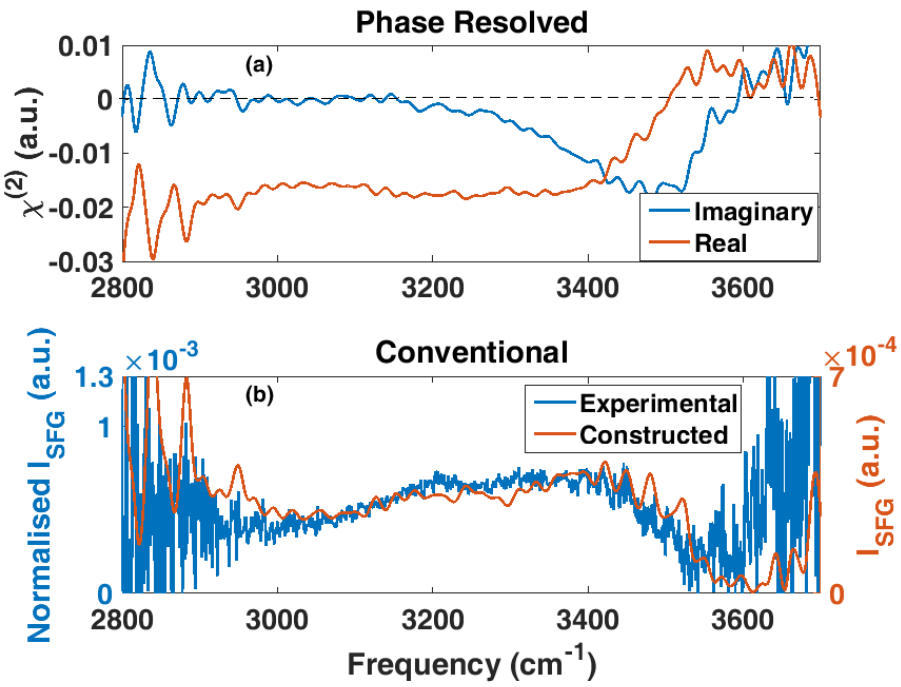

Figure 8: (a) Imaginary and real parts of the $\chi^{(2)}$ spectrum of the sample detected in a phase-resolved measurement. (b) The $|\chi^{(2)}|^2$ spectrum constructed (red) from the imaginary and real parts of $\chi^{(2)}$ and overlaid on top of the experimental intensity spectrum.

Both conventional and phase-resolved SFG are powerful tools to acquire information about the equilibrium structure of the system. However, it cannot provide any information on any dynamic changes that occur at thermodynamic non-equilibrium on a few picosecond timescales. To capture such dynamics spectroscopically, one needs a technique that can resolve such time-dependent changes. Therefore, in a time-resolved approach, a pair of pulses is used to *excite* the sample and *probe* the transient modifications of the optical responses caused by the excitation. Then, by changing the time delay between two pulses, one can extract dynamic information. There are different approaches to time-resolved experiments. We use a specific approach called 'Pump-Probe' SFG.

Time-Resolved (Pump-Probe) Homodyne SFG:

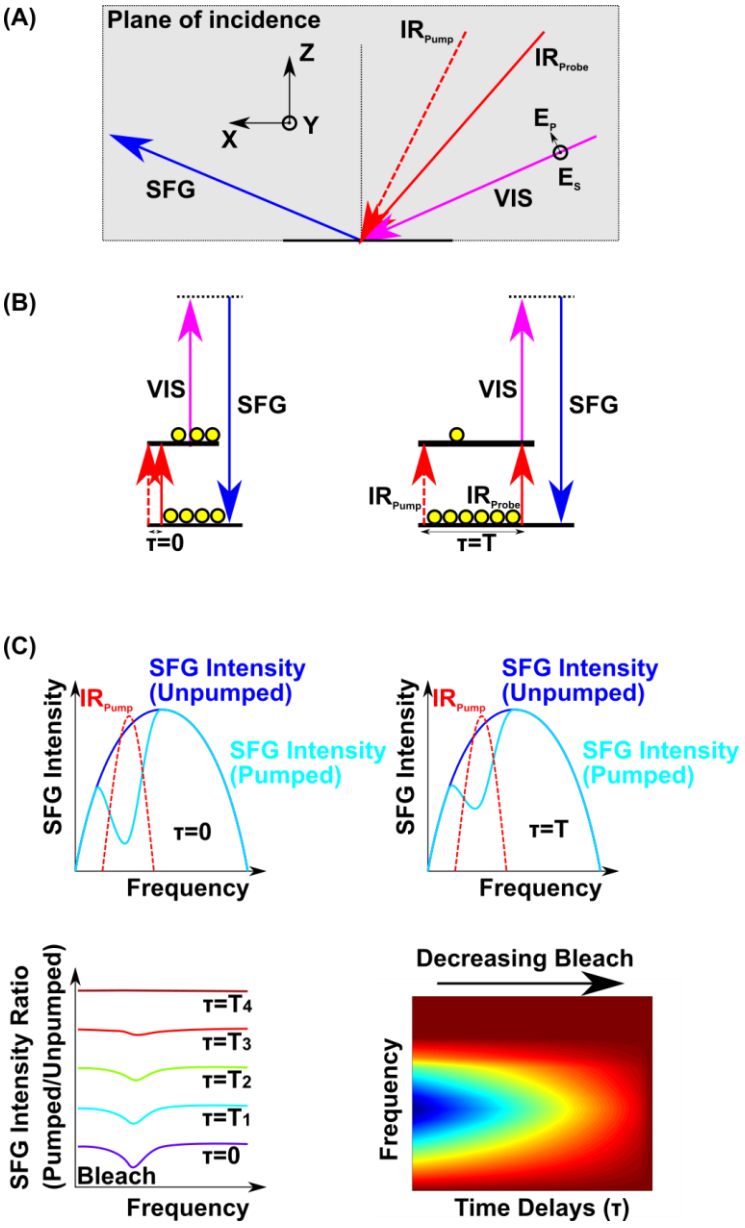

Figure 9: (A) schematics of the pump-probe experimental technique. (B) Energetics of pump-probe process. (C) Schematics of pump-induced changes in an SFG spectrum as a function of frequency and time delays.

As shown in figure 9 (A-B), in a pump-probe SFG experiment, a pump-IR pulse excites molecules from the ground state, $v = 0$, to the first vibrationally excited state, $v = 1$. The pump first creates a polarization between the ground and the excited state, which is followed by population transfer: $v = 0 \rightarrow 1$. The remaining population in $v = 0$ participate in the SFG process triggered by the probe pulse. As such, the probe pulse effectively measures the number density of the remaining molecules in the ground vibrational state. The recovery of the population in $v = 0$, measured as a function of time delay (τ) between the pump and the probe pulse, provides information about the possible pathways the population of the $v = 1$ relaxes back to the

$v = 0$. A $v = 1 \rightarrow 0$ transition also occur simultaneously but is not distinguished from the $v = 0 \rightarrow 1$ transition, in this scheme. In our pump-probe SFG scheme, we use a spectrally narrow IR pump pulse and a spectrally broad IR probe pulse.

It is important to note that neither the IR-'pump', nor the 'probe' is a surface-specific process, but, it is the interaction with the VIS that cancels all the responses from the centro-symmetric bulk medium and makes the pump-probe SFG a surface-specific process.

The SFG intensity decreases due to the population depletion from $v = 0$ induced by the IR pump and eventually recovers with increasing time. This intensity reduction is called 'bleach' (Fig 9(C)).

In the absence of any IR-pump, i.e. in the steady-state (ss), the SFG intensity is given by:

$$I_{ss} \propto \left|\chi_0^{(2)}\right|^2 \tag{33}$$

In the presence of a pump pulse (excitation, ex) the intensity can be written as:

$$I_{ex}(\tau) \propto \left|\chi_{ex}^{(2)}(\tau)\right|^2 \tag{34a}$$

$$I_{ex}(\tau) \propto \left|\chi_0^{(2)} + \Delta\chi^{(2)}(\tau)\right|^2 \tag{34b}$$

Since, $\chi_0^{(2)}$ is a complex number, an interesting question is if the pump-induced changes in time occur in both or either of the Imaginary and Real part of $\chi_0^{(2)}$. Expanding eq (34b), we get:

$$I_{ex}(\tau) \propto \left|\chi_0^{(2)}\right|^2 + \chi_0^{(2)*}\Delta\chi^{(2)}(\tau) + \chi_0^{(2)}\Delta\chi^{(2)*}(\tau) + \left|\Delta\chi^{(2)}(\tau)\right|^2 \tag{34c}$$

$\left|\Delta\chi^{(2)}(\tau)\right|^2$ is very small and can be neglected. Now we can rewrite the eq (34c) as:

$$\frac{I_{ex}(\tau)}{I_{ss}} \propto 1 + 2Re\left(\chi_0^{(2)}\right)Re\left(\Delta\chi^{(2)}(\tau)\right) + 2Im(\chi_0^{(2)})Im\left(\Delta\chi^{(2)}(\tau)\right) \tag{34d}$$

This shows that the changes in both the Imaginary and Real part of $\Delta\chi^{(2)}(\tau)$ are manifested in the intensity spectrum. Since the Imaginary and Real $\chi^{(2)}$ are related by the Kramers-Kronig relationship[49], the time evolution of the two parts are dictated by the same dynamics[55]. This gives us the opportunity to look at the dynamics as a sole function of changes in number of molecules in the ground and excited states.

The molecular susceptibility is related to the number density of molecules as $\chi^{(2)} = N\langle\beta\rangle$, therefore,

$$\chi_0^{(2)} \propto N_0 \tag{35}$$

A pump induced $v = 0 \rightarrow 1$ transition (bleach) and $v = 1 \rightarrow 0$ transition (stimulated emission) occur simultaneously at the same frequency and therefore, cannot be distinguished. If we assume that at any time delay τ, $\Delta N(\tau)$ is the population in the first excited vibrational state, then the transient change in effective susceptibility is proportional to the difference in population between the ground and vibrational excited state:

$$\chi_0^{(2)} + \Delta\chi^{(2)}(\tau) \propto N_0 - 2\Delta N(\tau) \tag{36}$$

Now, the ratio of the SFG intensities in the presence and absence of the excitation pulse is:

$$\frac{I_{ex}(\tau)}{I_{ss}} \propto \frac{\left|\chi_0^{(2)} + \Delta\chi^{(2)}(\tau)\right|^2}{\left|\chi_0^{(2)}\right|^2} \tag{37a}$$

$$\frac{I_{ex}(\tau)}{I_{ss}} \propto \frac{\left(N_0 - 2\Delta N(\tau)\right)^2}{(N_0)^2} \tag{37b}$$

$$\frac{I_{ex}(\tau)}{I_{ss}} = \frac{I_{pumped}(\tau)}{I_{unpumped}} \propto 1 - \frac{4\Delta N(\tau)}{N_0} \tag{37c}$$

So, at very long time delay, $\tau \rightarrow \infty$, $\Delta N(\tau \rightarrow \infty) = 0$, i.e. the excited state population is completely depleted, and $I_{ex}(\tau \rightarrow \infty) = I_{ss}$ or $I_{pumped}(\tau \rightarrow \infty) = I_{unpumped}$, i.e. the steady state is restored in the system.

Due to the interaction with the pump pulse, besides bleach, an excited state absorption (ESA) can also occur. Due to the anharmonicity of any chemical bond, the ESA occurs at a different frequency than bleach or SE. On top of that, the SFG intensity is proportional to the square of the very small population of the first excited state. Therefore, ESA is not observed in TR-SFG.

Higher-order contributions to SFG:

The $\chi^{(3)}$ contribution:

It is true that the SFG technique is a $\chi^{(2)}$-based technique that eventually makes it a surface-specific spectroscopic tool. However, if a charge is present at the surface, an electric field develops across the surface that can contribute to the overall SFG response[56, 57].

The general SFG polarization for a charged surface is given by:

$$P_{SFG}^{(2)} = \sum_{i}^{x,y,z} P_{i,SFG}^{(2,eff)} \tag{38a}$$

$$P_{SFG}^{(2)} = \epsilon_0 \sum_{i}^{x,y,z} \sum_{j}^{x,y,z} \sum_{k}^{x,y,z} \chi_{ijk}^{(2,eff)} E_{j,VIS}^{int} E_{k,IR}^{int} \tag{38b}$$

$$P_{SFG}^{(2)} = \epsilon_0 \sum_{i,j,k}^{x,y,z} \chi_{ijk}^{(2,eff)} E_{j,VIS}^{int} E_{k,IR}^{int} \tag{38c}$$

Where, $\sum_{i,j,k}^{x,y,z} = \sum_{i}^{x,y,z} \sum_{j}^{x,y,z} \sum_{k}^{x,y,z}$.

$$P_{SFG}^{(2)} = \epsilon_0 \left(\sum_{i,j,k}^{x,y,z} \chi_{ijk}^{(2)} E_{j,VIS}^{int} E_{k,IR}^{int} + \sum_{i,j,k}^{x,y,z} \chi_{ijkl}^{(3)} E_{j,VIS}^{int} E_{k,IR}^{int} \int_{-\infty}^{0} E_z^{dc} e^{i\Delta k_z z} dz \right) \tag{39a}$$

$$P_{SFG}^{(2)} = \epsilon_0 \left(\sum_{i,j,k}^{x,y,z} \chi_{ijk}^{(2)} E_{j,VIS}^{int} E_{k,IR}^{int} + \sum_{i,j,k}^{x,y,z} \chi_{ijkl}^{(3)} E_{j,VIS}^{int} E_{k,IR}^{int} \int_{-\infty}^{0} \left(-\frac{d}{dz} \Phi(z) \right) e^{i\Delta k_z z} dz \right) \tag{39b}$$

Where, $E_z^{dc} = -\frac{d}{dz}\Phi(z)$. $\Phi(z)$ is the electrostatic potential across at the surface. $\chi_{ijk}^{(2)}$ and $\chi_{ijkl}^{(3)}$ are the resonant second-order and third-order susceptibilities of the material,

respectively. $\frac{1}{\kappa} = \sqrt{\frac{\epsilon_0 \epsilon_r k_B T}{2000 e^2 N_A c}}$ is the Debye screening length (c=concentration of the electrolyte, N_A=Avogadro number, e=unit charge, k_B=Boltzmann constant, T= temperature), E_z^{dc} is the static electric field generated by the interfacial charges and /or net polarized dipoles, and $\Delta k_z = \sqrt{\frac{n_{SFG}^2 - \sin^2(\theta_{SFG})}{\omega_{SFG}}} + \sqrt{\frac{n_{VIS}^2 - \sin^2(\theta_{VIS})}{\omega_{VIS}}} + \sqrt{\frac{n_{IR}^2 - \sin^2(\theta_{IR})}{\omega_{IR}}}$ is the inverse of the coherence length of the SFG process (n_i= the refractive index of light).

Using a functional form $\Phi(z) = \Phi_0 e^{-\kappa z}$, the solution of eq (39b) reads:

$$P_{SFG}^{(2)} = \epsilon_0 \left(\sum_{i,j,k}^{x,y,z} \chi_{ijk}^{(2)} E_{j,VIS}^{int} E_{k,IR}^{int} + \frac{\kappa}{\kappa - i\Delta k_z} \Phi_0 \sum_{i,j,k}^{x,y,z} \chi_{ijkl}^{(3)} E_{j,VIS}^{int} E_{k,IR}^{int} \right) \quad (39c)$$

To a good approximation, the $\chi_{ijk}^{(3)}$-dependent term on the right-hand side can be neglected for interfaces with small interfacial electric potentials, such as water-air interface with a very high ionic concentration (~1M) in the sub-phase. It thus follows that within the *dipole moment approximation* the resonant SFG polarization for these interfaces only depends on $\chi_{ijk}^{(2)}$.

The Quadrupole contribution:

The SFG process is a surface-specific process strictly under the assumption of the electric-dipole approximation, which states that the signals generated by multipoles and magnetic moments are much smaller than that generated by the electrical dipoles. If the quadruple moment contributes[58, 59], SFG is no longer truly surface specific since there is no selection rule for quadrupole moments that can nullify the contributions from the bulk.

Considering quadrupole moment contributions to the SFG response, the effective second-order susceptibility can be written as:

$$\chi^{(2,eff)} = \chi^D + \chi^Q = \chi^{ID} + \chi^B + \chi^{IQB} + \chi^{IQ} \quad (40)$$

Where, $\chi^D = \chi^{ID}$, the interfacial dipole (ID) contribution, is the true dipole contribution in presence of a time-independent electric field across the surface, χ^B is the true bulk (B) contribution that can be determined experimentally, χ^{IQB}, the interfacial bulk quadrupole (IQB) contribution, is a bulk contribution located across the interfacial region, and the χ^{IQ}, the interfacial quadrupole (IQ) contribution, is the quadrupole contribution located only within the surface. The extent of contributions of the last three terms on the right-hand side of the above equation relative to the first can differ at different frequency regions[60] and is still under heavy debate. However, it is generally assumed that the quadrupole contributions for aqueous surfaces are negligibly small compared to the dipole

contributions for the OH(D) stretch vibrations but can contribute significantly in the bend vibration.

The $\chi^{(4)}$ contribution:

The pump-probe SFG spectroscopy, in practice, is *approximated* as a transient change in $\chi^{(2)}$-induced by the pump pulse. On closer observation, it is realized that the pump-induced process is actually a combined $\chi^{(2)}$ and $\chi^{(4)}$-process.

The pump causes a population transfer from the ground vibrational state to the first excited vibrational state. This population transfer is a dual step process: the first step is a creation of coherence between the ground and first excited state as a result of the first interaction with the IR-pump field. The coherence is then converted into a population state by a second interaction with the IR-pump field. The probe IR, that is delayed in time with respect to the pump, again interacts with the unexcited molecules in the ground state and creates a polarization with the first excited vibrational state, that is followed by the anti-stokes type Raman interaction with the VIS. Therefore, the interactions with the IR-probe and VIS are the third and fourth interactions respectively, making the entire process a combined $\chi^{(2)}$ and $\chi^{(4)}$ process, in true sense.

Thus, the combined second and fourth-order process can be represented as:

$$I_{SFG,pump,probe}(t,\tau) \propto \left| \sum_{\substack{i,j,k \\ x,y,z}}^{x,y,z} \chi_{ijk}^{(2)} E_{VIS}(t) E_{IR,probe}(t) + \sum_{i,j,k}^{x,y,z} \chi_{ijk}^{(4)} E_{VIS}(t) E_{IR,probe}(t) E_{IR,pump}(t-\tau) E_{IR,pump}(t-\tau) \right|^2 \tag{41a}$$

$$\begin{aligned} I_{SFG,pump,probe}(t,\tau) &\propto \left| \sum_{i,j,k}^{x,y,z} \chi^{(2)} E_{VIS}(t) E_{IR,probe}(t) \right|^2 \\ &+ \left(\sum_{i,j,k}^{x,y,z} \chi^{(2)} E_{VIS}(t) E_{IR,probe}(t) \right)^* \left(\sum_{i,j,k}^{x,y,z} \chi^{(4)} E_{VIS}(t) E_{IR,probe}(t) E_{IR,pump}(t-\tau) E_{IR,pump}(t-\tau) \right) + cc \\ &+ \left| \sum_{i,j,k}^{x,y,z} \chi^{(4)} E_{VIS}(t) E_{IR,probe}(t) E_{IR,pump}(t-\tau) E_{IR,pump}(t-\tau) \right|^2 \end{aligned} \tag{41b}$$

where, τ represents the time delay(s) between pump and probe pulses and *cc* corresponds to the complex conjugate of the second term on the right-hand side. The pure $\chi^{(4)}$ response (the last term on the right-hand side of the above equation) is small and negligible. Therefore, the cross terms, $\left(\sum_{i,j,k}^{x,y,z} \chi^{(2)} E_{VIS}(t) E_{IR,probe}(t)\right)^* \left(\sum_{i,j,k}^{x,y,z} \chi^{(4)} E_{VIS}(t) E_{IR,probe}(t) E_{IR,pump}(t-\tau) E_{IR,pump}(t-\tau)\right) + cc.$, dictate the time-dependent changes in SFG response. These terms can be considered the transient $\Delta\chi^{(2)}$ process, i.e. effectively; the pump induces a transient change in $\chi^{(2)}$ tensor elements.

Chapter 3

Experimental Methods:

The Laser system:

The laser system has four main parts: the seed laser, the pump laser, the amplifier and the optical parametric amplifier (OPA). The specifications are mentioned below:

Seed Laser:

Type: Titanium: Sapphire (Ti:Sa) oscillator (MaiTai, Spectra Physics)
Center wavelength: 800nm
Average power: >400mW
Bandwidth: 10nm (min),60nm (max)
Pulse width: <25fs
Peak power: >95kW @ 60nm
Repetition rate: 84±2 MHz
Beam diameter: <1.5mm

Pump Laser:

Type: Nd : YLF Laser (Empower-45, Spectra Physics)
Center wavelength: 527nm
Energy per pulse: 28mJ (max) @1kHz
Repetition rate: 1kHz
Polarization: Linear, Horizontal

Amplifier:

Type: Titanium: Sapphire (Ti:Sa) regenerative multi-pass,(Spitfire Ace-35F1k-5.0, Spectra Physics)
Wavelength: 795-805nm
Average power: >5W
Pulse width: <35fs
Repetition rate: 1kHz
Beam diameter: 10mm
Polarization: Linear, Horizontal

OPA:

Model: TOPAS-C (/-Prime)+(N)DFG, Light Conversion

Pumped with: 1-3 mJ
Wavelength: Signal:~1150-1600nm,
Idler:~1600-2700nm
DFG1:~2400-6100nm
Polarization: Signal: Linear, Vertical
Idler: Linear, Horizontal
DFG1: Linear, Horizontal
DFG1 Crystal (Signal + Idler→ IR): $AgGaS_2$, GaSe

The amplifier, pumped with the pump laser, amplifies the seed produced by the seed laser. The output from the amplifier is divided into three parts. One part is sent into OPA to produce IR light. Another part is sent to and transmitted through a Fabry Perot etalon (SLS optics ltd.). The transmitted 800nm light has ~15cm^{-1} bandwidth. The remaining part of the amplifier output is dumped.

Detector:

Type: Spectrometer (Acton Pro2300(i)) + Electron Multiplied Charged Coupled Device (EM-CCD) chip (Newton Andor)

Signals are dispersed by the spectrometer and the image is recorded by the CCD chip.

Specifics of different setups:

Conventional SFG:

TOPAS:
Pumped with: ~1.7mJ
Average power output: ~5 μJ (@ 4000nm)
Average FWHM: 450 cm^{-1}

Incident beam angles (w.r.t. surface normal): VIS: 34 deg, IR: 36deg
Beam diameters: ~0.2mm (both VIS, IR)

The schematics of the setup is given in Fig: 9.

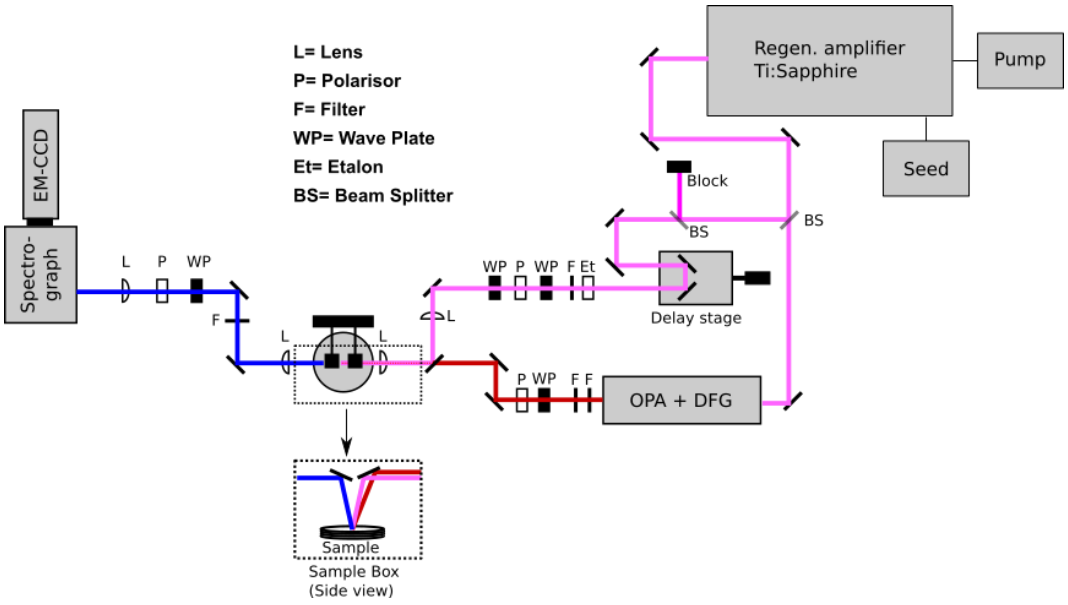

Figure 10: Schematic of conventional SFG setup. Beam paths are shown for VIS (pink), IR (red), and SFG (blue).

Phase-Resolved (**Heterodyne**) **SFG**:

TOPAS:
Pumped with: ~2 mJ
Average power output: ~10 μJ (@ 3000nm)
Average FWHM: 300 cm^{-1}

Incident beam angles (w.r.t. surface normal): VIS: 47 deg, IR: 62 deg
Beam diameters: ~0.2 mm (both VIS, IR)

Local oscillator (LO) generator: y-cut quartz (10 microns thick)
Delay plate: Silica plate (2 mm thick)

The IR and VIS beams are focused onto the y-cut quartz. The transmitted beams are refocused onto the sample surface using a concave mirror. The LO is passed through the delay plate to introduce a time delay relative to that of sample SFG.
The schematics of the setup is given in Fig: 11.

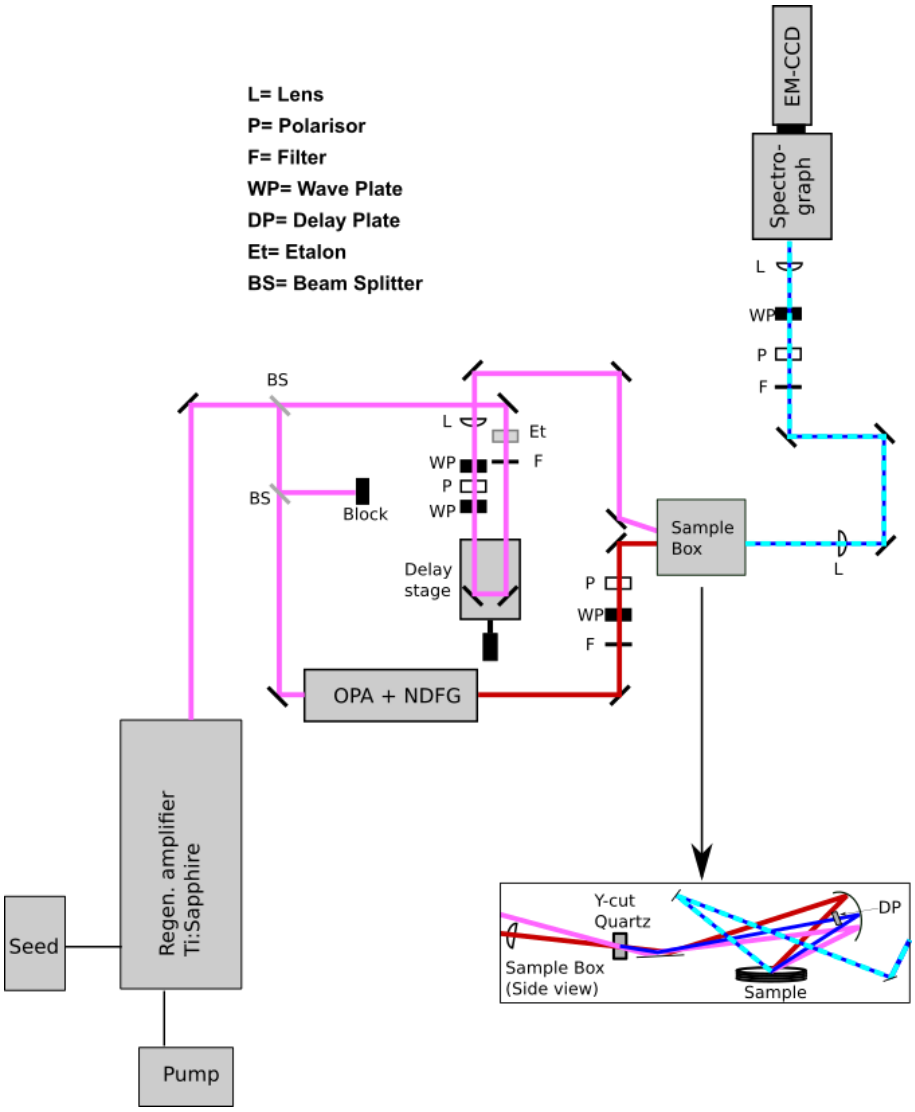

Figure 11: Schematic for phase-resolved SFG set up. Beam paths are shown for VIS (pink), IR (red), and SFG/ LO (blue/cyan).

Time-Resolved (Pump-Probe) Homodyne SFG:

TOPAS 1:
Pumped with: ~3 mJ
Average power output: ~20 μJ (@ 4000 nm)

TOPAS 2:
Pumped with: ~1 mJ
Average (Signal + Idler) output: ~185 μJ (@ Signal=1180nm)
Frequency Doubling (Idler, 2000→1000 nm) crystal: BBO

pump-IR generation crystal: Lithium Niobate (LN)

Average FWHM: IR-probe: ~400 cm^{-1}, IR-pump: ~80 cm^{-1}

Incident beam angles (w.r.t. surface normal): VIS: 70 deg, IR-probe: 40 deg, IR-pump: 55 deg

The laser system for this case is comparable to that described in earlier two cases. However, in this set up two pump lasers are used to generate ~10W output power from the amplifier as higher energy is required for pump-probe experiments.

The output from TOPAS 1 is used as a broadband probe pulse. The Idler from TOPAS 2 is first frequency-doubled and then mixed with a part of 800 nm to produce narrowband IR-pump pulse through an optical parametric amplification process.

Both IR-probe and IR-pump pulses have a 1kHz repetition rate in the beginning. In order to achieve a pair of SFG signals in the presence and absence of pump next to one another, every second pump pulse is blocked with an automated mechanical chopper after the generation of the pump pulse. Therefore, at the sample, the pump pulse has a 500 Hz repetition rate, but the probe has a 1kHz repetition rate. This mechanical chopper is synchronized with the amplifier output generation.

Both IR-pump and IR-probe pulses are guided through two automated delay stages that are used to change the time delays with respect to the VIS pulse at the sample. For the IR-probe, the delay is used to find the optimum SFG signal and then kept constant during the experiment. For IR-pump, the delay stage is used to change time delays during a time-resolved experiment.

Planoconvex lenses of focal lengths 5 cm and 15 cm are used to focus the IR-pump and probe pulses onto the sample, respectively, while an antireflection-coated planoconvex 40cm lens is used to focus the 800nm beam.

A 30 cm plano-convex lens collimates the SFG beam from the surface, and a 20 cm cylindrical lens subsequently focuses the signal vertically. The vertically focused beam is then guided through a vibrating mirror (Galvano) onto another cylindrical lens of focal length 5 cm that horizontally focuses the beam onto the spectrometer.

In a pump-probe experiment, consecutive SFG responses are recorded under pump-on and pump-off conditions. The SFG responses in the presence of pump are further spatially separated from the ones in the absence of pump before reaching the spectrometer using the Galvano-mirror that vibrates at 500 Hz synchronously with the laser and the mechanical chopper. All the automated delay stages are controlled, and data are acquired by Labview controlled software. The schematics of the time-resolved setup is shown in figure 12:

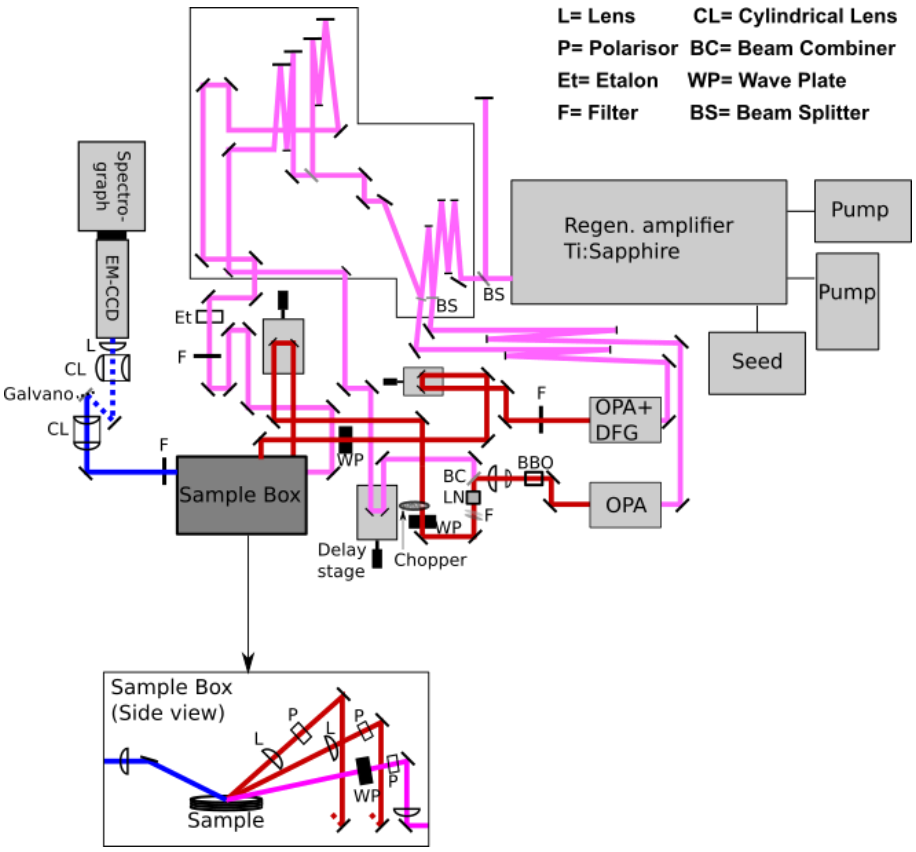

Figure 12: Schematics of time-resolved SFG setup. Beam paths are shown for VIS (pink), $IR_{pump\ and\ probe}$ (red), and SFG (blue).

The sample stages to probe solid-air and liquid-air interfaces are specifically designed to adjust sample height and tilt. For the time-resolved experiments, the trough of the sample is further rotated and cooled. The solvent is added drop-wise with a syringe to compensate for the change in the height of the liquid sample due to evaporation over time.

** In all of the above setups, there are three types of filters used: the one after the OPA is generally a long-pass filter used to block the residual 'signal+idler' from the OPA. The filter in front of the etalon is generally a band-pass filter used to transmit only the narrowband VIS centered at 800 nm and block all other additional fringes produced in the etalon during the narrowing process. The filter in the detection pathway is also generally a band-pass filter to transmit only the SFG response and block the reflected 800nm and/or any additional stray/scattered light from the sample.

Chapter 4

The surface affinity of cations depends on both the cations and the nature of the surface

Reproduced with some minor changes from "Das, S.; Bonn, M.; Backus, E. H. G. The surface affinity of cations depends both on the cations and the nature of the surface; J. Chem. Phys. 2018, 150, 044706". with the permission of AIP Publishing.

Abstract:

Specific ion effects at interfaces are important for a variety of thermodynamic properties of electrolyte solutions, like surface tension and the phase behavior of surfactants. We report the relative surface affinity of Na^+ and D_3O^+ at both the D_2O-air and the sodium dodecyl sulfate (surfactant)-covered D_2O surface by studying the alignment of interfacial D_2O, using Vibrational Sum Frequency Generation spectroscopy. The surface propensity of ions is found to be a function of both the nature of the ion and the nature of the surface. Specifically, for the charged, surfactant-covered interface, Na^+ has a higher affinity than D_3O^+. In contrast, D_3O^+ has a higher affinity than Na^+ at the air-D_2O interface. The relative surface affinity of cations thus depends on both details of the cation and the type of interface.

Introduction:

Ion specificity is important in various biochemical processes that frequently occur at the interface of water and lipid membranes of surfactants such as counter-ion dictated adsorption of surfactants at air-solution interfaces[61]. It is proposed that at water-air interface covered with charged organic monolayers coulomb interaction dictates the specific ion adsorption[35, 62]. On the contrary, properties such as ion polarizability[63], ion size[64], dispersion forces and hydration energy[65] have been proposed to be dictating the ion adsorption at neat water-air interface. It is indeed possible that different factors dominate specific ion adsorption at different interfaces. However, though water is an integral part of aqueous interfaces, the role of water itself in determining ion specificity in presence and absence of charged organic monolayers is not well understood. Therefore, it is important to understand the ion-specific effects on interfacial water organization in the presence of different types of ions and surfactants.

Surfactants are typically amphiphilic, owing to their characteristic nonpolar alkyl chains and polar head groups. They can adsorb at both polar (aqueous) and non-polar interfaces. At and beyond their critical micelle concentration (CMC), surfactants form a closely packed monolayer at the interface of water with air. The polar head groups directly interact with the water molecules and reduce the surface tension of water.

Due to this adsorption ability, surfactants are widely used in various industrial and biological applications, often in combination with salts and acids. The combination of surfactants and ions is also ubiquitous in the environment. In seawater, for instance, surfactants further interact with other chemicals and affect various physiochemical properties such as surface adsorption of these chemicals[66]. Amongst different surfactants, those with charged head groups are abundant and interact strongly with water and aqueous electrolyte solutions[67, 68]. Surface tension, radiochemical studies and simulations indicate that the counter-ions compete for surface adsorption at the water surface covered with charged surfactants[35, 62, 69]. In mixtures of monovalent cations, cations with smaller hydrated radius (i.e. higher charge density) tend to replace those with larger hydrated radius. Studies on charged lipid-covered aqueous interfaces have shown that the counter-ion concentration next to the lipid monolayer is much higher than in the subphase[70], as predicted by the Gouy-Chapman model[71]. The counter-ions screen the charge of the head groups and thereby

influence the way interfacial water molecules align and interact with the surfactant/lipid head groups.

The resulting properties of such charged lipid/surfactant covered interface thus depend on the interplay of the surface charge, the presence of the counter-ions and the water molecules[33]. While this general understanding of charged interfaces exists, the details of how the structure of such charged surfaces depends on the type and concentration of counter-ions in solution are a priori unknown. Somewhat remarkably, to our best knowledge, the effect of protons on alignment of water at such interface has not been reported, to date. This is surprising, considering the ubiquity of protons and their importance for countless physiochemical phenomena including protein (un-)folding and ion and charge transport through biological cell membranes.

To study the effect of protons on the alignment of water at a surfactant-covered aqueous surface, we have investigated a monolayer of Sodium dodecyl sulfate (SDS, R-O-SO_3^-) on a D_2O subphase containing excess D_3O^+. We have compared the results to those obtained from a subphase containing Na^+ and to the results from the same subphases without surfactant, i.e. at the D_2O-air interface. As shown in Figure 1A, SDS has a negatively charged head-group and Na^+ as counter-ion. It is a widely used component in, for example, shampoo, detergents, and toothpaste. As such, aqueous solutions of SDS containing various electrolytes are abundant in the environment. MD simulations[72] have shown that for an SDS-covered water surface, SDS-head groups are hydrated and a significant population of Na^+ is present within these hydration shells. These Na^+ bridge different surfactant head groups and thereby stabilize the self-assembled monolayer (SAM). As mentioned above, here, we compare the interaction of D_3O^+ and Na^+ with SDS. We determine the surface affinity of both ions by measuring the extent of water alignment, i.e., the extent of non-centrosymmetric organization of water, by vibrational Sum Frequency Generation (SFG).

SFG has been widely used to study the behavior of water in contact with surfactant and lipid monolayers[34, 73-75] and the bare water-air interface of aqueous electrolyte solutions[11, 12, 76]. In SFG spectroscopy, a broadband IR pulse, spatiotemporally overlapped with a narrowband 800 nm pulse, impinges the sample. When the IR light is resonant with a molecular vibration, the SFG response is enhanced, resulting in a strong sum frequency signal. Centrosymmetric media like bulk water have zero SFG response, owing to the selection rules of the method. At the interface, however, the centrosymmetry is broken, resulting in an SFG signal from the interfacial water. This preferential

alignment of water molecules is higher in the presence of charges at the surface like a monolayer of ionic surfactants. As a first order approximation, a more highly charged surface results in more aligned water molecules, giving rise to a higher SFG signal. At such surfactant-covered water surface, counterions present in the subphase can screen the charge and reduce the SFG intensity. Thus by monitoring the SFG intensity as function of the concentration of excess charges, we can quantify the relative surface affinity of Na^+ and D_3O^+. Please note that the correlation between the degree of water alignment and SFG signal intensity breaks down at low ionic strength[77, 78].

We find that at the SDS covered aqueous interface, the relative interfacial affinity of Na^+ is higher than that of D_3O^+. At the bare water-air interface, the affinity order is opposite. The relative surface affinity of counter-ions is thus interface dependent. Moreover, the order of the alkyl chain of the SDS-SAM is lower in the presence of D_3O^+ than in the presence of Na^+ indicating that the order of the SAM also depends on the type and concentration of counter-ion present.

Results and Discussions:

Figure 1A shows the SFG intensity as a function of infrared frequency, recorded from the surface of a 12 mM SDS solution in D_2O without any excess ion and with co-containing Na^+ and D_3O^+ at different concentration ratios with a total cation concentration of 0.1M. The pink curve shows the SFG intensity in absence of any excess ions, the red and the dark green in presence of 0.1M D_3O^+ and Na^+ respectively. The other three curves are responses in presence of co-existing Na^+ and D_3O^+, where the total cation concentration is fixed at 0.1M. Each spectrum has a broad response that extends from ~2100 cm^{-1} to ~2700 cm^{-1} and three narrower responses between ~2800 cm^{-1} and ~3000 cm^{-1}. The broad feature is the vibrational response of the O-D groups located near the monolayer of SDS. As discussed in detail in reference[34], there are two sub-ensembles of OD groups at this interface which vibrate at ~2390 cm^{-1} and ~2510 cm^{-1}. The OD groups that vibrate at ~2510 cm^{-1} are hydrogen bonded to the head groups of SDS ($R\text{-}O\text{-}SO_3^-$) and the ones that vibrate at ~2390 cm^{-1} are not directly in contact with $-O\text{-}SO_3^-$ groups, yet aligned under the influence of their electric field. The relatively sharp peaks at ~2846 cm^{-1}, ~2870 cm^{-1}, and ~2910-2980 cm^{-1} are different C-H vibrations of the alkyl chain of SDS.

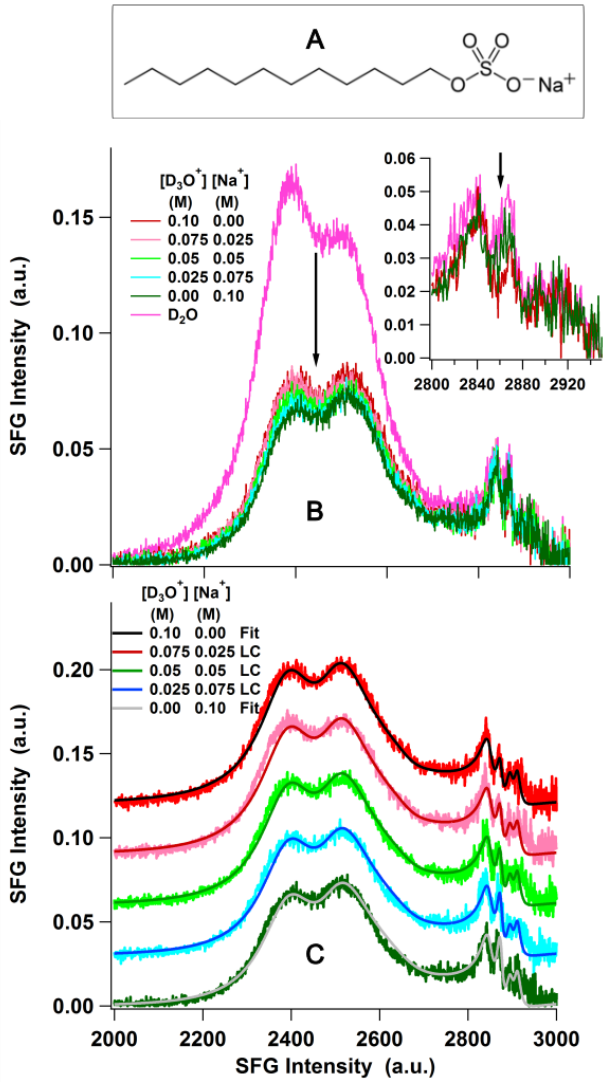

Figure 13: (A) the chemical structure of sodium dodecyl sulfate (SDS). (B) SFG spectra in SSP polarization of an SDS-SAM on pure D_2O (pink) and at different deuteron to sodium concentration ratios. The total concentration of cations is 0.1M in all cases. (C) A comparison of original experimental spectra with the square of the weighted linear combinations of the $\chi^{(2)}$ responses of solutions containing $[Na^+] = [D_3O^+] = 0.1$ M. The colors for experimental spectra in panel (B) and (C) are same and represented only in panel (B). The legends in panel (C) represents the colors of the fits and reconstructed spectra. The inset in panel (B) shows the zoom-in of the CH stretch region, where a marked decrease in the symmetric CH_3 intensity (highlighted by the arrow) is observed in the presence of D_3O^+.

The SFG intensity in presence of both 0.1M D_3O^+ and Na^+ is significantly lower in the OD stretch region than in absence of any excess ions in the solution. As predicted by the Gouy-Chapman model[71] and shown by simulations[72], the Na^+ concentration near the charged monolayer head groups is extremely high even in absence of any excess ion in the solution. Addition of excess Na^+ enhances the counter-ion concentration near the surface resulting in an increased charge screening

and a concomitant reduction of the aligned water (D_2O) molecules, thus reducing the SFG intensity. The SFG intensity along the OD stretch region gradually increases with increasing D_3O^+ to Na^+ bulk concentration ratio. It indicates that the preferential alignment of D_2O molecules near the charged head groups increases with replacement of Na^+ by D_3O^+. This, in turn, indicates that the concentration of cations at the SDS –D_2O interface decreases with increasing relative bulk concentration of D_3O^+. D_3O^+ apparently adsorbs slightly less than Na^+ at the interface.

This observation can be explained by considering the ion radii of the cations and the implicit size restrictions imposed by the finite dimension of the electrical double layer (EDL) near the charged interface. Previous works have already pointed out that smaller univalent cations are preferred within the EDL[35, 62, 69]. A larger number of smaller ions can remain within a constrained volume causing a better charge neutralization , thereby lowering the Gibbs free energy. Following this argument, our results thus indicate that D_3O^+ should have a larger ion radius than Na^+. X-ray and neutron diffraction studies indeed support that notion. The inter-nuclear distance between the central oxygen atom of H_3O^+ and the oxygen atom of its nearest neighbor is ~0.252 nm in HCl solution. For DCl it is even larger: ~0.288 nm. For sodium however, both simulations and diffraction methods consistently report that the nuclear distance between sodium ion and the nucleus of oxygen of nearest H_2O is ~0.235 nm[79].

Since these SFG responses arise from D_2O molecules strongly aligned due to the electrostatic field of the SDS head groups, they possibly involve both pure $\chi^{(2)}$ and $\chi^{(3)}$ driven responses[74, 77, 78, 80]. In the present work, we focus on the relative changes in the intensities in the presence of D_3O^+ and Na^+. Therefore, we treat these intensities as an effective $\chi^{(2)}$ response and we make no distinction between relative contributions of $\chi^{(2)}$ and $\chi^{(3)}$. The Debye length decreases from 1 micron in SDS covered pure D_2O surface to 1 nm in SDS covered D_2O containing 0.1 M D_3O^+ and/or Na^+ (see details in supplementary information). Possibly the SFG response from the pure D_2O case is a combined pure $\chi^{(2)}$ and $\chi^{(3)}$ response, while the SFG response in presence of 0.1M excess ion is dominated by the $\chi^{(2)}$ contribution.

Not only the preferential organization of interfacial D_2O, but the organization of the monolayer too seems to be different for D_3O^+ and Na^+. The CH stretch modes, simultaneously measured in the experiments, provide information about the alkyl chain conformation. In particular, the ratio of

intensities of the CH_2 and CH_3 symmetric stretch modes are known to serve as an order parameter of the alkyl chain.

The presence of 0.1M Na^+ does not affect the SDS conformation: The addition of 0.1M Na^+ changes the water response substantially, but not the intensities of both the CH_2 symmetric stretch (2846 cm^{-1}) and the CH_3 symmetric stretch (2870 cm^{-1}) modes of the SDS monolayer (see inset in figure 1A). In contrast, the presence of 0.1M D_3O^+ causes a ~50% reduction in the CH_3 symmetric stretch intensity. Since the SDS concentration (12 mM) is for al Na^+ and D_3O^+ concentrations studied here above the cmc of SDS, it is unlikely that the surface coverage changes significantly. The reduction in the CH vibration responses, therefore, indicates that the presence of D_3O^+ causes a disordering of the SAM alkyl chain.

The Na^+ concentration next to the SAM head groups is very high, due to the Coulomb interactions, even in absence of any excess ions in the solution[71]. In the presence of 0.1 M excess Na^+ in the sub-phase, the order of SAM alkyl chains hardly differs from that of neat D_2O. On the contrary, in the presence of 0.1 M D_3O^+, the SAM is disordered compared to that of neat D_2O, indicating that the directional characters of hydrogen bonding between the head groups and the counter-ions, in addition to the Coulomb interaction, apparently is important in determining the order of the SAM. The two cations are geometrically very different: D_3O^+ has a "tripod" structure[81], as opposed to the spherical shape of Na^+. As a result, the ability of those two cations to act as bridges between different head groups is undoubtedly different. Secondly, although, the pKa of SDS in bulk-H_2O is -1.5, the surface pKa is expected to be ~ 0, based on reports regarding similar systems[70, 82]. Therefore, at bulk D_3O^+ concentration of 0.1M i.e. pH=1, ~10% of the SDS molecules should be protonated. The protonation of SDS molecules reduces the repulsion amongst the head groups, which is also expected to affect alkyl chain arrangement. Nevertheless, the effects of the presence of 0.1M D_3O^+ in the subphase on the preferential alignment of D_2O molecules and the alkyl chains of the SAM at the interface are slightly different than in the presence of 0.1M Na^+. The D_2O molecules are preferentially more aligned but the alkyl chains are preferentially less aligned in presence of 0.1M D_3O^+ compared to that of 0.1M Na^+. Both effects occur simultaneously.

Evidently, Na^+ and D_3O^+ perturb the noncentro-symmetric order of interfacial D_2O and packing order of SDS-SAM to a different extent. An interesting question, therefore, is whether all these effects are (non-)additive when more than one type of cation coexist in the solution? If the effects

are additive with respect to their bulk concentrations then the intensity from a solution, containing a mixture of cations should be equal to the square of the linear combinations of the $\chi^{(2)}$ response from the solution containing only one or the other cation. If the effects are additive with respect to their surface concentrations requires precise knowledge of their surface concentration which is not known.

Since calculating mixtures of the spectra as a linear combination of the response of the pure solutions requires knowledge of the $\chi^{(2)}$, we have quantitatively analyzed the data by fitting with an established procedure. According to this procedure, the SFG signal is proportional to the square of the second-order nonlinear susceptibility $\chi^{(2)}$ of the sample and intensity of both incoming IR and Visible (VIS) light,

$$I_{SFG} \propto \left|\chi^{(2)}\right|^2 I_{VIS} I_{IR} \qquad (1)$$

The second order nonlinear susceptibility $\chi^{(2)}$ is a sum of a non-resonant contribution $\chi_{NR}^{(2)}$ (consisting of an amplitude A_{NR} and a phase ϕ_{NR}) and resonant contribution(s) $\chi_R^{(2)}$. Each $\chi_R^{(2)}$ is expressed in terms of a Lorentzian line-shape with area A_n, central frequency ω_n and bandwidth Γ_n (half width at half maximum):

$$\left|\chi^{(2)}\right|^2 = \left|\chi_{NR}^{(2)} + \chi_R^{(2)}\right|^2 = \left|A_{NR} e^{i\phi_n} + \frac{A_n}{\omega_n - \omega_{IR} + i\Gamma_n}\right|^2 \qquad (2)$$

The spectra recorded for the SDS-covered pure aqueous Na^+ and D_3O^+ solutions are fitted with eight resonant peaks (See Table 1 in the SI for assignment details). The bandwidths and peak positions of all the bands, as well as the non-resonant area and phase from this fit are subsequently interpolated to describe the intermediate spectra.

Panel (C) shows that the three spectra for co-existing Na^+ and D_3O^+ can be described very well by the square of the linear combinations of the $\chi^{(2)}$ response (see SI) from pure Na^+ and pure D_3O^+, implying that the effect is simply additive.

The observation that Na^+ has higher surface affinity at the SDS-water interface is in contrast with the conclusion drawn for the electrolyte-air interface, for which, at very high concentrations (~1M), H_3O^+ has been found[12, 83-85] to have higher interfacial affinity than Na^+. Here, we have monitored the modulation of interfacial D_2O alignment at the air- D_2O interface as a function of bulk D_3O^+

and Na^+ concentration ratio at 1M constant ionic strength using vibrational SFG spectroscopy. Unlike the SDS case presented above, the alignment of interfacial D_2O at the air-water interface is enhanced by the presence of ions, and the enhancement of the SFG intensity is a measure of the surface affinity of an ion. By systematically changing the Na^+ and D_3O^+ ion concentration ratio, and quantitatively monitoring the change in the SFG intensity change, we have studied not only the relative surface affinity of the two ions but also the gradual evolution of interfacial water alignment under the influence of the relative concentration ratio of these two ions.

Figure 2(A) shows the SFG responses in SSP polarization at the D_2O-air interface, for pure D_2O and in co-presence of Na^+ and D_3O^+ at different concentration ratios at 1M total ionic strength. As opposed to the SDS case, higher ionic concentration at the air-D_2O interface enhances the preferential D_2O alignment. To ensure an optimum signal to noise ratio, we have chosen here a 1M ionic strength.

Each spectrum consists of two main features: a sharp peak centered at ~2700 cm^{-1} and a relatively broad feature that extends between ~2000 cm^{-1} and ~2600 cm^{-1}. The sharp peak at ~2700 cm^{-1} originates from the non-hydrogen bonded O-D oscillator which points away from the surface into the air. The broad feature extending between 2000 and 2600 cm^{-1} originates from OD groups with a broadly distributed H-bond strength. Intra- and inter-molecular coupling among different OD vibrations causes the double-peak feature[86].

The SFG intensity hardly changes when adding 1M Na^+ to D_2O, meaning the alignment of interfacial D_2O molecules in the presence of 1M Na^+ is almost identical to that of pure D_2O: Na^+ has no or very weak surface affinity towards the D_2O-air interface, as, apparently, does Cl^-. In contrast, with increasing fraction of D_3O^+, the intensity around ~2000-2600 cm^{-1} increases and that around 2700 cm^{-1} decreases. The D_3O^+ ions add charges to the D_2O-air interface, increasing the alignment of interfacial water. Since D_3O^+ has a "tripod" structure and can make three strong hydrogen bonds with neighboring D_2O molecules, the preferential alignment of interfacial D_2O molecules with their D atoms pointing towards bulk increases with increasing bulk D_3O^+ concentration, thus resulting in an enhanced SFG intensity around ~2000-2600 cm^{-1} region. The reduction in intensity of dangling OD peak can be a result of a real reduction in vibrational amplitude and/or a change in its angular distribution with respect to the surface normal. More studies to comment conclusively on these observations are ongoing. In any case, we find that, at

the D_2O-air interface, D_3O^+ indeed is more surface active than Na^+ at 1M concentration, in agreement with the previous reports[8, 87].

Although for pure D_2O, $\chi^{(3)}$ does not contribute significantly to the SFG response, D_2O containing ions certainly can[57, 88, 89]. The increase in the SFG response in figure 2(A) is, therefore, possibly caused by simultaneous changes in pure $\chi^{(2)}$ along with changes in $\chi^{(3)}$ driven responses. In this study we are interested only in relative changes in the total SFG intensity, and we therefore consider the combined effects as changes in an effective $\chi^{(2)}$ response.

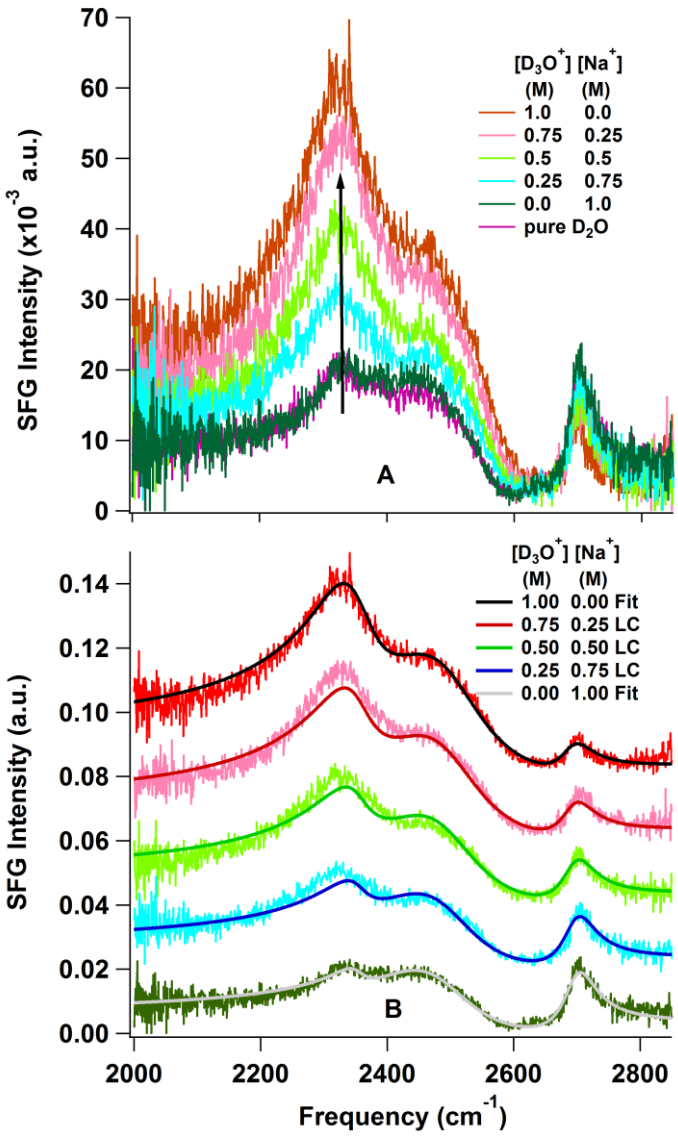

Figure 14: (A) SFG spectra in SSP polarization of the D_2O-air interface for different sodium to deuterium concentration ratios. The total concentration of cations is 1M in all cases. (B) A comparison of original experimental spectra with the square of the weighted linear combinations of the $\chi^{(2)}$ responses of solutions containing $[Na^+] = [D_3O^+] = 1$ M. The colors for the experimental spectra in panel (A) and (B) are the same and represented only in panel (A). The legend in panel (B) represents the colors of the fits and reconstructed spectra.

Panel (B) shows the experimental SFG spectra in the presence of 1M Na^+ and D_3O^+ along with the fitted spectra (Details of the fits are given in the SI). Panel (B) also shows the experimental SFG spectra in co-presence of Na^+ and D_3O^+ along with the corresponding squared $\chi^{(2)}$ spectra constructed with linear combinations of the $\chi^{(2)}$ response of 1M D_3O^+ and Na^+ solutions obtained

by fitting. The linear combinations (see Fig. 2) significantly differ from the experimental spectra specifically around 2350 cm^{-1}, meaning the effects are not additive, unlike in the case of SDS. It qualitatively proves that apparently, the surface concentration of adsorbed D_3O^+ does not increase linearly with its bulk concentration.

Conclusion:

In summary, we have reported the relative interfacial affinity of two ubiquitous cations, Na^+ and D_3O^+ (equivalent to H_3O^+ in H_2O) and their effects on interfacial water organization at both the water-air and the surfactant-covered aqueous solution interface using SFG spectroscopy. Due to ionized head groups ($-O-SO_3^-$) of SDS, the interface is negatively charged. Both cations screens this surface charge, yet the screening ability depends slightly on the charge and radius of the cation. The surface propensity of Na^+ is marginally higher than that of D_3O^+. Moreover, the order of the alkyl chain of SDS also depends on the type of ions in the solution: D_3O^+ makes the alkyl chains more disordered than Na^+. Also these two effects are additive with respect to the co-existence of the two ions.

Conversely, at the nominally neutral air-aqueous solution interface, D_3O^+ not only has higher surface propensity than Na^+, the degree of surface propensity and thereby the ability to perturb the interfacial D_2O structure is much higher than that of Na^+. As such, the surface propensity of Na^+ and D_3O^+ at the SDS-covered water surface is opposite to that at the air-water interface. However, the surface propensity and the ability to perturb the interfacial D_2O alignment is significantly non-additive with respect to co-existence of the two cations. Apparently, the surface adsorption of D_3O^+ is not linearly related with its bulk concentration at the air-D_2O interface. The ion-specific effect is larger for the nominally neutral air-water interface than for the charged SDS-D_2O interface, where screening of that charge is, to a first approximation, independent of details of the cation.

Acknowledgements:

The authors thank M. Knecht for purifying the SDS samples, M. Deiseroth, C. Bernhard, S. Pezzotti, D.R. Galimberti, M-P. Gaigeot, M. Grechko, and J. Hunger for fruitful discussions. This work is funded by a DFG grant (BA 5008/3).

Supplementary Information:

The surface affinity of cations depends on both the cations and the nature of the surface

Experimental Details:

Setup:

The experimental setup consists of a mode locked Ti:sapphire laser (Mai Tai SP, Spectra-Physics) and a regenerative amplifier (Spitfire Ace, Spectra-Physics) pumped by a Nd:YLF laser (Empower 45, Spectra-Physics). The amplifiers delivers 800 nm pulses with a power of 4.5 mJ, a pulse width of ~45 fs, and a 1 kHz repetition rate. ~1.7 mJ from its output is used to pump a commercial OPA (TOPAS-C, Light conversion) to produce tunable broadband IR pulses by mixing signal and idler in a $AgGaS_2$ crystal. The ~5 μJ IR pulses are centred around ~2500 cm^{-1} and have a FWHM of ~450 cm^{-1}. Another part of the amplifier output is spectrally narrowed to ~15 cm^{-1} (FWHM) using a Fabry-Perot etalon (SLS optics ltd.). The output energy is ~20 μJ. Both beams are focused onto the sample with beam diameters of ~0.2mm. The polarization is controlled by half wave plates and polarizers. The signal is collected by a spectrograph (Acton, Princeton Instruments) and detected with an electron multiplied charge coupled device (emCCD) camera (Newton, Andor instruments). The acquisition time is typically between 2 and 10 minutes, depending on the signal strength.

All spectra in the presented work are collected in SSP polarization (S: SFG, S: Vis, P: IR) and at incident angles of 34 degrees and 36 degrees for the VIS and IR, respectively. The data are normalized by the non-resonant signal from z-cut quartz.

Materials:

Since SDS is known to degrade to dodecanol, it was purified as described in literature[90]. Subsequently, a 12 mM solution of SDS was prepared in D_2O (pure or containing electrolytes) by

directly dissolving the purified SDS. The electrolyte solutions were made by dissolving HCl (37%) and/or NaCl in D_2O. H^+ instantly reacts with D_2O to produce D^+. Since 37% HCl has a concentration of 12 M (in H_2O), 1 M and 0.1 M HCl in D_2O will have 10% and 1% H_2O respectively in it.

Fitting parameters:

SDS – D_2O interface:

Table 1: ***Assignment of the different vibrations with their corresponding peak positions and bandwidths (used in the fitting procedure). The phase (0) of the non-resonant signal is constant. The assignments follow literature[91-93].***

Vibration	ω (cm^{-1})		2Γ (cm^{-1})		A	
	SDS-0.1M Na^+	SDS-0.1M D_3O^+	SDS-0.1M Na^+	SDS-0.1M D_3O^+	SDS-0.1M Na^+	SDS-0.1M D_3O^+
$OD_{stretch}$	2395	2395	155	155	15.5	16.6
$OD_{stretch}$	2505	2505	155	155	13	14.5
$OD_{stretch}$, Above surfactant head groups	2660	2660	150	100	-2	-1
CH_2-SS (d^+)	2850	2850	30	30	-1.6	-1.6
CH_3-SS (r^+)	2874	2874	15	15	-1	-0.7
CH_2-FR (d_{FR}^+)	2896	2896	18	18	-0.7	-0.7
CH_3-FR (r_{FR}^+)	2912	2912	18	18	-1.1	-1.1
Non-Resonant					-0.03	-0.01

Air – D_2O interface:

Table 2: ***Assignment of the different vibrations with their corresponding peak positions and bandwidths (used in the fitting procedure). The phase (3.14) of the non-resonant signal is constant.***

Vibration	ω (cm^{-1})		2Γ (cm^{-1})		A	
	1M Na^+	1M D_3O^+	1M Na^+	1M D_3O^+	1M Na^+	1M D_3O^+
Bonded $OD_{stretch}$	2355	2355	68	128	-0.9	-6.7
Bonded $OD_{stretch}$	2484	2496	204	214	-12.5	-17.2
Free $OD_{stretch}$	2697	2689	60	47	4.7	3.3
Non-Resonant					0.07	0.10

Linear combination:

The linear combinations for the spectra for coexisting Na^+ and D_3O^+ have been calculated using following equation:

$$I_{SFG} = \left| f_{Na^+} * \chi^{(2)}_{fit_{Na^+}} + f_{D_3O^+} * \chi^{(2)}_{fit_{D_3O^+}} \right|^2$$

Where, f_{x^+}=fraction of x^+ in solution, $\chi^{(2)}_{fit_{x^+}}$ =Susceptibility values obtained from fitting the spectra containing only x^+.

The SFG spectra obtained through linear combinations are shown in the main text in figure 1 and 2 as solid lines.

Debye length and surface charge density:

Area per SDS molecule[94]= 0.44 nm^2
Trough area used in the experiment = 50 mm^2
Number of SDS molecules at the surface= $1.14*10^{14}$
Charge density at the surface= $(1.14*10^{14} * 1.6*10^{-19}$ C)/50mm^2 = 0.36C/m^2

Debye length[71]= $\kappa^{-1} = \sqrt{\frac{\epsilon_0 \epsilon k_B T}{2*10^3 N_A e^2 I}} = 0.304 * \frac{10^{-9}}{\sqrt{M}}$

Ionic strength (I) /M	Debye Length (κ^{-1}) /nm
0 (pure water)	960
0.1	0.96

Chapter 5

The surface activity of the hydrated proton is substantially higher than that of hydroxide.

Reproduced with some minor changes from "Das, S.; Bonn, M.; Backus, E. H. G. The surface activity of the hydrated proton is substantially higher than that of hydroxide; Angew. Chem. Int. Ed. 10.1002/anie.201908420".

Abstract:

The behaviour of hydroxide and hydrated protons, the auto-ionization products of water, at surfaces is important for a wide range of applications and disciplines. However, it is unknown at which bulk concentration these ions start to become surface active at the water-air interface. Here, we report changes in the D_2O-air interface in the presence of excess D^+_{hyd}/OD^-_{hyd} determined using surface-sensitive vibrational Sum Frequency Generation spectroscopy. The onset of the perturbation of the D_2O surface occurs at a bulk concentration as low as 2.7±0.2 mM D^+_{hyd}. In contrast, a concentration of several 100s mM OD^-_{hyd} is required to change the D_2O surface. The hydrated proton is thus orders of magnitude more surface-active than hydroxide at the water-air interface.

Introduction:

The auto-ionization of water)$H_2O \rightleftharpoons H^+_{hyd}+OH^-_{hyd}$) produces hydrated protons and hydroxide ions. Their relative concentrations depend on the pH of the medium. The likelihood of surface adsorption of either of those two ions is yet to be accurately determined[95]. As overviewed recently[95], both from an experimental and theoretical point of view contradictory results have been obtained regarding the surface affinity of both ions. Part of this inconsistency may originate from comparing results from different methods that have unequal probing depths at the aqueous surface.

However, also different results are reported by using the non-linear, surface-specific optical spectroscopies, second harmonic generation (SHG) and sum-frequency generation (SFG). These methods have been used to extract molecular-level information from these interfaces. Symmetry breaking at the water surface results in an SHG/SFG response from interfacial water molecules. The presence of ions adsorbed at the surface affects the interfacial arrangement of water molecules and subsequently enhance or reduce the SFG intensity. SHG studies of the strongly acidic and basic solution conclude surface adsorption of the hydrated proton and surface depletion of hydroxide, respectively [8, 96]. However, a previous phase-resolved SFG study of highly concentrated (>1M) hydrated proton and hydroxide solutions showed that for high concentrations, both ions are surface-active[11]. Moreover, conventional SFG intensity studies on concentrated acid[9, 12, 13] and base[9] solutions (≥0.55 M) also established surface adsorption of hydrated protons and hydroxide. In contrast, a very recent study, combining SFG with molecular dynamics, found no adsorption of either H^+_{hyd} or OH^-_{hyd} at an air-water interface over a range of pH=2-11[14]. Combined, these studies indicate that hydrated protons adsorb at the water-air interface. However, it is not apparent at which bulk concentration the surface adsorption of the hydrated proton starts to influence the nonlinear response. Less seems to be known about the surface propensity of hydroxide.

Here we use SFG spectroscopy to study the modulation in the vibrations of the interfacial D_2O molecules at the D_2O-air interface, in the presence of D^+_{hyd}/OD^-_{hyd} ions for different concentrations in the subphase. We note that the hydrated proton can exist in various conformations including hydronium (D_3O^+), Eigen ($D_5O_2^+$), and Zundel ($D_9O_4^+$). Here, we represent all those moieties as $D^+_{hyd.}$ We find that both D^+_{hyd} and OD^-_{hyd} perturb interfacial water at the water-air interface. However, D^+_{hyd} affects the water surface already at a few mM bulk concentration, whereas for OD^-_{hyd} the surface remains unperturbed beyond 100 mM concentration. The surface adsorption of OD^-_{hyd} becomes prominent at a bulk concentration that is two orders of magnitude higher than that of D^+_{hyd}.

Results and Discussions:

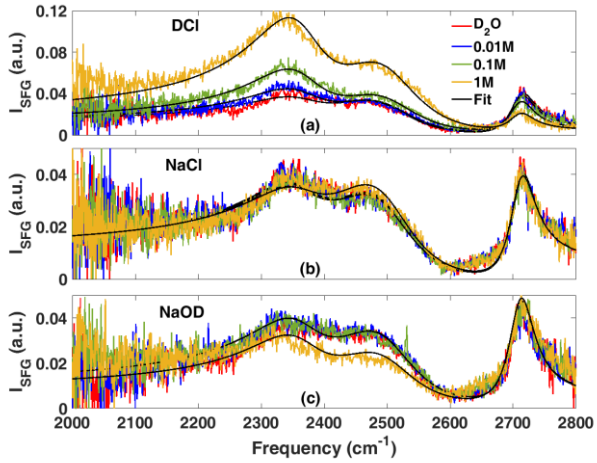

Figure 1 *SFG spectra in SSP polarization from the D_2O-air interface at different bulk concentrations of (a) DCl, (b) NaCl, and (c) NaOD. The red spectrum is a pure D_2O spectrum. The black lines on each experimental spectrum are the fits with a Lorentzian lineshape model (details in the text).*

Figure 1 shows the SFG intensity (I_{SFG}), from the D_2O-air interface with different concentrations of)a(DCl,)b(NaCl, and)c(NaOD in the subphase as a function of the infrared frequency in SSP polarization (S: SFG, S: VIS, P: IR). Each spectrum has a broad response from ~2000 cm^{-1} to ~2600 cm^{-1} due to hydrogen-bonded D_2O molecules at the D_2O-air interface[86] and a sharp response centered at ~2700 cm^{-1} from the vibration of OD groups 'dangling' in the air[97, 98]. With increasing acid concentration)Fig 1)a((, I_{SFG} in the hydrogen-bonded region increases, and that of the dangling OD groups decreases implying interfacial adsorption of hydrated protons: free OD groups are displaced by the hydrated protons at the interface, and the presence of charges at the surface aligns water molecules, thereby increasing the signal in the hydrogen-bonded region. The surface is affected already at 0.01 M acidic concentration, suggesting hydrated protons have adsorbed to the D_2O-air interface already at 10 mM.

To exclude effects due to counterions, we have monitored I_{SFG} from an interface containing NaCl in the subphase. I_{SFG} is independent of bulk NaCl concentration, as shown in Fig 1(b), providing evidence that neither Na^+ nor Cl^- adsorb at the interface at 0.01 M ionic strength. At 1 M ionic

strength, according to literature[10, 76], Cl^- can adsorb, but Na^+ does not. Therefore, the spectral changes occurring already in the presence of 10 mM DCl can be attributed entirely to D^+_{hyd} adsorbed at the surface. Control experiments to rule out impurities as the cause for the increase in the I_{SFG} with increasing acid concentration are detailed in the SI. Measurements on H^+_{hyd} in H_2O give similar results as for D_2O, and experiments using comparable angles of incidence for infrared and visible pulses as those used by Tyrode *et al*.[14], reproduce the results of Tyrode *et al*. These results showed no effect of protons on interfacial response up to 10 mM, implying that the threshold for observing protons at the interface depends on the experimental geometry (details in SI).

Upon addition of base into the subphase, I_{SFG} in the hydrogen-bonded region remains unchanged up to, and including 0.1 M bulk concentration (Figure 1(c)). Only upon the addition of 1 M base, the I_{SFG} in the hydrogen-bonded region decreases, while in the dangling OD region the spectrum remains unchanged: OD^-_{hyd} seems to adsorb at the D_2O-air interface significantly only around 1 M ionic strength. Surfactant studies have shown that the presence of positive and negative charge at the surface affects the magnitude of the SFG response in the H-bonded region very similarly[33]. Hence, for a given surface concentration, both D^+_{hyd} and OD^-_{hyd} are expected to perturb the D_2O-air interface response equally strongly. However, OD^-_{hyd} adsorption requires a bulk concentration that is two orders of magnitude higher than that of D^+_{hyd}.

D^+_{hyd} and OD^-_{hyd} have opposite effects on I_{SFG} in the H-bonded region: with increasing D^+_{hyd} (OD^-_{hyd}) concentration, I_{SFG} increases)decreases). This difference can be explained, in line with ref (10) as follows: at a nominally neutral D_2O surface, on average the hydrogen-bonded D_2O molecules orient with their deuterium atoms pointing towards the bulk[99]. Due to adsorption of D^+_{hyd} at the surface, the preferential alignment of the D_2O molecules with deuterium towards bulk increases, giving rise to a higher I_{SFG}. In contrast, the adsorption of OD^-_{hyd} at the surface causes a decrease in the orientation of D_2O molecules with their deuterium atoms pointed towards bulk, resulting in a lower I_{SFG} compared to that of neutral D_2O interface. The presence of charges at the interface can also give rise to a $\chi^{(3)}$ signal, that is equally consistent with the observed signal variations.[56]

To determine the onset of D^+_{hyd}/OD^-_{hyd} adsorption at the interface, we quantify the amplitudes of the different resonances in the SFG spectra using an established fitting procedure[9]. According to this fitting procedure, the I_{SFG} is proportional to the square of the second-order susceptibility $\chi^{(2)}$ of

the sample and intensity of the incoming IR and Visible (VIS) light:

$$I_{SFG} = \left|\chi^{(2)}\right|^2 I_{IR} I_{VIS} \tag{1}$$

The $\chi^{(2)}$ is a sum of a non-resonant term, $\chi_{nr}^{(2)}$ (comprising of a non-resonant amplitude A_{nr} and a non-resonant phase φ_{nr}) and resonant ($\chi_r^{(2)}$) contribution(s). Each $\chi_r^{(2)}$ is expressed as a Lorentzian line shape with area A_n, central frequency ω_n, and bandwidth Γ_n (half-width at half maximum):

$$\left|\chi^{(2)}\right|^2 = \left|\chi_{nr}^{(2)} + \chi_r^{(2)}\right|^2 = \left|A_{nr} e^{i\phi_{nr}} + \sum_n \frac{A_n}{\omega_n - \omega_{IR} + i\Gamma_n}\right|^2 \tag{2}$$

First, the spectrum for pure D_2O is fitted with three resonant peaks and a frequency-independent non-resonant response. The peak positions (2367, 2498, and 2710 cm^{-1}) and FWHM bandwidths (140, 170, and 50 cm^{-1} respectively) of the bands, as well as the phase (0.0 rad) from this fit, are subsequently used in the fits of the spectra containing different electrolytes. The resonant areas are the only free parameters for a specific dataset. The obtained values of the non-resonant amplitude are enlisted in table S-2 in the SI. The fits are shown as black lines in figure 1. Please note that the $\chi^{(2)}$ is an effective $\chi^{(2)}$ also including possible contributions from the electrostatic potential driven $\chi^{(3)}$[57].

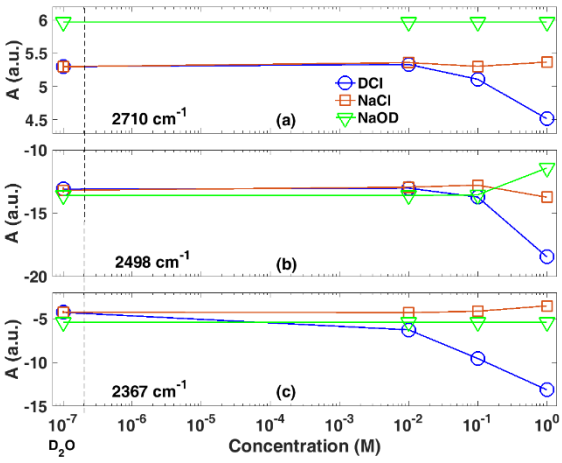

Figure 2. *Areas (A_n) of (a-c) different OD vibrations as a function of ionic strength of the solution. A positive sign of the OD stretch vibration indicates that the D atoms of D_2O molecules are pointing towards air. Negative sign means*

the opposite. The connecting lines are to guide the eyes. The differences of the A_n values for D_2O (most prominent in panel (a)) arise from variations between data sets.

Figure 2 depicts the areas)A_n(of the different vibrations as a function of DCl, NaCl, and NaOD concentration, obtained from the fits to the data in figure 1. Panel (a) shows that the 2710 cm^{-1} resonant contribution practically does not change in the presence of up to 1 M NaCl and NaOD, yet decreases by ~15% in the presence of 1 M D^+_{hyd}. Assuming that the free OD orientation does not change in line with Ref [4a], the 15% area reduction implies a ~15% decrease in the number of 'dangling' ODs due to the displacement of free OD groups by D^+_{hyd} ions. Panel (b) shows that the signal at 2498 cm^{-1} increases by ~45% for 1M D^+_{hyd}, marginally increases for 1 M NaCl, and decreases weakly for 1 M OD^-_{hyd}. The 2367 cm^{-1} resonant contribution (panel (c)) does not change significantly for 1 M NaCl and NaOD and increases by ~250% for 1 M D^+_{hyd}. These changes in the signal intensity of the low-frequency features, report on a change of the response of the water molecules due to a change in the interfacial charge distribution. Similar to the structure of H^+_{hyd} , at least in part present as H_3O^+ at the interface[81,10] of H_2O, the "tripod" structure of D_3O^+ orients at the water-air interface pointing its D-atoms towards the bulk, donating three strong hydrogen bonds. The increase in the hydrogen-bonded OD signal can, therefore, originate from hydronium-OD groups, the enhanced downward orientation of the interfacial D_2O molecules, or a bulk $\chi^{(3)}$ contribution[57].

To quantify the onset of surface activity for the two ions, we use the resonance most sensitive to that particular ion: the 2367 cm^{-1} for the hydrated proton and 2498 cm^{-1} for the hydrated hydroxide. The areas of these two resonances are plotted in Fig. 3. As the amplitude of the 2498 cm^{-1} mode for hydroxide changes between 0.1 (no apparent reorganization of the water molecules at the surface) and 1 M, we determine the threshold of surface activity at ~0.5±0.4 M. As the amplitude enhancement of the 2367 cm^{-1} resonance for hydrated proton shows a linear behavior on a log scale from 10^{-2} M onwards, we linearly extrapolate the concentration-dependent signals to the signal intensity observed for pure water (Fig. 3) and find the onset of surface adsorption at ~2.7±0.2 mM for hydronium. Given the estimated detection efficiency of surface charge of around 0.1-1 % (see SI), we conclude that we could detect as low surface concentration as 0.05-0.5 M of D^+_{hyd}/OD^-_{hyd} ions. From the observed onset of surface adsorption of the hydrated proton at ~2.7 mM, we conclude that the partition coefficient of the hydrated proton is larger than 1, i.e. the protons are

attracted to the water-air surface. For hydroxide, the partition coefficient seems to be in the range of 1.

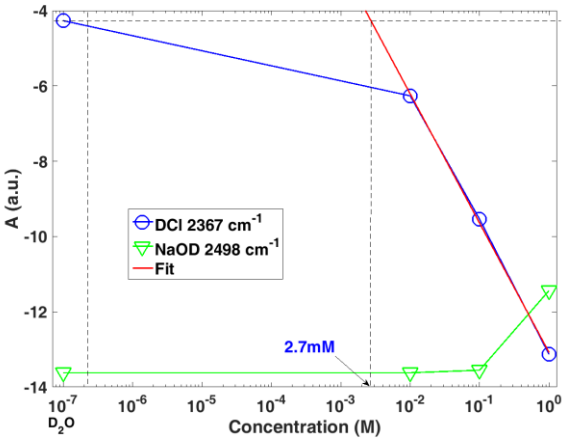

Figure 3. *Fitted areas of the 2367 cm^{-1} peak in the presence of DCl and 2498 cm^{-1} peak in the presence of NaOD. The blue dotted horizontal line represents the A_n value for the 2367 cm^{-1} resonance band of pure D_2O. The vertical dotted blue line represents the onset concentration of the surface propensity of hydronium.*

Although it has often been argued that the surface of neat water in contact with air has an excess negative charge, i.e. the hydroxide formed through the autoionization of water adsorbs more than hydronium[100-102], this seems to be unlikely based on our SFG results. The SFG spectra in Fig.1 shows that the OD^-_{hyd} concentration at the surface at thermodynamic equilibrium is apparently very small in the range pD)H(=7-13; i.e. only above pD(H)=13 the SFG spectrum changes.

Conclusion:

In summary, we have determined the onset concentrations of surface adsorption at the water-air surface of hydrated protons and hydroxide ions. Protons adsorb at the D_2O-air interface at a bulk concentration around 2.7±0.2 mM. For OD^-, the interfacial water structure remains unaffected until a significantly higher bulk concentration of 0.5±0.4 M is reached. Given our estimated detection limit for charges present at a surface, we conclude that the partition coefficient for D^+_{hyd} is higher than 1 meaning that D^+_{hyd} is expelled from the bulk. For OD^-_{hyd} we estimate a partition coefficient around 1. The surface adsorption ability likely anti-correlates with the hydrogen bond formation

ability of the two species[103], especially within the first solvation shell[104]. As D_3O^+ is a very weak hydrogen bond acceptor[10], it prefers to stay close to the surface[103, 105] where the number of neighboring species to make a hydrogen bond with, specifically at the immediate water-air interface, are naturally scarce[106]. However, the most recent multi-state empirical valence bond model-based calculation comparing the instantaneous air-water interfacial structure and the Gibbs dividing surface, shows that also the second solvation shell structure can influence surface affinity[105]. The free energy minimum very close to the interface (~1 Å) is similar for hydrated proton and hydroxide. However, the hydroxide has a higher maximum in free energy than the hydrated proton at 2-3 Å away from the instantaneous surface, increasing the barrier for hydroxide to come to the interface.

Experimental Section

SFG Spectroscopy:

Two different experimental set-ups have been used for this work. The setup that is used to collect the data shown in Fig. 1 here and S1-2 in the SI consists of a mode-locked Ti:sapphire laser (Mai Tai SP, Spectra-Physics) and a regenerative amplifier (Spitfire Ace, Spectra-Physics) pumped with a Nd:YLF laser (Empower 45, Spectra-Physics). The amplifier produces 800 nm pulses with 4.5 mJ power, ~45 fs pulse width, at a 1 kHz repetition rate. From its output, ~1.7 mJ is used to pump a commercial OPA (TOPAS-C, Light conversion) that mixes signal and idler in a $AgGaS_2$ crystal and produces tuneable broadband IR pulses. The IR pulses, centered around ~2500 cm^{-1}, have a full width at half maximum (FWHM) of ~450 cm^{-1} and ~5 μJ pulse energy. The remainder of the amplifier output is spectrally narrowed to ~15 cm^{-1} FWHM using a Fabry-Perot etalon (SLS optics ltd.). The output energy is ~20 μJ. The diameters of the beams focused onto the sample are ~0.2 mm. The incident angles for the *IR* and *VIS* (800 nm) beams are 36° and 34° respectively. The signal is collected by a spectrograph (Acton, Princeton Instruments) and detected with an electron multiplied charge coupled device (emCCD) camera (Newton, Andor instruments). The acquisition time is typically 5 to 10 minutes, depending on the signal strength. All spectra in the presented work are collected in SSP polarization (S: SFG, S: Vis, P: IR). The data are normalized by the non-

resonant signal from z-cut quartz. The details of the other setup and a comparison of the incident angles are given in the SI.

Sample Preparation:

The electrolyte solutions were made by dissolving HCl (37%) and/or NaCl in D_2O and H_2O. H^+ instantly reacts with D_2O to produce D^+. Since 37% HCl has a concentration of 12 M (in H_2O), 1 M and 0.1 M HCl solutions in D_2O will have 10% and 1% H_2O in it, respectively.

Acknowledgement:

This work is funded by the Deutsche Forschungsgemeinschaft (DFG, German Research Foundation) - BA 5008/3.

Supplementary information:

The surface activity of hydrated proton is considerably higher than that of hydroxide

Set up:

Two different experimental set-ups have been used for this work. The setup that is used to collect the data shown in Fig. 1 in the main text and S1-2 in this SI is described in the main text.

The other setup, used to collect the data shown in S3 in this SI is comparable to the one described before, but with ~9.5 mJ output power from the amplifier, of which ~3 mJ is used to pump a commercial OPA to produce IR pulses of ~20 μJ energy, with an FWHM spectral width of ~350 cm^{-1} centered at ~2500 cm^{-1}.

All spectra in the presented work are collected in SSP polarization (S: SFG, S: Vis, P: IR). The data are normalized by the non-resonant signal from z-cut quartz. The details of incident angles are presented in table S-1 in the section: ‘Spectra at different geometries’ below.

Check of surface-active impurities:

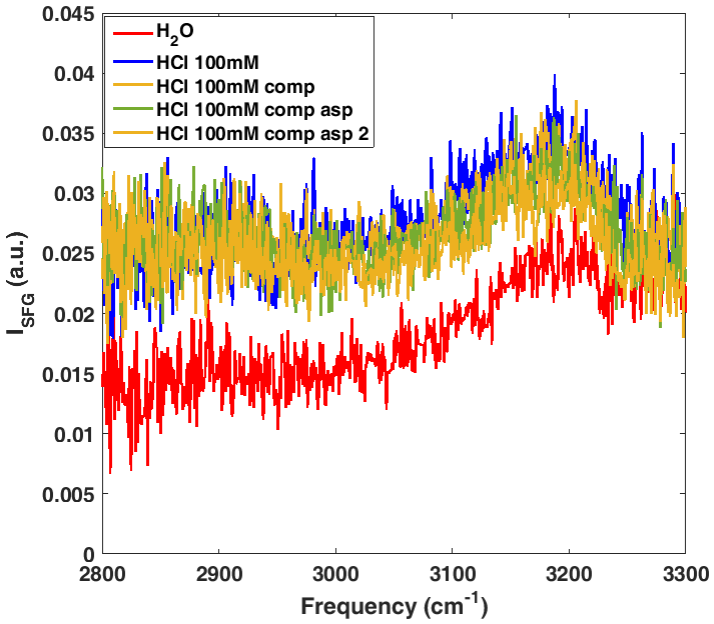

Figure S-1: Comparison of SFG intensity of pure H_2O and 0.1M HCl. The spectra are collected using a Langmuir trough. 'HCl comp' corresponds to the spectrum taken from a compressed HCl surface immediately after compression. 'HCl comp asp' corresponds to the spectrum taken after aspirating the compressed HCl surface. 'HCl comp asp2' corresponds to the spectrum taken after (de-)compression and aspiration of the surface three times subsequently.

Figure S-1 shows the comparison of the spectra obtained from the surfaces of pure H_2O and 0.1 M HCl solutions, the latter being checked for the presence of any surface active impurity in a Langmuir trough. First, the spectrum of a 0.1 M HCl sample is recorded. Then the surface is compressed to ~1/4th of its initial surface area in order to compress the surface-active impurities, if any, inside the smaller area. An SFG spectrum is recorded immediately ('HCl 100 mM comp' in figure S-1). Some amount of sample from the surface is sucked out using an Eppendorf pipette (aspiration) in order to remove potentially present surface active impurities, and immediately another SFG spectrum is taken that is referred to as 'HCl 100 mM comp asp' in figure S-1. The surface area is further decompressed, compressed and aspirated three times subsequently and another SFG spectrum is recorded at the end that is referred to as 'HCl 100 mM comp asp 2' in figure S-1. None of the four HCl spectra shows any CH vibration response or differs from each other in either intensity or spectral shape implying that there is no surface-active impurities present and we probe a clean HCl surface.

Spectra in OH region:

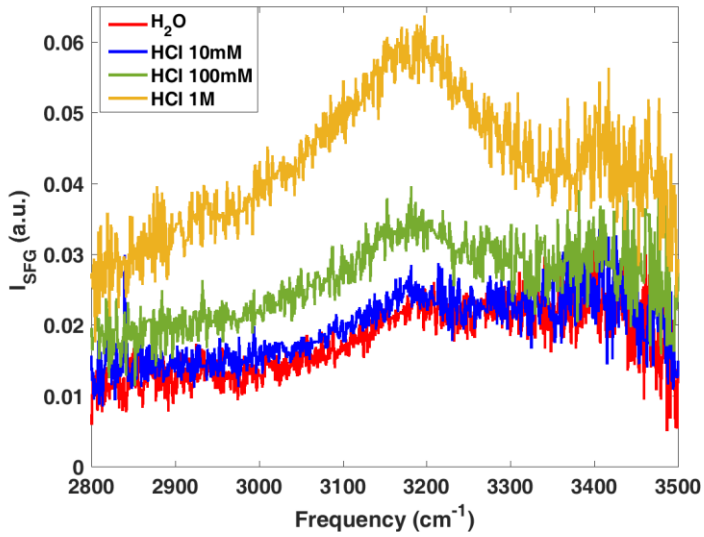

Figure S-2: The SFG intensity in SSP polarization from H_2O-air interface containing HCl at different concentrations in the subphase.

Figure S-2 shows the SFG response in SSP polarization from an air-H_2O interface for pure H_2O and H_2O containing acid in the subphase as a function of frequency in the H-bonding region of H_2O. The intensity of the H-bonding region increases in the presence of 10mM acid, indicating significant adsorption of hydrated protons at the surface.

Spectra at different geometries:

To verify if the difference between our work and the work by Tyrode *et al.*[14] can be explained by the different experimental geometries, we have obtained spectra in SSP polarization from the D_2O-air interface in two different experimental geometries. The incoming angles of IR and VIS pulses in these two geometries are tabulated below (Table S1) along with the geometry used by Tyrode *et al.*[14] for comparison. The spectra shown in Fig S-3 in this SI are recorded in Geometry 2. The spectra shown in Fig 1 in the main text and Fig S(1,2) in this SI are recorded in Geometry1.

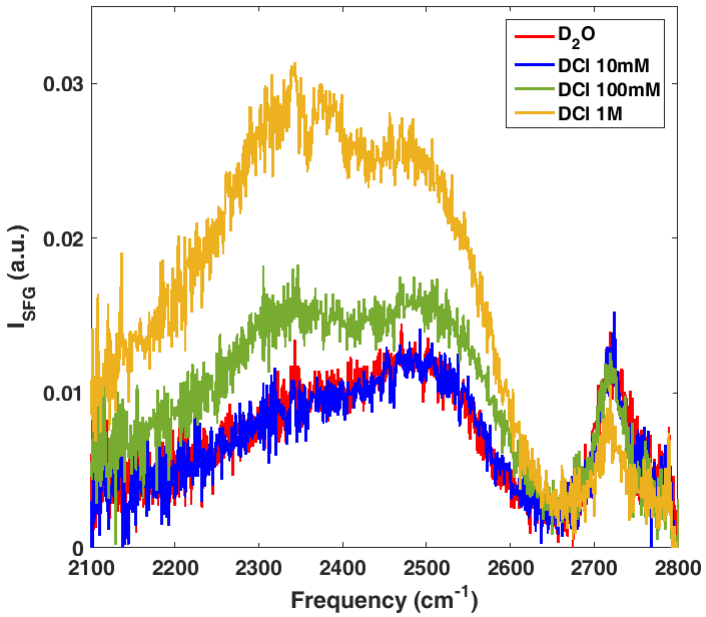

Figure S-3: SFG spectra in SSP polarization from the D_2O-air interface from pure D_2O and at different concentrations of DCl in the subphase, recorded in geometry 2 (details in Table S1).

Figure S-3 represents the SFG intensity spectra as a function of frequency for pure D_2O and at different concentrations of DCl in the subphase. The SFG intensity remains unchanged in the presence of 10 mM DCl. However, the intensity in the hydrogen-bonded region (~2100-2600 cm^{-1}) increases and that of the free OD region (~2710 cm^{-1}) decreases with increasing concentration of acid.

Table S-3: Incoming angles of IR and VIS pulses in different experimental geometries.

	Geometry 1	Geometry 2	Tyrode *et al.*[14]
IR	36	40	55
VIS	34	70	70

Non-resonant SFG response obtained from the fits with eq. 2 in the main text:

Table S-4: Non-resonant amplitudes obtained from the fits with eq. 2 in the main text.

	DCl	NaCl	NaOD
0.00M (D_2O)	-0.10	-0.10	-0.095
0.01M	-0.10	-0.10	-0.095
0.1M	-0.10	-0.10	-0.095
1M	-0.12	-0.10	-0.095

The small variations in the non-resonant SFG response for pure D_2O arise from different data sets.

Calculation of the SFG sensitivity for surface charge at the water-air interface:

To estimate how sensitive SFG is to a charge density at the air-water interface, we use SFG spectra for the lipid-water interface. We estimate that a lipid density of 1 charged lipid per 1000-10000 $Å^2$ will result in a noticeable change of the water spectrum, based on the observation of a clear change in water signal for the zwitterionic lipid DPPC at 300 $Å^2$ per lipid[92]. Therefore, we set our detection limit to one charge at 1000-10000 $Å^2$, which equals 10^{14}-10^{15} charges per dm^2. Assuming a surface concentration of water molecules of 10^{17} molecules per dm^2 (55 M x 3 Å thick surface layer), we can conclude that we have a detection limit of about 0.1-1%. Given the water concentration of 55 M, we estimate that we could see an interfacial concentration as low as 0.05-0.5 mol – i.e., we have a detection threshold of 50 mM at best.

Chapter 6

Nature of excess hydrated proton at the water-air interface

Abstract:

Despite the importance of the interfacial structure of acidic aqueous solutions in the context of, e.g., atmospheric chemistry, biophysics, and electrochemistry, our understanding of protons at interfaces is incomplete, owing to the limited number of techniques that are able to selectively probe interfacial protons. Here, using surface-specific vibrational spectroscopy, we probe the response of interfacial protons at the water-air interface, and reveal the interfacial proton continuum. Combined with ab initio molecular dynamics simulations, the response of the proton at the water-air interface is shown to be consistent with the coexistence of both Eigen and Zundel structures at the interface. A quantitative analysis reveals an interfacial stabilization by -1.3±0.2 kcal/mol, in reasonable agreement with previous theoretical predictions. Our results illustrate the surface propensity of protons, and the ability to characterize interfacial protons using surface-specific vibrational spectroscopy.

Introduction:

The proton in water is as ubiquitous as water itself, given that the proton is a product of the auto-ionization of water ($2H_2O \rightleftharpoons H_3O^+ + OH^-$). Hydrated protons are important for a wide range of disciplines, as charge carrier in membrane biology, photosynthesis, and as electron acceptors in electrochemistry.

As such, the structure of protons in bulk water has been studied in detail and it has become evident that, much like the hydrogen-bonded network of water, the proton and its hydration shell are highly dynamic. For hydrated protons in bulk, two limiting structures, namely Zundel and Eigen, have been proposed[27]. An Eigen moiety is a proton as part of a hydronium (H_3O^+) ion, which is solvated by three additional water molecules to produce $H_9O_4^+$. An ideal Zundel structure constitutes of a proton equally shared between two water molecules to produce the moiety $H_5O_2^+$. Steady-state[3]

and time-resolved[27, 28, 107] vibrational spectroscopy have shown that both of these moieties are present inside the bulk in both of their ideal and significantly distorted conformations producing a typical proton continuum absorption spanning a wide vibrational frequency range, between the bend and stretch vibrations of pure water from 1600 to 3400 cm^{-1}.

While hydrated protons in bulk have been intensely studied, less is known about protons at interfaces. Protons at interfaces are important for several systems, including atmospheric aerosols[4], biological membranes[108], fuel cells[109] and electrochemical systems[110]. At the interface of acidic solutions with air, the concentration of protons at the surface is elevated compared to that in bulk. Although the presence of the hydrated proton at the surface has been evidenced from both surface-specific spectroscopies, such as second harmonic[8] and sum frequency[11, 12] generation and theoretical studies[10, 19, 29, 81], it is experimentally challenging to elucidate the structure of the interfacial proton. Moreover, the energetics of interfacial proton adsorption is somewhat controversial: Voth and coworkers[103] have concluded that the proton is weakly attracted to the water-air interface with a free energy of~0.55 kcal/mol. However, Jungwirth and coworkers have previously concluded the proton to be strongly adsorbed at the surface based on their calculated free energy of adsorption of ~3 kcal/mol [111]. Pegram and Records' analysis of the surface tension increase[6] had predicted an enhanced surface concentration of protons relative to the bulk with a partition coefficient ~1.5, corresponding to about ~0.24 kcal/mol.

The reason for the surface activity of the hydrated proton can be well illustrated by considering simply the hydronium ion, and its amphiphilic character[103]: while the three hydronium-OH groups are excellent hydrogen bond donors, the remaining lone electron pair on the oxygen atom is a poor hydrogen bond acceptor due to the net positive charge of the hydronium ion. Hence, the hydronium ion has been predicted to sit on the surface with its three OH groups pointing down towards the bulk, with the lone pair pointing towards the vapor phase[10, 19, 81, 103]. Yet it is not clear how the hydrated proton is present at the interface: in addition to hydronium, it is more likely to be present as Eigen and Zundel moieties, as in the bulk. In addition, an experimental value for the surface free energy of the hydrated proton is highly desirable. In order to address these questions, we have used surface-specific vibrational spectroscopy, i.e., conventional and phase-sensitive (PS-) sum frequency generation (SFG) spectroscopy, at the water-air interface in presence of HCl in the bulk solution.

From our experiments, we find that the protons indeed adsorb at the surface and produce a 'proton continuum' response similar to that in the bulk. By comparing the observed experimental response with calculations, we find that the spectral response can be accounted for by the coexistence of the Eigen and the Zundel forms of interfacial solvated protons. We quantify the absorption free energy of the proton at the surface to be ~-1.3 kcal/mol, substantially higher than k_BT.

In conventional SFG spectroscopy, an IR laser pulse is spatiotemporally overlapped with an 800 nm pulse at the sample surface and the reflected sum frequency response is detected. The generation of SFG light requires symmetry to be broken. Bulk water is centrosymmetric and has zero SFG response. However, at the water surface the symmetry is broken, resulting in an SFG response. Moreover, when the IR light is in resonance with a molecular vibration, the SFG signal is enhanced, so that the SFG intensity as a function of IR frequency in essence provides the vibrational response of interfacial molecules. Specifically, the spectral intensity distribution in the OH stretch vibrational frequency region (~3000-3750 cm^{-1}), reports on the presence and alignment of interfacial water and hydronium molecules.

Results and discussions:

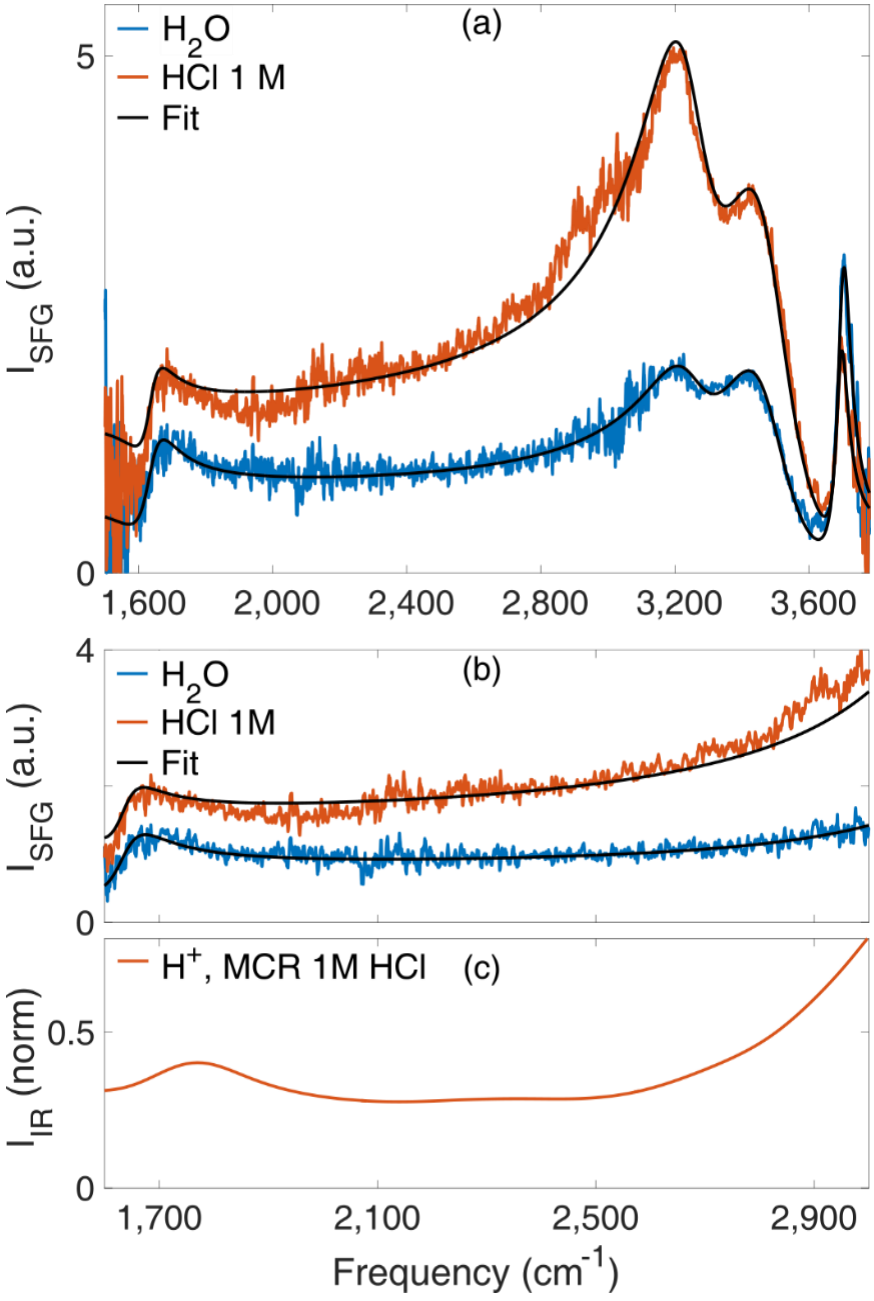

Figure 15: SFG spectroscopy of the acidic water surface. *(a): The SFG intensity in SSP (S: SFG, S: VIS, P: IR) polarization from the water-air interface for pure H_2O, and H_2O containing 1M HCl in the subphase. The black lines are fits to the spectra obtained using eq s2 mentioned in SI. (b) Zoom-in of the 1600-3000 cm^{-1} region of the SFG response from pure H_2O and 1M HCl solution. (c) The contribution to the bulk IR absorption spectrum from the*

hydronium ion obtained from multivariate curve resolution (MCR) analysis. The IR-MCR data are reproduced from Ref.[3].

Figure 1(a) shows the SFG intensity spectra for pure H_2O, and H_2O containing 1M HCl in the subphase. Each spectrum has a sharp response centered at ~3700 cm^{-1}, a broad response with a dual peak feature extending between ~3000 cm^{-1} to ~3650 cm^{-1}, a broad featureless response spanning the range ~2000-3000 cm^{-1} and a peak at ~1600 cm^{-1}. The sharp response at ~3700 cm^{-1} originates from the vibration of non-hydrogen-bonded OH groups from water pointing into the air. The broad response with dual peak feature is the vibrational signature of hydrogen-bonded H_2O molecules at the H_2O-air interface. Vibrational coupling between hydrogen-bonded O-H groups causes the dual-peak line-shape[86]. The flat featureless response for pure water is generally considered to be a non-resonant response of the interfacial water molecules. The peak at ~1600 cm^{-1} is the bend vibrational response of the water molecules[60, 112, 113]. In the presence of 1M HCl, the intensity rises throughout the ~1600-3600 cm^{-1} region, and decreases around 3700 cm^{-1}. Both observations evidence interfacial proton propensity: protons at the interface displace the free OH groups, and give rise to additional signal in the hydrogen-bonded region. The presence of 1M NaCl does not significantly affect the surface water spectrum (Figure S1), so that it is apparent that the signal changes are primarily due to the proton. Figure 1b shows the SFG intensity in the ~1600-3000 cm^{-1} region, illustrating the enhancement of intensity in this region as a result of the presence of protons. This observation is reminiscent of the so-called proton continuum absorption in bulk acid solution, exemplified in the panel (c), which shows the proton-related IR absorption in HCl solution, obtained using a multivariate curve resolution (MCR) analysis[3]. The Raman MCR signal has been shown to have a similar shape[3]. Recently, using 2DIR spectroscopy, this region has been shown to arise due to couplings amongst several vibrational modes of Zundel ($H_5O_2^+$)-moieties in the bulk[114]. An earlier conventional SFG study on the H_2O-air interface containing halogen acid in the subphase had also predicted the presence of H_3O^+ and $H_5O_2^+$ at the interface based on similar intensity enhancement[12].

The proton-induced increase of the SFG intensity clearly shows that the proton is surface active, yet the signal increase can be due to (i) OH groups of a surface-adsorbed hydrated proton (i.e. an interfacial proton continuum response); (ii) an enhanced orientation of water; or (iii) a result of the presence of charge at the surface, giving rise to a bulk contribution, expected for charged

interfaces[56, 57]. It is challenging to distinguish amongst these different possible contributions from the SFG intensity spectra. One of the reasons is that SFG intensity spectra, being proportional to the absolute square of the response function ($\chi^{(2)}$), are not quantitative: $I_{SFG} \propto \left|\chi^{(2)}\right|^2$. This means that the real (*Re*) and an imaginary (*Im*) components of $\chi^{(2)}$ cannot be disentangled. In particular, *Im*[$\chi^{(2)}$] directly reflects the response and orientation of interfacial molecules. Phase-resolved measurements allow the real and imaginary parts of $\chi^{(2)}$ to be determined independently.

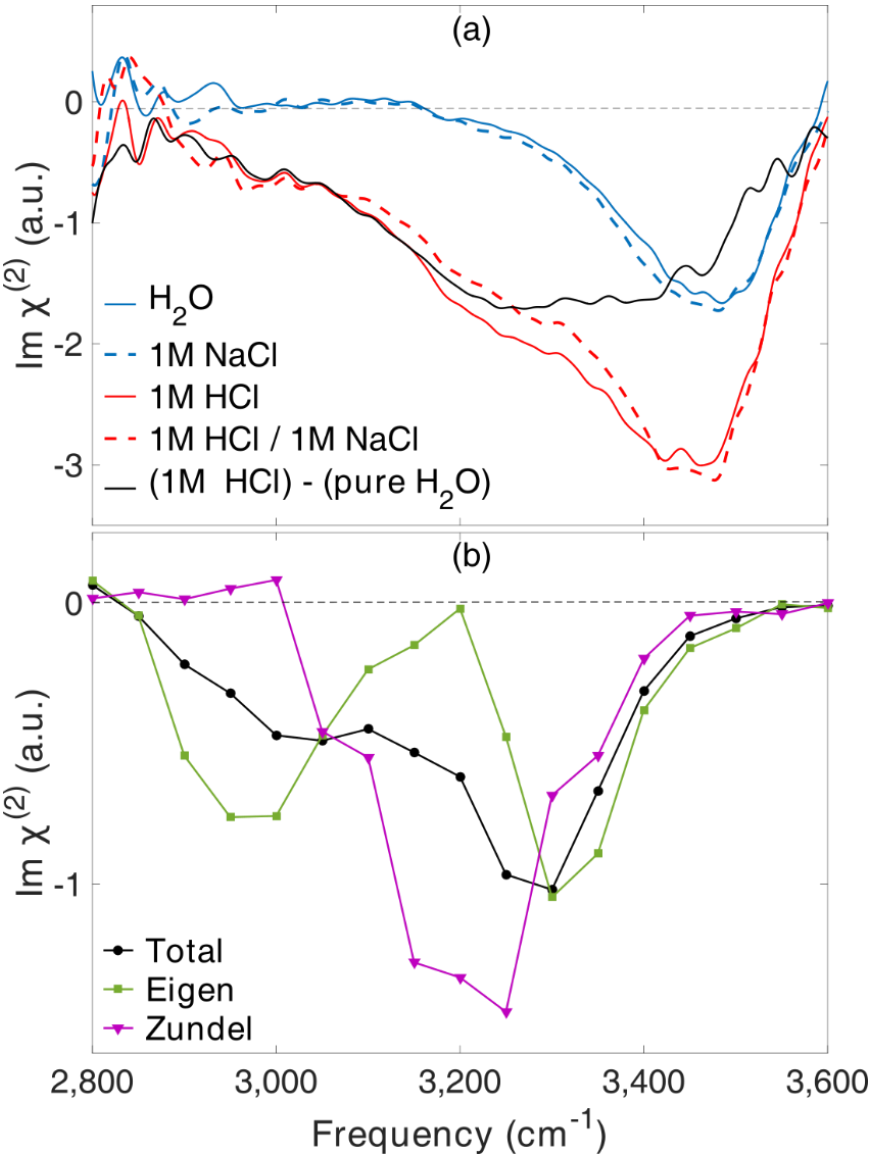

Figure 2: ***Phase-resolved measurements of the proton continuum and theoretical calculations.*** *(a) Experimentally determined imaginary part of $\chi^{(2)}$ spectra as a function of frequency in SSP polarization from H_2O-air interface for*

pure H_2O and in presence of 1M NaCl, 1M HCl and a solution containing both 1M NaCl and 1M HCl in the subphase. The black line shows the difference spectrum between the presence and absence of 1M HCl (b) Simulated individual and total contributions from Eigen and Zundel moieties to the total imaginary $\chi^{(2)}$ response of 1M HCl. The inset represents the number density profiles of H_2O, H_3O^+ and Cl^-.

To shed more light on the origin of the proton signal, we, therefore, have performed phase-sensitive measurements. Figure 2 (a) shows $Im[\chi^{(2)}]$ responses as a function of frequency in SSP polarization from the water-air interface of pure H_2O, H_2O containing 1M NaCl and 1M HCl, and a solution containing both of 1M NaCl and 1M HCl in the subphase. The close resemblance between the $Im[\chi^{(2)}]$ response of pure water (blue solid line) and 1M NaCl solution (blue dotted line) show that neither sodium nor chloride alter the SFG response of interfacial water.

In the presence of protons (red solid line), the response is much broadened, and has a distinct tail towards lower frequency, compared to that of the pure H_2O surface. To check for a possible bulk ($\chi^{(3)}$-) contribution[56] that is expected to enhance the intensity more evenly or less disproportionately than we see in Fig 1(a), we added 1M NaCl to the 1M HCl solution. The resulting doubling of the ionic strength of the solution will result in stronger screening of the charge of the interfacial protons, reducing the Debye screening length from ~3 to ~2 Å. Yet, the addition of NaCl does not affect the $Im[\chi^{(2)}]$ response (red dotted line), indicating that the $\chi^{(3)}$ effect does not dominate the proton-induced response of the acidic water surface.

However, we cannot experimentally distinguish between the contributions to the signal from (i) the hydronium O-H groups and (ii) the increased orientation of water molecules with their H-atoms pointing towards the bulk due to accumulation of protons at the surface. Since overall contribution to the $Im[\chi^{(2)}]$ spectra are additive, we consider the difference spectrum of 1M HCl and pure H_2O as the 'effective' $\chi^{(2)}$ response of the adsorbed protons at the surface. We note that this is a very crude approximation: it assumes a vanishingly small $\chi^{(3)}$-bulk contributions to the signal, and that the increase in downward water orientation due to the presence of protons is counteracted by the displacement of interfacial water by hydronium ions. The difference spectrum (black) is broad with a dual peak feature. One peak is centered on ~3400 cm^{-1} and another around ~3250 cm^{-1}, suggesting the appearance of new vibrational modes. The resulting spectrum attributed primarily to the proton at the interface is very broad, with a width of about 450 cm^{-1}, with a tail extending to low frequencies. While this general shape is reminiscent of the

proton continuum previously reported in bulk[3, 27], the interfacial proton continuum approaches zero at higher frequency than that in the bulk. This difference between surface and bulk response may be traced to either different selection rules for the different species at the interface, or a difference in relative occurrence of the different hydrated proton types at the surface.

To further investigate the nature of the proton at the surface, we therefore compare the experimentally obtained spectrum with that obtained using simulations. The simulation methodology must be able to dynamically readjust the chemical bonding topology. This reactive nature of the chemical process is automatically captured with ab initio molecular dynamics (AIMD) simulation methods, where the electronic degrees of freedom are treated explicitly[115].

Figure 2(b) shows the simulated individual and total contributions from both Eigen and Zundel moieties to the $Im[\chi^{(2)}]$ SFG response from the surface of a 1M HCl solution. The shape of the calculated total $Im[\chi^{(2)}]$ response (red spectrum in panel (b)) agrees reasonably well with the very broad $Im[\chi^{(2)}]$ response determined experimentally (red spectrum in panel (a)) implying that both Eigen and Zundel moieties are present at the surface, i.e. the structural nature of the proton at the surface appears similar to that inside bulk. We note that the minima of the calculated $Im[\chi^{(2)}]$ is red shifted by ~150 cm^{-1} with respect to the experimental minima. The red shift possibly arises from the overestimation of the H-bond strength due to structural optimization for harmonic analysis, typical for the theory.

Undoubtedly, our results showing the substantial surface affinity of the proton at the order of 1M concentration agree well with the previous reports[10, 11]. An important question in this regard is that how strongly does the proton bind to the surface? In other words, what is the free energy of adsorption for protons to the surface? Previous theoretical reports have predicted both weak binding[103, 116] (binding strength, $\Delta E_{bind} \leq$ *0.6 kcal/mol*) and strong binding[29, 111, 117-119] ($\Delta E_{bind} >$ *0.6 kcal/mol*).

However, to the best of our knowledge, there is no experimental report of this value. To determine the value experimentally, we have monitored the SFG intensity as function of D_3O^+ to Na^+ concentration ratio as total bulk concentration of 1M from a D_2O-air interface, i.e. at constant ionic strength. The reason to use D_2O, instead of H_2O is to avoid any uncertainty due to the absorbance of IR intensity by the water vapor in the air at free OH region (~3700 cm^{-1}). We focus on the free OD intensity to quantify the surface propensity of protons at the D_2O-air

interface, since the free OD intensity does not suffer from potential complications due to vibrational coupling and bulk contributions to the signal, and thereby provides the most direct measure for the interfacial proton density.

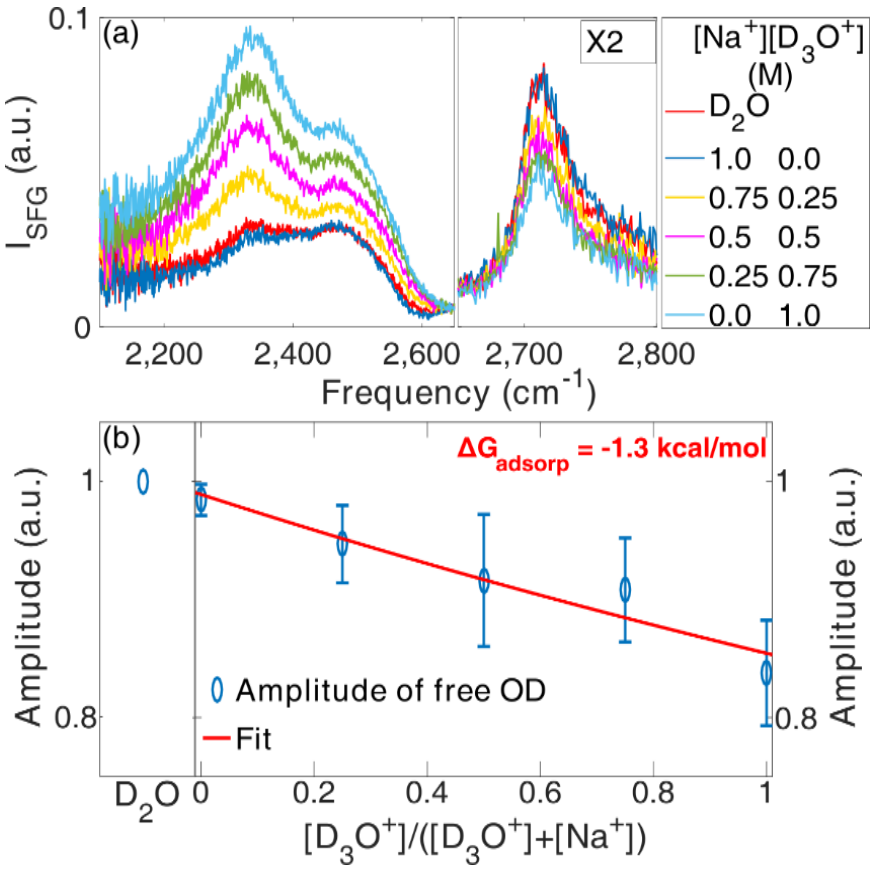

Figure 3: ***Displacement of free OD groups by the hydrated proton allows determining free energy of interfacial adsorption.*** *(a) The mean SFG response in SSP polarization from air –D_2O interface for pure D_2O and D_2O containing NaCl and DCl at different concentration ratios obtained in three separate experiments The black lines are fits to the spectra. (e)Amplitude (A_n) of the 'free' OD vibrations as function of the relative concentration of D_3O^+ to Na^+ in the subphase The red line is the fit obtained with eq 3.*

Figure 3(a) represents the SFG intensity as a function of frequency in SSP polarization from the D_2O -air interface containing NaCl and DCl in different concentration ratios in the subphase. The SFG intensities shown here are the average of three spectra for each concentration ratio obtained through three separate experiments. The SFG responses of 'free' OD region obtained in these individual set of experiment are shown in panel (b-d). The SFG responses of the hydrogen

bonded region are shown in the SI. The SFG intensity in presence of 1M NaCl (dark blue) does not significantly differ from that of pure D_2O (red). The intensity of the hydrogen bonded region (~2200-2650 cm^{-1}) increases with increasing acid fraction in the subphase, identical to the results for H_2O. The intensity of the 'free' OD groups decreases with increasing concentration of acid indicating a displacement of 'free' ODs by the adsorbed D_3O^+ ions - again in line with the H_2O results.

In order to get the amplitude of the free OD response, we have fitted the data obtained in the individual experiments separately using an established procedure[9], using Lorentzian lineshapes to reproduce the observed resonances (details in SI). First, the spectrum for the 0.5M mixture of NaCl and DCl is fitted with four resonant peaks and a frequency independent non-resonant response (See table 1 for details). The peak positions (2360, 2500, 2660 and 2705 cm^{-1}) and FWHM bandwidths (120, 180, 100 and 40 cm^{-1}) of all the bands[120], as well as the non-resonant phase (0.0 rad) from this fit, are subsequently used in the fits of the spectra containing different electrolytes. The amplitudes are the only free parameters. The fits for the 'free' OD vibration region are shown as black lines in figure 3(b-d).

Figure 3(e) represents the amplitude of the 2705 cm^{-1} peak ('free' OD) as a function of fraction of D_3O^+ to the total cation concentration in the solution. Since the total ionic strength of the solution is 1 M, the fraction of D_3O^+ in figure 3(e) equals its absolute bulk concentration. The fit results show that the number of free OD groups decreases by up to ~15% in presence of 1M acid in the subphase.

We verified that this reduction is solely because of the reduction in number of 'free' OD groups through displacement by the hydronium moieties, and not because of the change in the angular distribution with respect to the surface normal (see SI for details) in agreement with previous reports[10, 12]. Therefore, the reduction of the amplitude of the free OD band (ΔA_{freeOD}) can be directly related to the interfacial proton concentration $N_{D_3O^+}^{Surf}$:

$$N_{D_3O^+}^{Surf} \propto \Delta A_{freeOD} \quad (1)$$

In order to determine the proton adsorption free energy, we relate the adsorption free energy ΔG_{adsorp} to $N_{D_3O^+}^{Surf}$, through ΔA_{freeOD}.

In line with refs [96, 121-123], the surface concentration of hydronium is calculated by describing ΔA_{freeOD} as a function of D_3O^+ concentration $C_{D_3O^+}$with the Langmuir isotherm:

$$\Delta A_{freeOD} = A_{freeOD}^{D_2O} - \frac{A_{freeOD}^{D_2O} * C_{D_3O^+}}{C_{D_3O^+} + C_{water} * e^{\frac{\Delta G_{adsorp}}{RT}}} \quad (3)$$

Here, $A_{freeOD}^{D_2O}$ is the amplitude of the free OD band in absence of protons, $C_{D_3O^+}$ and C_{water} are the bulk concentrations of hydronium and water respectively, and ΔG_{ads} is the Gibbs free energy of adsorption of hydronium to the surface. In this equation, we assume that all free OD intensity is gone when the surface is fully covered with hydrated protons.

The model describes the data well assuming an adsorption free energy of -1.3 ±0.2 kcal/mol (red line in figure 3e) indicating a strong adsorption of the hydrated proton in agreement with specific theoretical studies[29, 111, 117-119].

Conclusion:

In summary, we have characterized the nature of the hydrated proton adsorbed at water-air interface. Our experimental data, together with theoretical calculations, are consistent with coexistence of Eigen and Zundel moieties of the interfacial proton, similar to that in the bulk. We also find that the adsorption free energy of the proton at the water-air interface is substantially larger than 0.6 kcal/mol (1 k_BT) at room temperature, implying strong surface adsorption.

Supplementary information

Nature of excess hydrated proton at the water-air interface

Comparison H_2O and 1M NaCl:

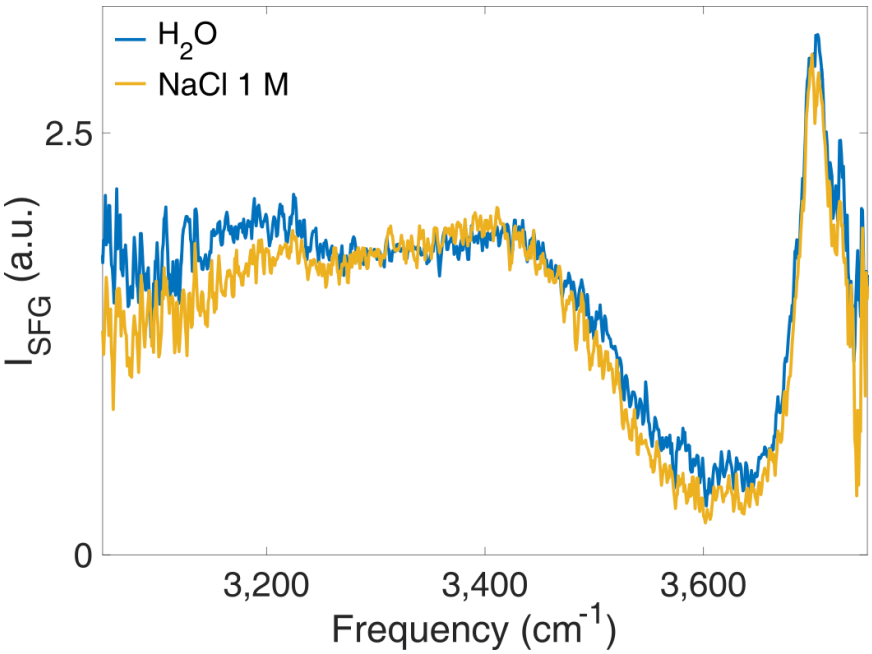

Figure S1: The SFG intensity in SSP polarization from the H_2O-air interface in presence of 1M NaCl in the subphase.

The intensity spectrum for a 1 M NaCl aqueous solution-air interface differs very little from that of pure H_2O, implying the concentration either both Na^+ or Cl^- is minimal at water-air interface. It further bolsters the idea that whatever changes we see in case of acid/proton is indeed caused by hydrated protons.

Fitting methods:

We quantify the amplitudes of the different resonances in the SFG spectra using an established fitting procedure[9]. According to this fitting procedure, the I_{SFG} is proportional to the square of the second-order susceptibility $\chi^{(2)}$ of the sample and intensity of the incoming IR and Visible (VIS) light

$$I_{SFG} = \left|\chi^{(2)}\right|^2 I_{IR} I_{VIS} \quad \text{(s1)}$$

The $\chi^{(2)}$ is a sum of a non-resonant term, $\chi_{nr}^{(2)}$ (comprising of a non-resonant amplitude A_{nr} and a non-resonant phase φ_{nr}) and resonant ($\chi_r^{(2)}$) contribution(s). Each $\chi_r^{(2)}$ is expressed in terms of a Lorentzian line shape with area A_n, central frequency ω_n, and bandwidth Γ_n (half width at half maximum)

$$\left|\chi^{(2)}\right|^2 = \left|\chi_{nr}^{(2)} + \chi_r^{(2)}\right|^2 = \left|A_{nr} e^{i\phi_{nr}} + \sum_n \frac{A_n}{\omega_n - \omega_{IR} + i\Gamma_n}\right|^2 \quad \text{(s2)}$$

Non-resonant SFG response:

To check if the enhancement in SFG intensity in presence of 1M HCl in the subphase (Fig 1, main text) is a result of an enhancement in the non-resonant background or not we have measured the SFG responses from 1M HCl, 1M NaOH, and 1M NaCl by tuning the IR frequency off-resonant with the OH stretch region of pure H_2O. We have also measured the non-resonant SFG response from 1M DCl, NaCl, and NaOD by tuning the IR frequency off-resonant with the OD stretch

vibration.

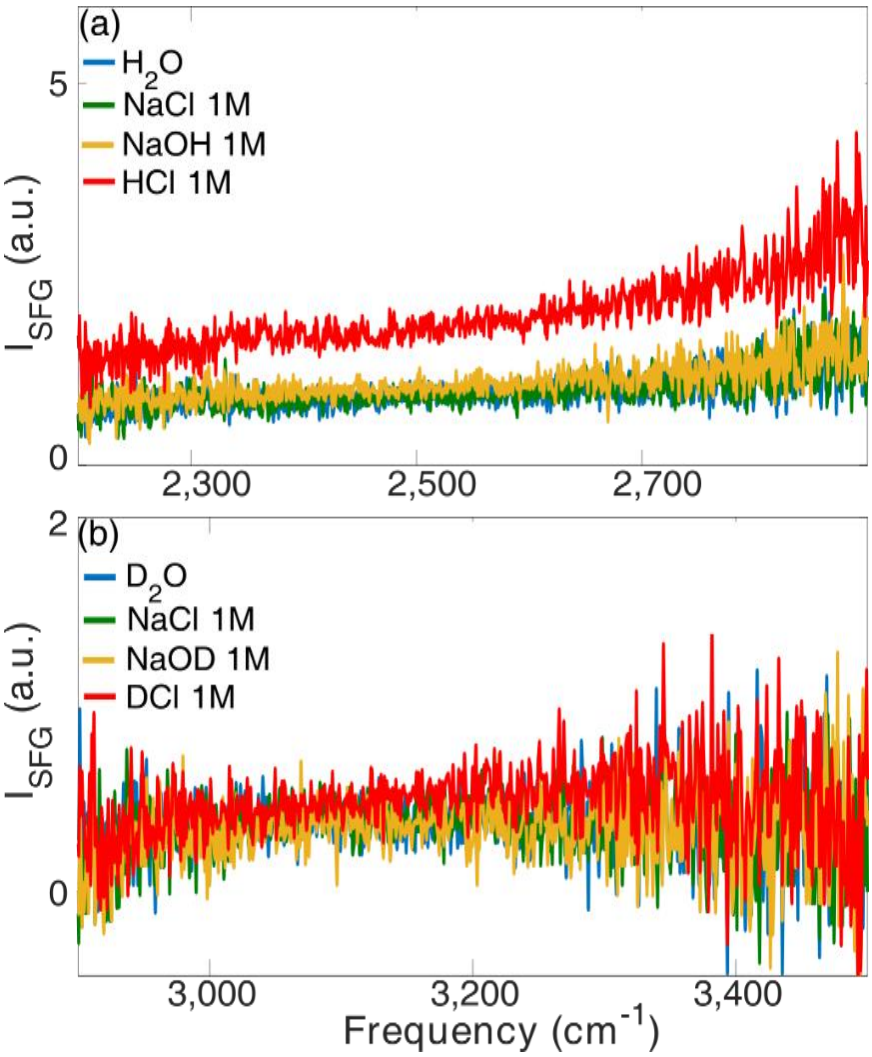

Figure S2: (a) The off-resonant SFG intensity in SSP polarization from the H_2O-air interface in presence of 1M NaCl, 1M NaOH and 1M HCl in the subphase. (b) The off-resonant SFG intensity in SSP polarization from the D_2O-air interface in presence of 1M NaCl, 1M NaOD and 1M DCl in the subphase.

Fig S1 (a) shows the off-resonant SFG response from the H_2O-air interface for pure H_2O and H_2O containing 1M HCl, NaCl and NaOH in the subphase as a function of infrared frequency in the OH stretch vibrational region. Indeed, neat H_2O does not show any resonant contribution. The frequency-independent non-resonant SFG response does not change in the presence of either 1M NaCl or NaOH, but 1M HCl shows a frequency dependent SFG response that is an extended part of the resonance around 3000 cm^{-1}. This means that the non-resonant response does not change at 1M ionic strength and the changes in the hydrogen-bonded OH region in the presence of HCl must be an effect of presence of protons at the surface.

Figure S1 (B) shows a similar experiment: we look at the SFG responses from the D_2O-air interface containing 1M DCl, NaCl and NaOD in the subphase as a function of infrared frequency in the OD stretch vibration region. Indeed, neat D_2O does not show any resonant contribution. Moreover, the non-resonant SFG response does not change in the presence of 1M DCl, NaCl and NaOD. This means that the non-resonant response in presence of protons at the interface is the same as that of pure water suggesting that the rise of the SFG response in presence of 1M HCl may be an effect of appearance of new vibrational modes and/or simply a change of dispersion.

The phase of the 'proton-continuum':

The broad featureless SFG response throughout the range ~2000-3000 cm^{-1} increases in presence of 1M HCl in the subphase (Fig 1, main text), similar to the enhancement of IR and Raman response for HCl in the bulk water. Following the studies in the bulk, this enhancement is identified as an enhancement due to presence of different vibrational modes of the Eigen and Zundel moieties of the proton. The question is if it is appearance of new vibrational modes at the surface similar to the bulk? The enhancement in the SFG intensity response can be an associated modulation in the imaginary and/or real part of the susceptibility (Im and Re $\chi^{(2)}$). The sign of the Im $\chi^{(2)}$ (-/+) in the stretch vibrational region of OH (~3000-3750 cm^{-1}) corresponds to water molecules oriented with their H-atoms pointing towards/away (down/up) from the bulk. In the bend vibration region (~1600 cm^{-1}) a contribution of quadrupoles has been proposed and thereby any direct correlation of the sign of the Im $\chi^{(2)}$ (-/+) and orientation of the water molecules (down/up) has been argued. To the best of the knowledge of the authors, there is no report of any (in-)direct correlation between the sign of the Im $\chi^{(2)}$ (-/+) and orientation of the water molecules (down/up) established in the frequency region ~2000- 3000 cm^{-1}. An effort, therefore, we make to find if there is any correlation between the sign of the Im $\chi^{(2)}$ throughout the proton continuum region with the direction of water alignment at the interface and if it arises due to any vibration of any of the hydronium moieties. It

is important to note that the Re $\chi^{(2)}$ represents the dispersion of the medium and is related to the Im $\chi^{(2)}$ by Kramers-Krönig relationship.

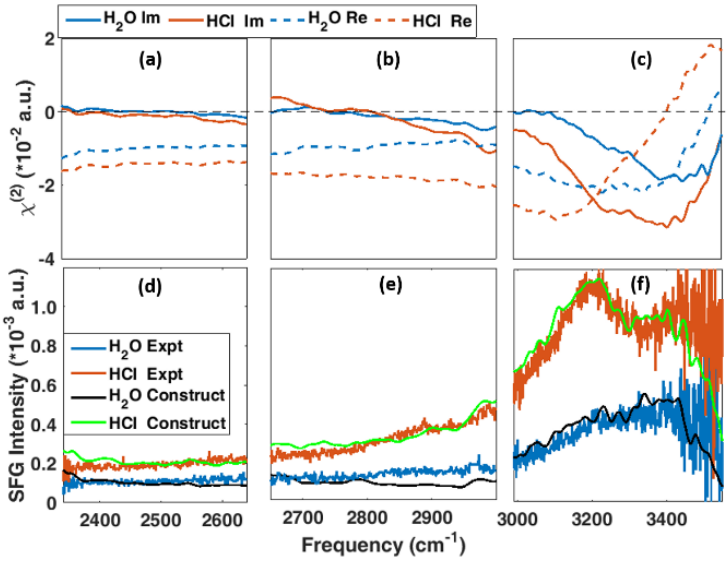

Figure S3: (a-c) Imaginary and real part of $\chi^{(2)}$ spectra as a function of frequency in SSP polarization from pure H_2O-air interface and in presence of 1M HCl in the subphase. (d-f) Experimentally measured SFG intensity overlaid with the intensity spectra constructed from the experimental imaginary and real $\chi^{(2)}$ spectra

Figure S2 (a-c) represent the imaginary (solid lines) and real (dotted lines) of the $\chi^{(2)}$ responses as a function of frequency in SSP polarization from the water-air interface of pure H_2O and H_2O containing 1M HCl in the subphase. Within the experimental noise level the Im $\chi^{(2)}$ response of H_2O seems to be nearly zero in the range ~2350-3000 cm^{-1} and definitely negative in the range ~3000-3400 cm^{-1}. The Im $\chi^{(2)}$ becomes more negative in the range ~2900-3400 cm^{-1} and nearly identical to that of H_2O in the range ~2350-2900 cm^{-1}. The real part of the response in presence of 1M HCl is definitely more negative than that of pure H_2O in the range ~2350-2900 cm^{-1}, implying that the enhanced SFG intensity in this region is dominated by the Re $\chi^{(2)}$ response.

As discussed before, within the OH stretch vibrational range (~3000-3400 cm^{-1}) a more negative Im $\chi^{(2)}$ indicates a higher alignment of H_2O molecules in the presence of the adsorbed protons at the surface compared to that for neat H_2O surface. However, an Im $\chi^{(2)}$ response in presence of adsorbed protons identical to the neat H_2O seems to be inconclusive with respect to any variation in orientation of the H_2O molecules. An absence of any Im $\chi^{(2)}$ response corresponds to an absence of any resonance. Since the non-resonant SFG response of 1M HCl is also the same as that of pure

H_2O, the more negative Re $\chi^{(2)}$ points towards an increased dispersion of interfacial H_2O in presence of 1M HCl in the subpahse.

Figure 6 (d-f) represent the experimental SFG response overlaid with the constructed intensity from the experimental $\chi^{(2)}$ spectra. The constructed intensity spectra match fairly well with the experimental spectra bolstering the fidelity of the data.

Angular distribution of the orientation of the 'free' OD:

As seen before (Fig 1, 4; main text), the intensity of the 'free' OH/ OD decreases in presence of acid in the subphase. This can be a result of a reduction in number of 'free' OH/OD oscillators without a change in their average angular distribution, or vice versa or a combination of both. The $\chi^{(2)}$ is given by the product of number of oscillators (N) and molecular hyperpolarizability (β) averaged over all possible angles of orientations: $\chi^{(2)} = N\langle\beta\rangle$. This means for a constant number of oscillators, a change in the average angular orientation may also result in a reduction of the $\chi^{(2)}$ leading to a decreased SFG intensity. A way to investigate if the observed reduction (Fig 1,4; main text) is due to a combination or either of reduction in number of oscillators and change in average angular distribution is to look at the ratio of the $\chi^{(2)}_{xxz}$ and $\chi^{(2)}_{zzz}$ tensor elements for the 'free' OH/OD. The $\chi^{(2)}_{xxz} = \chi^{(2)}_{yyz}$ and $\chi^{(2)}_{zzz}$ are related to the measured SFG intensity in SSP (S: SFG, S: VIS, P: IR) and PPP (P: SFG, P: VIS, P: IR) polarizations (proportional to $|\chi_{ssp}^{(2),eff}|^2$ and $|\chi_{ppp}^{(2),eff}|^2$, respectively) in the following ways:

$$\chi_{ssp}^{(2),eff} = L_{yy}(\omega)L_{yy}(\omega_1)L_{zz}(\omega_2)\sin\beta_2\chi_{yyz}^{(2)}$$

$$\chi_{ppp}^{(2),eff} = -L_{xx}(\omega)L_{xx}(\omega_1)L_{zz}(\omega_2)\cos\beta\cos\beta_1\sin\beta_2\chi_{xxz}^{(2)} + L_{zz}(\omega)L_{zz}(\omega_1)L_{zz}(\omega_2)\sin\beta\sin\beta_1\sin\beta_2\chi_{zzz}^{(2)}$$

where $L_{ii}(i = x, y, z)$ is the Fresnel factor and β_i is the incidence or reflection angle of the light of frequency ω_i with respect to the surface normal along z axis, to the surface in x-y plane. The

amplitudes of the 'free' OH/OD peak A_{xxz} and A_{zzz} in the $\chi_{xxz}^{(2)}$ and $\chi_{xxz}^{(2)}$ spectra, respectively are related to $<\cos\theta>/<\cos^3\theta>$ via

$$\frac{A_{xxz}}{A_{zzz}} \propto \frac{(1+r) < cos\theta > -(1-r) < \cos^3\theta >}{2r < cos\theta > +2(1-r) < \cos^3\theta >}$$

in the slow motion limit. For the slow motion limit, the decay of the orientational memory of the free OH/OD is much slower than its vibrational relaxation. *r* is given by the ratio of the transition polarizability $\alpha_{\parallel}/\alpha_{\perp}$, where $\parallel$ and $\perp$ denote directions parallel and perpendicular to the OH bond, respectively.

Therefore, we have carried out the SFG measurements with SSP and PPP polarization combinations at the D_2O-air interface for pure D_2O and D_2O containing 2M DCl in the subphase. The intensities are then fitted with an established Lorentzian model to extract the areas of the 'free' OD vibration.

Since the intensity SFG response is proportional to the square of the $\chi^{(2)}$, all the information regarding the orientation of the dipole moment of water given by the sign of the $\chi^{(2)}$ is lost. In order to obtain the orientation information too we have also experimentally measured the PS-SFG and extracted the Im and Re $\chi^{(2)}$ values.

The reason to use 'free' OD instead of 'free' OH is to reduce the intensity and phase uncertainties in measurements that may arise from absorption of IR intensity by water vapor around 3700 cm^{-1} region and faster evaporation rate of H_2O compared to that of D_2O.

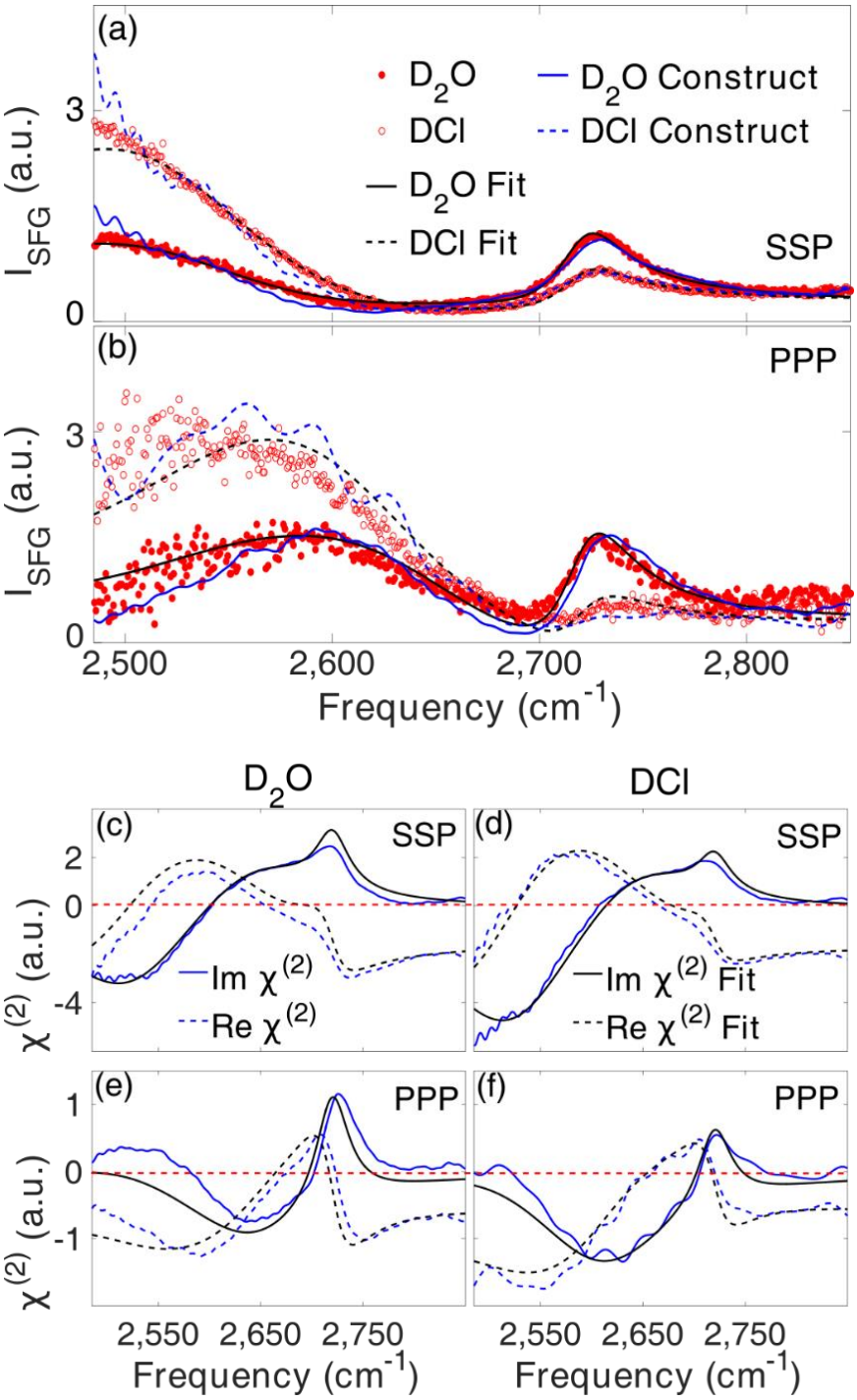

Figure S4: SFG intensity spectra at D_2O-air interface for pure D_2O (red closed circles) and 2M DCl (red open circles) in SSP (panel a) and PPP (panel b) polarizations. The fits to the intensity spectra are shown in black in both panel a and b. The intensity spectra constructed from the imaginary and real $\chi^{(2)}$, obtained with phase resolved SFG experiments, are shown in blue in both panel a and b. The experimental imaginary and real $\chi^{(2)}$ SFG spectra are shown in blue in panel c-f. The imaginary and real $\chi^{(2)}$ SFG spectra calculated from the fits of intensity spectra are overlaid on the experimental imaginary and real SFG responses.

Figure S3(a-b) show SFG intensity as a function of infrared frequency in SSP and PPP polarization combinations respectively from a D_2O- air interface for neat D_2O and D_2O containing 2M DCl in

the subphase. The spectra shown with red circles correspond to the experimental intensity spectra. The black lines correspond to the fit to these experimental spectra. The spectra in blue correspond to the conventional SFG intensities constructed from the experimental imaginary and real $\chi^{(2)}$ SFG responses obtained using phase resolved SFG experiments. Figure 1(c-f) show the experimental imaginary and real parts of $\chi^{(2)}$ spectra (in blue) along with the imaginary and real parts of $\chi^{(2)}$ (in black) calculated from the fits shown in panel a and b.

Each spectrum has a sharp response at ~2720 cm^{-1} and a broad response that extends into low frequency region. The sharp feature is the vibration of the non-hydrogen bonded OD oscillators that point away from the surface into the air ('free' OD). The broad feature is the vibration response of hydrogen bonded OD groups that broadly vary in hydrogen bond strength. Compared to that of pure D_2O, the intensity of the free OD decreases and the hydrogen bonded region increases upon addition of 2M DCl into the subphase.

Since, both the experimental intensity and $Im\chi^{(2)}$ spectra comprise of interfering resonant vibrations of different signs; we have fitted the experimental homodyne spectra using an established procedure under the constraint that the shape of the imaginary and real $\chi^{(2)}$ of the fits match the same that are extracted from the experimental spectra. The areas of the "free OD" thus obtained from the fits are used to calculate the ratios, A_{xxz}/A_{zzz}. The calculated ratios are 0.42 and 0.41 for D_2O and 2M DCl respectively.

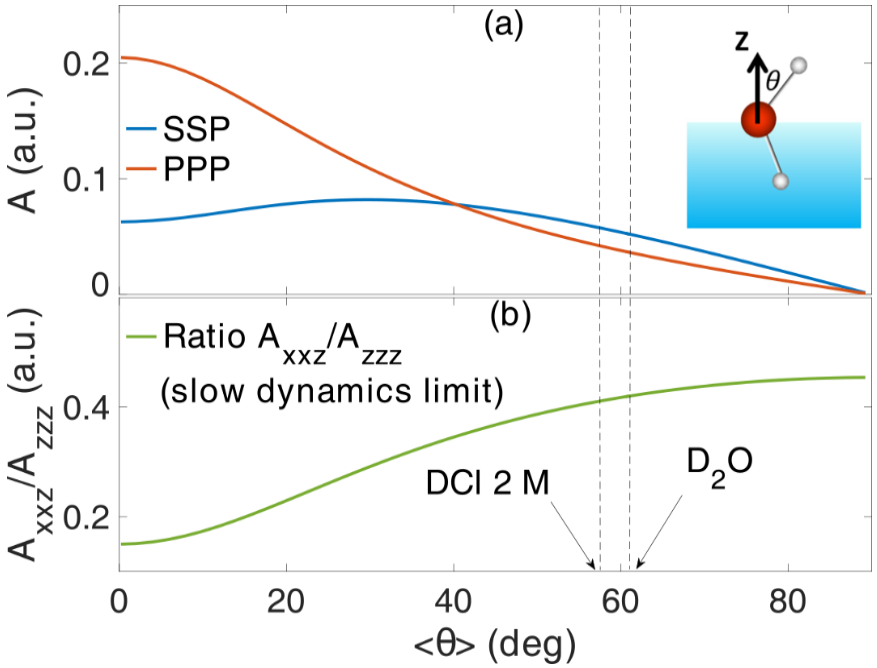

Figure S5: (a)The area of the SFG response of the "free OD" in SSP (red curve) and PPP (blue curve) polarization as a function of the angle the "free OD" makes with the surface normal. (b) The ratio of the xxz and zzz components of the areas as a function of the angles in slow dynamics limit.

Figure S4 (a) shows the calculated area of "free OD" stretch vibration in SSP and PPP polarizations as a function of average angle that "free OD" makes with the surface normal. It shows that the area in SSP polarization depends on the angles very differently from that in PPP.

Figure S4 (b) shows the calculated A_{xxz}/A_{zzz} from the A_{ssp}/A_{ppp} as a function of average angle of the free OD with respect to the surface normal in slow dynamics limit. The ratios for D_2O and 2M DCl (0.42 and 0.41 respectively) correspond to the angles 61.3^0 and 57.5^0, i.e. a difference of ~4^0 which is negligible given the noise of the measurement and uncertainties of the fits. Therefore, our results show that the average angular distribution of 'free' OD does not change in presence of acid, but only the number of oscillators decreases.

Individual set of spectra (Fig 3(b-d)):

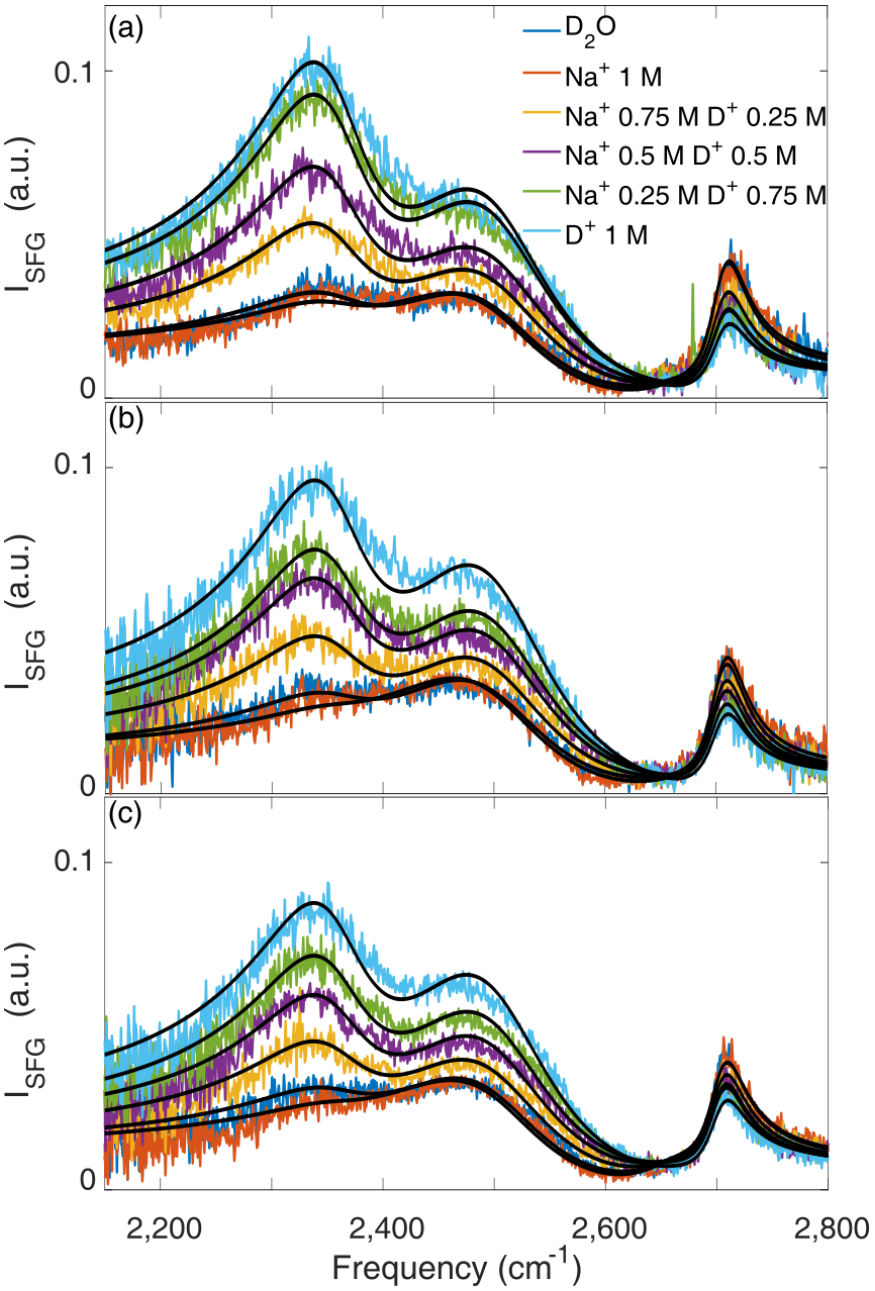

Figure S6: (a-c) The SFG responses in SSP polarization from air –D_2O interface for pure D_2O and D_2O containing NaCl and DCl at different concentration ratios obtained in three separate experiments The black lines are fits to the spectra.

Chapter 7

The effect of protons on the vibrational dynamics of the water-air interface

Abstract:

Despite being ubiquitous in nature and having paramount importance in several industrial, biological and environmental processes, our understanding of hydrated proton and its effect on the water at the interface is incomplete. Here, using surface-specific time-resolved vibrational spectroscopy, we probe the response of the water molecules at water-air interface enriched with hydrated protons. We observe that following the vibrational excitation and relaxation on sub-picosecond time scales, the infrared excitation also affects the SFG response on ~125 ps time scale. This effect scales with the concentration of hydrated protons in the system. We attribute this slow transient signal to the formation of a new equilibrium between interfacial and bulk protons, following the quasi-instantaneous temperature jump following vibrational relaxation of the interfacial water molecules.

Introduction:

Hydrated protons are not only ubiquitous in nature, but they are also tremendously important in various industrial, biological and environmental processes[124-126]. Because of such importance, a great deal of research has focused on understanding the molecular-scale structure and dynamics of hydrated protons in water.

The structure of hydrated proton is generally understood in terms of two key forms, namely the Eigen ion, a single proton solvated by a water molecule to produce a hydronium ion, that is further solvated by three other water molecules ($H_3O^+(H_2O)_3$ or $H_9O_4^+$) and a Zundel ion, a single proton equally shared by two water molecules ($H_5O_2^+$). An in-depth understanding of these two key conformations of hydrated protons has been obtained through gas-phase protonated water cluster studies at low temperatures, which have identified vibrational features of both the Zundel and Eigen motifs[26, 127]. In low-temperature gas-phase studies of small clusters, it has been relatively easy to identify the different protonated species since the small number of degrees of freedom give rise to specific normal modes of vibrations and result in narrow IR spectra.

As the number of hydrating water molecules grows in number beyond 6 in protonated water clusters, multiple conformers coexist[128], making the interpretation of the spectrum difficult. This difficulty increases in the liquid phase because extensive hydrogen bonds exist and the different conformers can interconvert in ultrashort time scale. Indeed pump-probe[28] and 2D-IR[27] studies in aqueous solution of acids have identified sub-ps time scales of such conformational interconversions.

Compared to hydrated protons inside the bulk, hydrated protons at the water surface are predicted to have notably different properties, since the dimensionality of the surface is nearly 2D as opposed to 3D bulk water. Probing the hydrated protons and the hydrated water at the surface while suppressing the responses of the overwhelmingly large number of molecules inside the bulk is a challenging task. The vibrational responses of surface-only species can be obtained with Sum Frequency Generation (SFG) spectroscopy. In SFG, a broadband (*BB*-) *IR* pulse, which is in resonance with the vibrations of the water molecules, is overlapped with a non-resonant *VIS* pulse at the surface of water. The *IR* pulse can create a resonant polarization between the ground and the first excited vibrational states of, typically, the OH stretch vibration. This polarization can interact with the *VIS* field, to generate a polarization that radiates an electric field whose frequency is equal to the sum of the two incoming frequencies. Due to the selection rules of SFG spectroscopy, centro-symmetric bulk water does not produce any SFG response. Therefore, an SFG spectrum effectively represents the vibrational response of the molecules only at the surface of the water. Indeed, SFG spectroscopy on water-air interface for pure water[97, 98], and water containing salts[10, 83, 129] and acids[11, 12, 14, 130] have provided detailed understanding of the structural similarities/differences of the ion-enriched water surfaces.

However, SFG spectra of aqueous surfaces in the OH stretch region are typically broad, similar to IR/Raman spectra of bulk water or aqueous electrolyte solutions, largely due to inhomogeneous broadening. An inhomogeneous broadening is caused by multiple reasons such as the inhomogeneous hydrogen bonding configurations[37], intermolecular vibrations[38, 39], coupling amongst delocalized symmetric and asymmetric modes[40, 41], and Fermi resonances caused by the coupling with bending overtones[43]. Besides the inhomogeneous broadening there exists considerable amount of homogeneous broadening, caused by time dependent decay of amplitude and phase coherence amongst different molecular oscillators. The homogeneous linewidths provide insights into the structural dynamics of the hydrogen bonding networks of water and the dynamics

of vibrational energy redistribution. Time-Resolved (TR-) SFG spectroscopy, can experimentally access these time-related parameters.

In TR-SFG spectroscopy, a narrowband *IR* pulse excites ("pumps") a population from the ground state to the first vibrationally excited state. The "probe" pair (*BB-IR* and *VIS*) monitor the transient changes in the system caused by the pump pulse, as a function of time delay between the pump and the probe pulses. A number of significant studies have looked into the vibrational dynamics at water-air interface of pure water[46, 48, 131-135] and water containing alkali halide salts[136-138].

Therefore, we have significant knowledge about the vibrational dynamics of pure and halide anions-rich water-air interface. However, the same is not true for hydrated proton-rich water-air interface. Given the fact that hydrated proton also has strong surface propensity, it would be interesting to know how (dis-)similar the vibrational dynamics of a hydrated proton-rich water-air interface is, relative to that of pure water. Here, we investigate the TR-SFG responses from the DCl–air interface of different acid concentrations as a function of pump-probe time delays. We study deuterated water D_2O, and deuterated HCl, since our experimental setup works better in the OD stretch region than the OH stretch region. We find that the SFG intensity from the hydrated proton-rich water surface decays on a hundred ps time scale. Our results indicate that the hydrated protons depart from the water surface as a result of the transient heating caused by the pump pulse.

Results and Discussions:

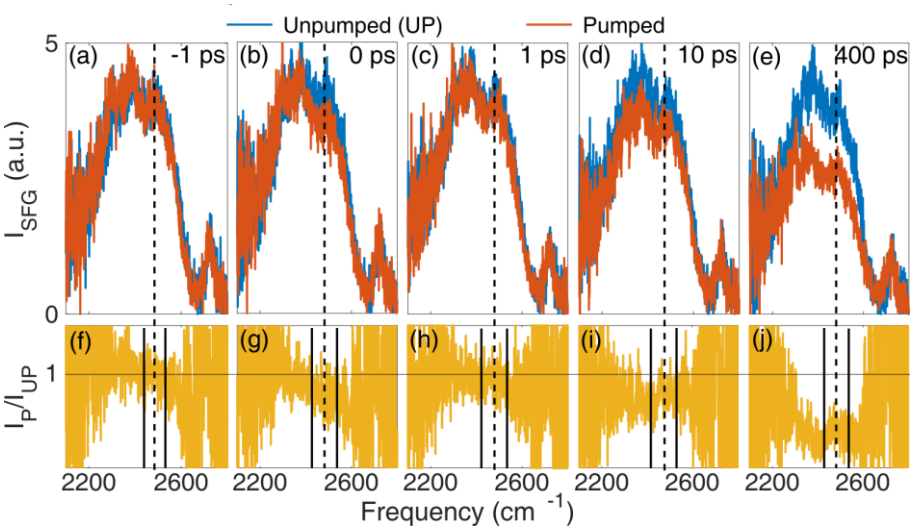

Figure 16: (a-e) The unpumped and pumped SFG signal intensities as a function of frequency in SSP (S: SFG, S:VIS, P: IR) polarization from 1 M DCl-air interface at -1, 0, 1, 10 and 400 ps pump-probe time delays. (f-j) The ratio of pumped to unpumped SFG response at corresponding time delays. The dotted black vertical lines represent the center of the pump-frequency. The solid vertical lines represent the boundaries of integration (details in the text).

Figure 1 (a-e) depicts the changes in the SFG intensities as a function of frequency recorded from the surface of a 1 M DCl solution, In presence and absence of the *IR*-pump pulse centered at ~2500 cm^{-1}, at five exemplary pump-probe time delays. Figure 1 (f-j) depicts the ratios of the pumped (P) to unpumped (UP) SFG intensities.

At negative time-delays, the probe-pair (*BB-IR* and *VIS*) interact with the DCl-air interface before the pump, producing an identical pair of pumped and unpumped SFG responses of the interfacial D_2O molecules. At zero time delay, the probe pair interact with the D_2O molecules together with the pump. The pump pulse centered at ~2500 cm^{-1} depletes the ground vibrational state and transfers a population into the first excited vibrational state. Thus, a smaller number of oscillators in the ground state interact with the probe pair and produce a slightly weaker SFG response. Therefore, the intensity of the pumped SFG spectrum (red) is less than the unpumped spectrum (blue) at ~2500 cm^{-1} (panel (b)). With the advancing pump-probe time-delay, the transferred population gradually relaxes and repopulates the ground state, on sub-picosecond timescales; hence, the pumped-SFG has recovered its intensity after ~1 ps (panel (c)).

Interestingly, at substantially later time-delays, e.g. ~2ps and beyond, the pumped SFG intensity decreases again (panel (d)). At 400 ps pump-probe delay, the pumped SFG intensity is significantly less than the unpumped intensity (panel (e)).

A reduction in SFG intensity indicates a reduction in the alignment of D_2O molecules at the interface. The D_2O molecules at the interface are less strongly aligned at 400 ps time delay compared to at -1, 0, and 1 ps time delays, following the vibrational relaxation process. To shed more light on the loss of alignment of the interfacial D_2O molecules, we monitored the relative

intensities of the pumped and unpumped SFG responses as a function of pump-probe time delays for different concentration of DCl, i.e. hydrated proton at the interface.

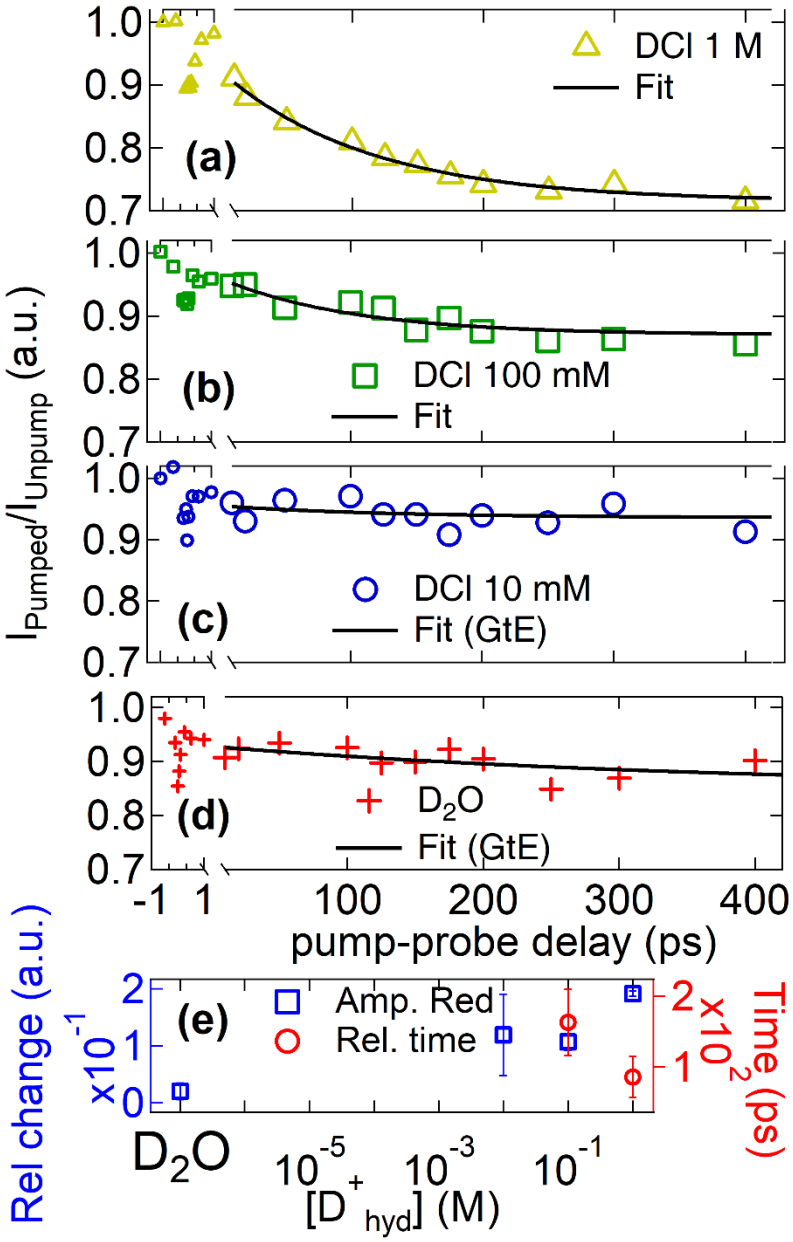

Figure 17: The ratio of integrated SFG intensity (2500 ±30 cm^{-1}) of pumped to unpumped response in SSP polarization at D_2O-air interface for (a) 1 M DCl, (b) 100 mM DCl, (c) 10 mM DCl, and (d) pure D_2O pumped at ~2500 cm^{-1} as a function of pump-probe time delays. The black traces are fits using a single exponential model. Only the ratios after10ps time delays have been fitted with this model. The fits to 10 mM DCl and D_2O are guide to the eye (GtE) and lack any physical/statistical meaning. (e) The difference of amplitudes between 10 ps and 400 ps (blue squares, left axis) as a function of DCl concentration in D_2O. The lifetimes of the dynamic process at 2500 cm^{-1} for 100 mM and 1 M DCl (red circles, right axis). The error bars represent the standard errors obtained by averaging over two data sets.

Figure 2 (a-d) depicts the ratios of pumped to unpumped SFG responses as a function of pump-probe time delay, pumped at ~2500 cm^{-1}, from DCl solution-air and pure D_2O-air interface. The ratio is ~1 at -1 ps in accordance with the equal intensities of both the pumped and unpumped spectra. With advancing time delay, it decreases and reaches minima at ~0 ps due to the population depletion in the ground vibrational state. Soon after the ratio increases due to the relaxation process. The ratio recovers close to 1. The ratio decreases again after ~2ps for 1 M DCl. The time-dependent relative reduction is less prominent for 100 mM DCl and absent for 10 mM DCl and pure D_2O. For 10 mM DCl and pure D_2O the ratio remains nearly constant at ~0.95.

A possible reason of such intensity reduction may be heat. In a pump-probe SFG experiment, the excitation process is not surface sensitive. The pump pulse excites the vibration of water molecules ~1 μm into the bulk. Following relaxation, this bulk excitation is converted into heat within a few picoseconds. Hence, the excitation with a femtosecond *IR* pulse leads to local heating of the water. The pump-induced temperature elevation is typically of the order of ~10 K. An important question, at this point, is whether the intensity reduction is caused by the pump-induced temperature elevation of the solutions. Therefore, we have raised the temperature of the solutions externally,

i.e., in steady-state, by 6 and 10 K to compare the relative changes in SFG intensity due to elevation of temperature with the changes seen in time-resolved SFG measurements.

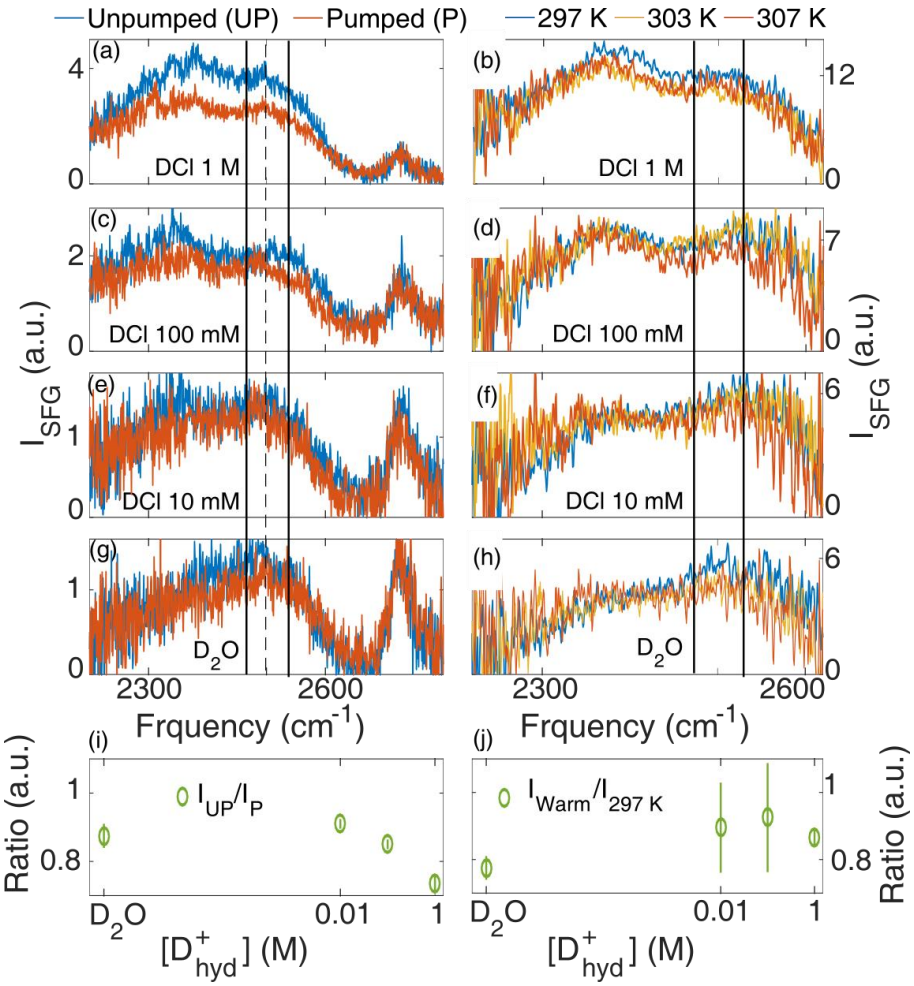

Figure 18:(a,c,e,g) The unpumped and pumped SFG intensities as a function of frequency in SSP polarization from D_2O-air interface containing different concentration of DCl in the subphase at 400 ps pump-probe time delay. (b,d,f,h) The SFG intensity at three different temperatures for corresponding sample solutions. The dotted black vertical lines represent the center of the pump-frequency. The solid vertical lines represent the boundaries of integration. (i) The ratios of integrated intensities of pumped to unpumped spectra as a function of hydrated proton concentration in the solution. The error bars represent standard errors obtained from two separate data sets. (j) The average ratios of integrated intensities of spectra at two higher temperatures to spectra at 297 K as a function of hydrated proton concentration in the solution. The error bars represent standard errors of the averages.

Figure 3 (a,c,e,g) shows the changes to the SFG intensities from D_2O-air interface in the presence of DCl at different concentrations in the sub-phase in response to the *IR*-pump pulse centered at ~2500 cm^{-1} as a function of frequency at 400 ps pump-probe time delay. The relative reduction of the SFG intensity of the pumped spectrum compared to the unpumped spectrum decreases with

decreasing concentration of DCl in the solution. Clearly, the pumped induced effect is strongly correlated to the DCl concentration of the solution.

Figure 3 (b,d,f,h) shows the changes to the SFG intensities from D_2O-air interface in the presence of DCl at different concentrations in the sub-phase in response to the elevation of the temperature by 6 and 10 K. Upon elevation of temperature, the SFG intensity reduction is little to none, regardless of the DCl concentration of the solution.

Figure 3 (i) shows that the relative reduction of pumped intensity increases with increasing hydrated proton concentration in the solution, while the relative reduction due to temperature elevation is nearly the same for all samples (Fig 3 (j)). This indicates that the substantial SFG intensity reduction in time-resolved experiment does not seem to originate from temperature elevation and correlates with the interfacial hydrated proton concentration.

A reason of such a substantial reduction of intensity upon the pumping process might be because the protons leave the surface, hence the interfacial D_2O molecules reorganize themselves such that they are less strongly aligned at the interface on a timescale of ~100 ps. We have previously established that protons at the interface displace the free OH groups. Therefore, to test this hypothesis, we investigated whether the number of free OD oscillators increase upon the pumping process. To this end, we have quantified the amplitudes of the different resonances in both pumped and unpumped spectra for all concentrations of DCl and pure D_2O with a well-established model, using Lorentzian lineshapes[9]. According to this fitting procedure, the SFG intensity, I_{SFG} is proportional to the square of the second-order susceptibility $\chi^{(2)}$ of the sample and intensity of the incoming *IR* and Visible (*VIS*) light:

$$I_{SFG} = \left|\chi^{(2)}\right|^2 I_{IR} I_{VIS} \qquad (1)$$

The overall $\chi^{(2)}$ is a sum of a non-resonant term, $\chi_{nr}^{(2)}$ (comprising of a non-resonant amplitude A_{nr} and a non-resonant phase φ_{nr}) and resonant ($\chi_r^{(2)}$) contribution(s). Each $\chi_r^{(2)}$ is expressed in terms of a Lorentzian line shape with area A_n, central frequency ω_n, and bandwidth Γ_n (half-width at half maximum)

$$\left|\chi^{(2)}\right|^2 = \left|\chi_{nr}^{(2)} + \chi_r^{(2)}\right|^2 = \left|A_{nr}e^{i\phi_{nr}} + \sum_n \frac{A_n}{\omega_n - \omega_{IR} + i\Gamma_n}\right|^2 \quad (2)$$

First, the unpumped spectrum for the 1 M DCl is fitted with four resonant peaks and a frequency-independent non-resonant amplitude and phase. The peak positions (2366, 2512, 2650 and 2717 cm^{-1}) and FWHM bandwidths (140, 180, 130 and 36 cm^{-1}) of all the peaks, as well as the non-resonant phase (0.0 rad) from this fit, are subsequently used in the fits of the other pumped and unpumped spectra of different concentrations of acid and pure D_2O. The amplitudes of the 2650 cm^{-1} peak and non-resonant response are held constant between pumped and unpumped spectra. All other amplitudes are free parameters.

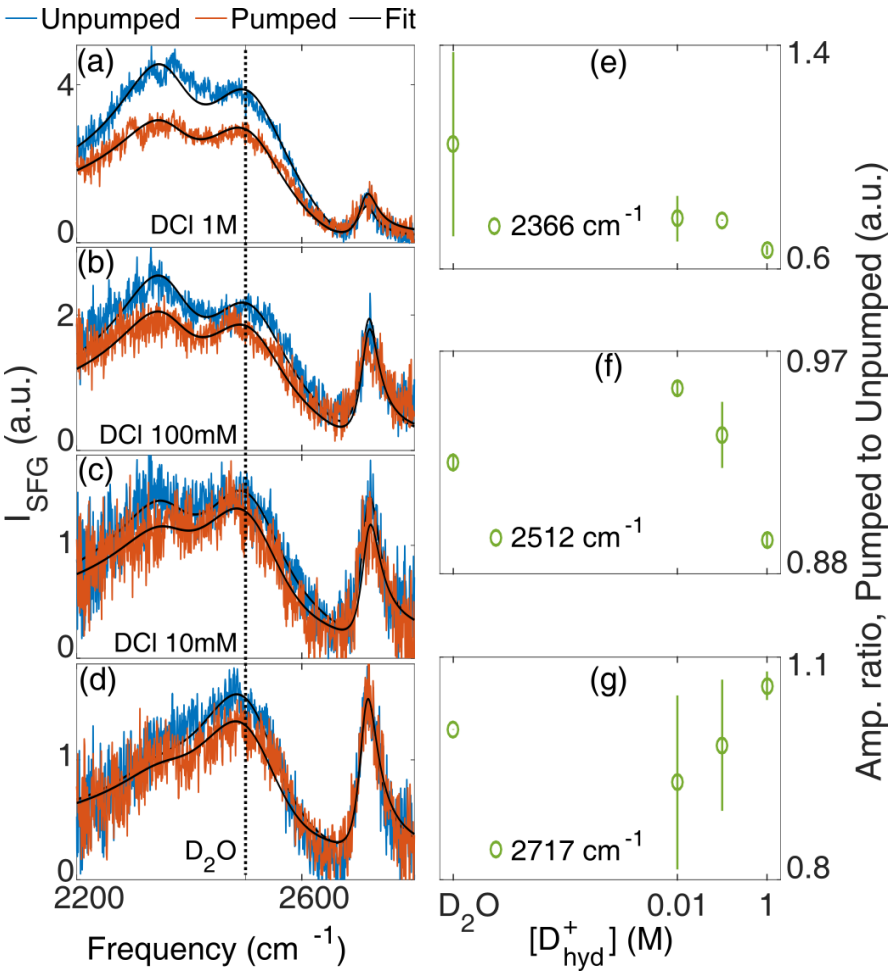

Figure 19: (a-d) The unpumped and pumped SFG intensities as a function of frequency in SSP polarization from the D_2O-air interface containing different concentration of DCl in the subphase at late pump-probe time delays. These spectra are produced by averaging spectra at six different late time delays (ranging from 150 to 400 ps) in order to obtain better signal to noise ratio for fitting. The black traces represent the fits to the spectra. The vertical dotted line represents the center of the pump frequency.

(e-g) The ratio of amplitudes of the resonant (2717, 2512, 2366 cm^{-1}) responses in the pumped spectra to unpumped spectra obtained from fitting.

Figure 4 (a-d) represent the SFG intensities as a function of frequency from the D_2O-air interface in the presence of DCl at different concentrations in the sub-phase along with the fits. Panel (e-g) depict the amplitudes of the resonant responses as a function of the DCl concentration in the subphase.

The amplitudes of the hydrogen-bonded regions (2512 and 2366 cm^{-1}) are smaller in the pumped spectra than in the unpumped spectra for all samples. The 2366 cm^{-1} peak amplitude in the pumped spectrum is similar to unpumped spectrum for pure D_2O (panel (e)) but decreases significantly by ~35% in presence of acid. The reduction of 2512 cm^{-1} peak (panel (f)) is ~5-7 % for D_2O, 10 mM, and 100 mM DCl solutions, but is ~10% for 1 M DCl. This indicates that the hydrogen-bonded water molecules become randomly oriented at long time delays and the extent of loss of alignment is larger for elevated concentrations of acid present in the solution.

The amplitude of the free OD (2717 cm^{-1}) remains nearly the same in both the pumped and unpumped spectra of D_2O (panel (g)) implying that the number of free ODs does not change upon pumping. However, it is ~6% larger for 1 M DCl, implying that the number of free ODs increases at late time delays. For, 10 and 100 mM DCl, the noise is too large to conclude anything. All of the above observations bolster the hypothesis that the hydrated protons leave the interface.

In order to understand the mechanism of proton departure from the interface we turn our attention back to the dynamics presented in figure 2. The long-time dynamics can be fitted with a single exponential, the inverse of the exponential decay constant of which represents the relaxation time of this dynamics and shown in figure 2 (e). For 100 mM and 1 M DCl, the time constant is ~125±35 ps. In absence of any decaying dynamics in the D_2O and 10 mM DCl, the fit diverges. This implies that the slow, ~125 ps scale dynamics is related strongly to presence/absence of hydrated protons at the surface and can indeed be rationalized by considering disappearance of the hydrated protons from DCl-air interface.

The single exponential fit implies that the disappearance of hydrated protons from the surface may be a uni-pathway process. Proton hopping through Grothuss mechanism is less likely to be the cause of such dynamics, since the reported time scale[139, 140] of the proton hop considering Grothuss

mechanism is ~1±0.5 ps, which is at least two orders of magnitude faster than the time scale we find here. Within ~2.5 Å from the instantaneous water-air interface, hydrated protons reside by constructing long chains of hydrogen bonds with neighboring water molecules that run parallel to the instantaneous interfacial topographical structure[81, 141]. A possibility, therefore, could be that the interfacial water structure is substantially reorganized due to the heat in such a way that it facilitates the departure of hydrated protons from the surface by breaking such proton wires at the surface. Since the diffusion constant of hydrated proton (~1.02±0.78 $Å^2$/ps)[140] is significantly higher than that of chloride (0.15 $Å^2$/ps)[142] a departure of proton from the interfacial region would result in less positive charge and possibly a relative abundance of negative charges at the interface leading to less aligned water molecules. Therefore, at ~10 ps and beyond time delays, the SFG process probably monitors a quasi-equilibrium state at the surface that develops over our experimental time window of a few hundred ps. This process is schematically represented in figure 5.

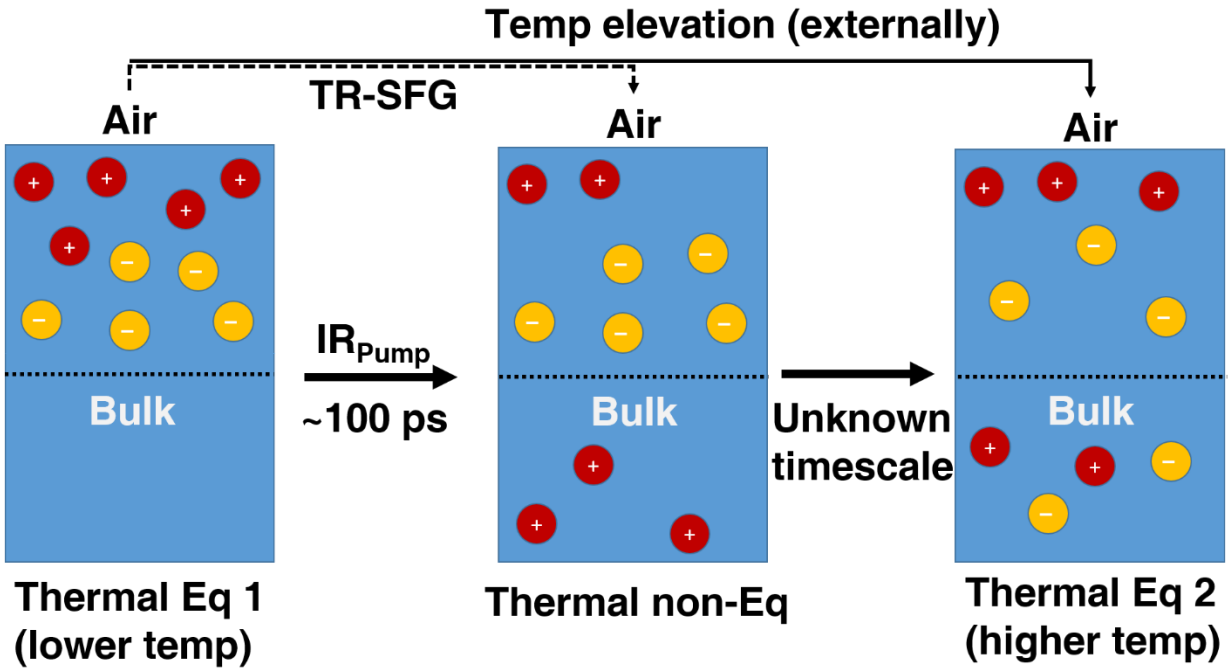

Figure 20: ***Schematic representation of the non-equilibrium state created by the IR_{pump} pulse and its subsequent recovery to the thermodynamic equilibrium state.*** *The IR_{pump} pulse excites the interfacial D_2O molecules that are aligned due to the charges present at the interface in thermodynamic equilibrium (Thermal Eq 1). Upon vibrational relaxation, due to the released heat the protons (red balls) depart from the surface creating a non-equilibrium condition (Thermal non-Eq). In such a non-equilibrium, at the interface, possibly there are larger number of anions (yellow balls) present. Water molecules are less aligned due to less hydrated protons at the surface. The thermodynamic equilibrium is restored in an unknown time scale at a higher temperature and contains fewer ions at the interface. The black dotted horizontal line represents an apparent division between bulk and interface.*

However, since the hydrated protons have a strong surface affinity, they possibly come back to the surface several 100 ps later and settle into thermodynamic equilibrium again. The thermodynamic non-equilibrium condition cannot be reached by simply raising the temperature of the solution externally. Therefore, the temperature-dependent study shows the effect when the thermodynamic equilibrium is already re-established, while the time-resolved experiment captures a glimpse of the thermodynamic quasi-equilibrium condition.

Conclusion:

In summary, we have observed remarkably slow dynamics of the SFG intensities that decay on a hundred ps time scale, recorded from a hydrated proton-rich water surface. We study the origin of such decaying dynamics by varying the acid concentration of the solution. We find strong evidence that the IR-pump process causes depletion of the hydrated protons from the water-air interface. A hypothesis for such a depletion is a modification of the hydrogen bonding network and/or the topology of the instantaneous surface by the heat released due to the vibrational relaxation process followed by the IR-pump. Such heat induced modifications possibly disrupt the proton wires and facilitates the release of hydrated protons from the surface.

Chapter 8

Conclusion and Outlook

Hydrated proton along with water are ubiquitous in nature and play key roles in many industrial, biological, and environmental processes. In this thesis, we have investigated the effect of hydrated protons on the structure and dynamics of water-air interface. The results presented in this thesis enhance our knowledge about water surfaces enriched with hydrated protons. However, a lot of questions remain unanswered even after these results. The following paragraphs briefly summarize the main results from each chapter and present ideas for experiments that might answer some of the open questions.

In chapter 4 we have presented the relative surface affinity of hydrated proton and sodium ion at nominally neutral water-air interface and water surface covered with a negatively charged surfactant monolayer. We have investigated the alignment of the heavy water molecules at these two interfaces in presence/absence of sodium and hydrated protons in the sub-phase using the conventional SFG spectroscopy. We have found out that hydrated proton has marginally lower surface affinity than sodium at the negatively charged surfactant covered water-air interface as opposed to having a substantially higher surface affinity at a nominally neutral water-air interface. Evidently, the surface affinity of hydrated protons depends on the type of interface. Aside from affecting the alignment of water molecules at the surfactant covered aqueous interface, hydrated protons and sodium seem to have different effects on the alignment of the alkyl chains of the surfactants. It would be interesting to know if such an effect scales with the alkyl chain length. In this study, we have compared the effects of hydrated proton with uni-positive ion sodium. Although, a bare proton itself is unipositive, it has much higher charge density than other unipositive alkaline metal ions. Partly due to that, the proton remains in strongly hydrated forms, e.g., hydronium, Eigen, Zundel etc. Therefore, it would be worth comparing hydrated proton's behavior with the doubly charged alkaline earth metal ions (e.g. Mg^{2+}) to understand, how (dis-)similar effects hydrated protons have, compared to that of the alkaline earth metal cations, on the structure of interfacial water. This would help us understand how the modulations in interfacial

water structure scales with the charge density of the electrolyte present in the solution.

In chapter 5, using conventional SFG spectroscopy we have investigated the bulk concentrations at which the hydrated proton and its conjugate base hydroxide show significant surface affinity. Thus, we have quantified that hydrated proton starts to significantly perturb the alignment of D_2O molecules at the D_2O-air interface at a bulk concentration of ~2.3 mM, that is nearly two orders of magnitude lower than that of hydroxide. Thus, we understand hydrated proton has more surface affinity than hydroxide at water-air interface. We have also seen that the spectral changes are different for different ions: for hydrated protons, the lower frequency side of the SFG spectrum gains intensity and for hydroxide, the higher frequency side of the SFG spectrum loses intensity. We have attributed this difference to the differences in hydrogen bonding abilities of the two conjugate acid-base pair. It would be worthwhile to connect the subsequent changes in the bulk water with the changes occurring at the surface. A simultaneous benefit and challenge of SFG spectroscopy is that the isotropic average of the transition moments is zero, which makes it (aqueous-) surface specific. It also means that a decrease (increase) in SFG response occurs due to surface-desorption (-adsorption) of molecules or a more disordered (ordered) arrangement at the surface. Now since, the SFG cross-section is proportional to the product of the IR transition dipole moment and Raman transition polarizability, a mode that is weak in both IR and Raman spectrum, but produces strong SFG response would come from a strongly oriented species at the surface and vice versa. A combined IR-Raman bulk probe can therefore has the potential for surface-bulk hetero-spectral correlation with SFG.

A way to proceed would be to correlate the IR and Raman spectra with the SFG intensity and/or $Im\chi^{(2)}$ spectra. The IR absorbance, Raman scattering, and vibrationally resonant SFG, the imaginary components of the respective susceptibilities can be written as:

$$Im\chi_{ii}^{(1)} \approx N \sum\nolimits_n \langle \left(\frac{\partial \mu_i}{\partial Q}\right)^2 \rangle_n \left(\frac{\Gamma_n}{(\omega_n - \omega_{IR})^2 + \Gamma_n^2}\right) \approx N \sum\nolimits_n A_{IR,n} \left(\frac{\Gamma_n}{(\omega_n - \omega_{IR})^2 + \Gamma_n^2}\right)$$

$$Im\chi_{ijij}^{(3)} \approx N \sum\nolimits_n \langle \left(\frac{\partial \alpha_{ij}}{\partial Q}\right)^2 \rangle_n \left(\frac{\Gamma_n}{(\omega_n - \Delta\omega)^2 + \Gamma_n^2}\right) \approx N \sum\nolimits_n A_{Raman,n} \left(\frac{\Gamma_n}{(\omega_n - \Delta\omega)^2 + \Gamma_n^2}\right)$$

$$Im\chi_{ijk}^{(2)} \approx N\sum_n \langle\left(\frac{\partial\alpha_{ij}}{\partial Q}\frac{\partial\mu_i}{\partial Q}\right)\rangle_n \left(\frac{\Gamma_n}{(\omega_n-\omega_{IR})^2+\Gamma_n^2}\right) \approx N\sum_n A_{SFG,n}\left(\frac{\Gamma_n}{(\omega_n-\omega_{IR})^2+\Gamma_n^2}\right)$$

where, N is the number density of the oscillators, μ is the dipole moment, α_{ij} is the polarizability, Q is the normal mode, ω_n is the frequency of the nth vibrational mode, Γ is the homogeneous linewidth, ω_n is the frequency of IR pulse, $\Delta\omega$ is the Stokes shift, and $A_{q,n}$ is the amplitude of the q-type transition of the n-th mode.
If we define the oscillator strength in the combined IR-Raman bulk signal as:

$$A_{IR*Raman} = \sqrt{A_{IR} * A_{Raman}}$$

and correlate it with A_{SFG}, we shall be able to tell that an SFG transition is weak simply because one or both of the corresponding IR or Raman cross-sections are small.

In chapter 6, we have focused on the structure of hydrated proton itself and using both conventional and phase-sensitive SFG spectroscopy combined with computational calculation established that both Eigen and Zundel types of moieties coexist at the water-air interface. Furthermore, we have quantified the Gibbs free energy of adsorption of hydrated proton at the interface to be ~1.3 kcal/mol, which is in agreement with certain theoretical calculations.

In chapter 7, using time-resolved SFG spectroscopy we have unveiled the effects of hydrated proton on the vibrational dynamics of D_2O-air interface. We find that due to the excitation ('pump') process, following the vibrational excitation and relaxation a different type of dynamics occur as evidenced by the slow decay of the SFG intensities with time. We attribute this dynamics to formation of a new quasi-equilibrium state between the surface and the bulk proton. However, due to the low signal to noise ratio (SNR), it has been difficult to explore the effect of hydrated protons on the vibrational excitation-relaxation process that occur in sub-ps time scale. Improving SNR can be achieved by simply acquiring the signal for longer time or pump-probing with higher IR pulse energy. In nominally neutral water surface, the vibrational modes are shown to be strongly coupled.

It would be beneficial to understand how the couplings change due to presence of hydrated proton as well by performing 2D-SFG experiments.

Acknowledgements

I have learnt a lot in these last four years that I have worked in Molecular Spectroscopy department in MPIP. There are many people who have accompanied me in this process, who taught me, encouraged me. I thank you all from the deepest of my heart.

First and foremost, I thank Ellen for believing in me, for being there in and outside of the lab, for teaching me the concepts of SFG and helping me out in analyzing and interpreting the data and for helping me dream to be a successful scientist. I would always look up to you for your supervision style. I reckon the students in Vienna are extremely lucky to have you as their teacher. Mischa, I dream that I shall grow into as wise and enthusiastic a scientist as you are. Thank you for your keen, critical suggestions on my research. Ellen and Mischa, both of you have helped me grow into a better 'student' of science. And, I hope, that in future I can help others to become the same.

Dear Ruth and Saman, thank you for being patient with a slow learner like me in the lab. Ruth, I am grateful for the countless hours you spent to teach me how to use Viktor. Saman, I have thoroughly enjoyed the time when I had the opportunity to help you rebuild Vivian; I have learnt a lot form you then. As I am taking the next step of being a postdoc in a new group, I wish to take the role you used to carry in our group: being an enthusiastic as well as empathetic Postdoc who unconditionally helps the novices.

Dear Alejandra, I vividly remember your remark: "you'll have to write a thesis one day, and you'll realize"…and you were right…I have realized it. Thank you for your wisdom ☺ Dear Jan, it was fun sharing the office with you (since most of the times you were not there and I could steal your chair☺). Dear Simon "the curly", long live your 'curl', keep kicking…you know what you like to kick…of the people who do not follow the rules. In addition, thank you for the bouldering sessions we had together.

Dear Shumei, thank you for teaching me phase-resolved SFG. It was such a pleasure rebuilding the setup with you. I have learnt a lot while working with you. Dear Jenée, thank you for all the cookies you made. It was such a bliss to build the carts for the defenses with you downstairs. I guess I shall remember: "You know nothing, glitter fixes everything☺" All the very best for your job in Baylor University.

Dear Malte, thank you for all your help with data analysis. The days we spent together in fixing Viktor were painful yet lovely. I shall always be envious of your skills with codes. Keep it up.

Dear Max, Veronika, and Patrick, good luck for your PhD and life in general. Max, keep being the Sno-Max hero. Patrick, damn… you are an excellent cake-police. And Veronica, good luck with your time in Vienna and good luck with building the lab.

Dear Prerna, keep being the ice queen ☺ The following is for you:

नायाब नहीं मंजिल, दूर है सिर्फ
नामुमकिन नहीं इम्तेहान, मुस्किल हैं सिर्फ
अगली मंज़िल, आसमान हैं
अभी तो मुट्ठी भर ज़मीन टोली हैं सिर्फ

Good luck to you ☺

Dear Laurie, thank you for always being so kind and listening to all of my concerns. It is amazing how tactfully you organize everything in the department. Dear Marc-Jan and Florian, thank you for the helps in the lab with all the technical challenges. Dear Hansjörg, thank you very much for taking care of the Lasers. The department won't be able to work at all without you people. Thank you gain for being there for us.

Dear Maksim, or I should say Henry Louis, congratulations on having a new smartphone. Now get a pair of proper spectacles or contact lenses. I dearly like when you pay us a visit in the old office just with the excuse of printing something. Thank you very much for all the 'scientific discussions' we had together.

Dear Lisa and Christian, I wish you a very happy and prosperous married life. Thank you for all you helps. It was such a joy to play badminton together with you.

Dear Christoph and Mischa, you ba******….I mean bald-duos…YOU have turned me inside out and I am loving it. I cannot forget our time together in office 2.504. Mischa, your deep philosophical questions like "would you rather pet a chicken or an alligator ?" have stretched my analytical thinking abilities :P Christoph, I do not know how to describe you, but I love you. You'll always be in the deepest of my heart.

Dear Soham, you were the first friend, philosopher and guide I had in this unknown land. সবকিছুর জন্য তোমাকে ধন্যবাদ। আমি জানি না কীভাবে আমি এই বিদেশে বেঁচে থাকতে পারতাম, তুমি যদি আমার জন্য সারাক্ষণ না থাকতে। আমি খুব দুঃখিত যে তোমাকে এভাবে চলে যেতে হয়েছিল। Therefore, when I shall defend my thesis, I shall defend it for both of us.

And, last but not the least, my Mom and Dad. আমি কেবল তোমাদের জন্যই আমি এতদূর আসতে পেরেছি। তোমাদের অসুস্থতার সময় ওখানে না থাকতে পেরে আমি দুঃখিত, তবে আমি আশা করি, আমি তোমাদের এই ডিগ্রির মাধ্যমে গর্বিত করব। ভবিষ্যতে আরও ভাল ছেলে হওয়ার প্রতিশ্রুতি দিচ্ছি। Thank you for being there in my life☺

References

1. Fraxedas, J., Water at interfaces : a molecular approach. **2014**.
2. Palese, S.; Mukamel, S.; Miller, R. J. D.; Lotshaw, W. T., Interrogation of Vibrational Structure and Line Broadening of Liquid Water by Raman-Induced Kerr Effect Measurements within the Multimode Brownian Oscillator Model. *The Journal of Physical Chemistry* **1996,** *100* (24), 10380-10388.
3. Daly, C. A.; Streacker, L. M.; Sun, Y.; Pattenaude, S. R.; Hassanali, A. A.; Petersen, P. B.; Corcelli, S. A.; Ben-Amotz, D., Decomposition of the Experimental Raman and Infrared Spectra of Acidic Water into Proton, Special Pair, and Counterion Contributions. *The Journal of Physical Chemistry Letters* **2017,** *8* (21), 5246-5252.
4. Roberts, J. M.; Osthoff, H. D.; Brown, S. S.; Ravishankara, A. R., N_2O_5Oxidizes Chloride to Cl_2 in Acidic Atmospheric Aerosol. *Science* **2008,** *321* (5892), 1059-1059.
5. Beattie, J. K.; Djerdjev, A. M.; Gray-Weale, A.; Kallay, N.; Lützenkirchen, J.; Preočanin, T.; Selmani, A., pH and the surface tension of water. *J Colloid Interf Sci* **2014,** *422*, 54-57.
6. Pegram, L. M.; Record, M. T., Partitioning of atmospherically relevant ions between bulk water and the water/vapor interface. *Proceedings of the National Academy of Sciences* **2006,** *103* (39), 14278.
7. Takahashi, M., ζ Potential of Microbubbles in Aqueous Solutions: Electrical Properties of the Gas−Water Interface. *The Journal of Physical Chemistry B* **2005,** *109* (46), 21858-21864.
8. Petersen, P. B.; Saykally, R. J., Evidence for an Enhanced Hydronium Concentration at the Liquid Water Surface. *The Journal of Physical Chemistry B* **2005,** *109* (16), 7976-7980.
9. Tarbuck, T. L.; Ota, S. T.; Richmond, G. L., Spectroscopic Studies of Solvated Hydrogen and Hydroxide Ions at Aqueous Surfaces. *Journal of the American Chemical Society* **2006,** *128* (45), 14519-14527.
10. Mucha, M.; Frigato, T.; Levering, L. M.; Allen, H. C.; Tobias, D. J.; Dang, L. X.; Jungwirth, P., Unified molecular picture of the surfaces of aqueous acid, base, and salt solutions. *Journal of Physical Chemistry B* **2005,** *109* (16), 7617-7623.
11. Tian, C. S.; Ji, N.; Waychunas, G. A.; Shen, Y. R., Interfacial structures of acidic and basic aqueous solutions. *Journal of the American Chemical Society* **2008,** *130* (39), 13033-13039.
12. Levering, L. M.; Sierra-Hernandez, M. R.; Allen, H. C., Observation of hydronium ions at the air - Aqueous acid interface: Vibrational spectroscopic studies of aqueous HCI, HBr, and HI. *J Phys Chem C* **2007,** *111* (25), 8814-8826.
13. Schnitzer, C.; Baldelli, S.; Shultz, M. J., Sum frequency generation of water on NaCl, NaNO3, KHSO4, HCl, HNO3, and H2SO4 aqueous solutions. *Journal of Physical Chemistry B* **2000,** *104* (3), 585-590.
14. Sengupta, S.; Moberg, D. R.; Paesani, F.; Tyrode, E., Neat Water–Vapor Interface: Proton Continuum and the Nonresonant Background. *The Journal of Physical Chemistry Letters* **2018,** *9* (23), 6744-6749.
15. Ottosson, N.; Wernersson, E.; Söderström, J.; Pokapanich, W.; Kaufmann, S.; Svensson, S.; Persson, I.; Öhrwall, G.; Björneholm, O., The protonation state of small carboxylic acids at the water surface from photoelectron spectroscopy. *Physical Chemistry Chemical Physics* **2011,** *13* (26), 12261-12267.
16. Ottosson, N.; Cwiklik, L.; Söderström, J.; Björneholm, O.; Öhrwall, G.; Jungwirth, P., Increased Propensity of Iaq− for the Water Surface in Non-neutral Solutions: Implications for the

Interfacial Behavior of H3Oaq+ and OHaq−. *The Journal of Physical Chemistry Letters* **2011,** *2* (9), 972-976.
17. Shapovalov, V. L.; Möhwald, H.; Konovalov, O. V.; Knecht, V., Negligible water surface charge determined using Kelvin probe and total reflection X-ray fluorescence techniques. *Physical Chemistry Chemical Physics* **2013,** *15* (33), 13991-13998.
18. Dang, L. X., Solvation of the hydronium ion at the water liquid/vapor interface. *The Journal of Chemical Physics* **2003,** *119* (12), 6351-6353.
19. Petersen, M. K.; Iyengar, S. S.; Day, T. J. F.; Voth, G. A., The Hydrated Proton at the Water Liquid/Vapor Interface. *The Journal of Physical Chemistry B* **2004,** *108* (39), 14804-14806.
20. Buch, V.; Milet, A.; Vácha, R.; Jungwirth, P.; Devlin, J. P., Water surface is acidic. *Proceedings of the National Academy of Sciences* **2007,** *104* (18), 7342.
21. Wick, C. D.; Kuo, I. F. W.; Mundy, C. J.; Dang, L. X., The Effect of Polarizability for Understanding the Molecular Structure of Aqueous Interfaces. *Journal of Chemical Theory and Computation* **2007,** *3* (6), 2002-2010.
22. Tobias, D. J.; Stern, A. C.; Baer, M. D.; Levin, Y.; Mundy, C. J., Simulation and Theory of Ions at Atmospherically Relevant Aqueous Liquid-Air Interfaces. **2013,** *64* (1), 339-359.
23. Yan, L.; Alexandre, P. d. S., Ions at hydrophobic interfaces. *Journal of Physics: Condensed Matter* **2014,** *26* (20), 203101.
24. Hub, J. S.; Wolf, M. G.; Caleman, C.; Maaren, P. J.; Groenhof, G.; van der Spoel, D., Thermodynamics of hydronium and hydroxide surface solvation. *Chem Sci* **2014,** *5* (5), 1745-1749.
25. Jagoda-Cwiklik, B.; Cwiklik, L.; Jungwirth, P., Behavior of the Eigen Form of Hydronium at the Air/Water Interface. *The Journal of Physical Chemistry A* **2011,** *115* (23), 5881-5886.
26. Headrick, J. M.; Diken, E. G.; Walters, R. S.; Hammer, N. I.; Christie, R. A.; Cui, J.; Myshakin, E. M.; Duncan, M. A.; Johnson, M. A.; Jordan, K. D., Spectral Signatures of Hydrated Proton Vibrations in Water Clusters. *Science* **2005,** *308* (5729), 1765.
27. Thämer, M.; De Marco, L.; Ramasesha, K.; Mandal, A.; Tokmakoff, A., Ultrafast 2D IR spectroscopy of the excess proton in liquid water. *Science* **2015,** *350* (6256), 78.
28. Woutersen, S.; Bakker, H. J., Ultrafast Vibrational and Structural Dynamics of the Proton in Liquid Water. *Physical Review Letters* **2006,** *96* (13), 138305.
29. Iuchi, S.; Chen, H.; Paesani, F.; Voth, G. A., Hydrated Excess Proton at Water−Hydrophobic Interfaces. *The Journal of Physical Chemistry B* **2009,** *113* (13), 4017-4030.
30. Hub, J. S.; Wolf, M. G.; Caleman, C.; van Maaren, P. J.; Groenhof, G.; van der Spoel, D., Thermodynamics of hydronium and hydroxide surface solvation. *Chem Sci* **2014,** *5* (5), 1745-1749.
31. Wolf, M. G.; Grubmüller, H.; Groenhof, G., Anomalous surface diffusion of protons on lipid membranes. *Biophys J* **2014,** *107* (1), 76-87.
32. Yamashita, T.; Voth, G. A., Properties of Hydrated Excess Protons near Phospholipid Bilayers. *The Journal of Physical Chemistry B* **2010,** *114* (1), 592-603.
33. Dreier, L. B.; Nagata, Y.; Lutz, H.; Gonella, G.; Hunger, J.; Backus, E. H. G.; Bonn, M., Saturation of charge-induced water alignment at model membrane surfaces. *Sci Adv* **2018,** *4* (3).
34. Livingstone, R. A.; Nagata, Y.; Bonn, M.; Backus, E. H. G., Two Types of Water at the Water–Surfactant Interface Revealed by Time-Resolved Vibrational Spectroscopy. *Journal of the American Chemical Society* **2015,** *137* (47), 14912-14919.

35. Shapovalov, V. L.; Brezesinski, G., Breakdown of the Gouy− Chapman model for highly charged Langmuir monolayers: counterion size effect. *The journal of physical chemistry B* **2006,** *110* (20), 10032-10040.
36. Biesheuvel, P. M.; van Soestbergen, M., Counterion volume effects in mixed electrical double layers. *J Colloid Interf Sci* **2007,** *316* (2), 490-499.
37. Lawrence, C. P.; Skinner, J. L., Vibrational spectroscopy of HOD in liquid D2O. II. Infrared line shapes and vibrational Stokes shift. *The Journal of Chemical Physics* **2002,** *117* (19), 8847-8854.
38. Buch, V., Molecular structure and OH-stretch spectra of liquid water surface. *Journal of Physical Chemistry B* **2005,** *109* (38), 17771-17774.
39. Auer, B.; Kumar, R.; Schmidt, J. R.; Skinner, J. L., Hydrogen bonding and Raman, IR, and 2D-IR spectroscopy of dilute HOD in liquid D₂O. *Proceedings of the National Academy of Sciences* **2007,** *104* (36), 14215.
40. Choi, J.-H.; Cho, M., Computational IR spectroscopy of water: OH stretch frequencies, transition dipoles, and intermolecular vibrational coupling constants. *The Journal of Chemical Physics* **2013,** *138* (17), 174108.
41. Zhang, C.; Khaliullin, R. Z.; Bovi, D.; Guidoni, L.; Kühne, T. D., Vibrational Signature of Water Molecules in Asymmetric Hydrogen Bonding Environments. *The Journal of Physical Chemistry Letters* **2013,** *4* (19), 3245-3250.
42. Zhang, C.; Guidoni, L.; Kühne, T. D., Competing factors on the frequency separation between the OH stretching modes in water. *J Mol Liq* **2015,** *205*, 42-45.
43. Rey, R.; Møller, K. B.; Hynes, J. T., Hydrogen Bond Dynamics in Water and Ultrafast Infrared Spectroscopy. *The Journal of Physical Chemistry A* **2002,** *106* (50), 11993-11996.
44. Cowan, M. L.; Bruner, B. D.; Huse, N.; Dwyer, J. R.; Chugh, B.; Nibbering, E. T. J.; Elsaesser, T.; Miller, R. J. D., Ultrafast memory loss and energy redistribution in the hydrogen bond network of liquid H2O. *Nature* **2005,** *434*, 199.
45. Ramasesha, K.; De Marco, L.; Mandal, A.; Tokmakoff, A., Water vibrations have strongly mixed intra- and intermolecular character. *Nature Chemistry* **2013,** *5*, 935.
46. Hsieh, C.-S.; Campen, R. K.; Okuno, M.; Backus, E. H. G.; Nagata, Y.; Bonn, M., Mechanism of vibrational energy dissipation of free OH groups at the air–water interface. *Proceedings of the National Academy of Sciences* **2013,** *110* (47), 18780.
47. van der Post, S. T.; Hsieh, C.-S.; Okuno, M.; Nagata, Y.; Bakker, H. J.; Bonn, M.; Hunger, J., Strong frequency dependence of vibrational relaxation in bulk and surface water reveals sub-picosecond structural heterogeneity. *Nature communications* **2015,** *6*, 8384-8384.
48. Hsieh, C.-S.; Okuno, M.; Hunger, J.; Backus, E. H. G.; Nagata, Y.; Bonn, M., Aqueous Heterogeneity at the Air/Water Interface Revealed by 2D-HD-SFG Spectroscopy. *Angewandte Chemie International Edition* **2014,** *53* (31), 8146-8149.
49. Boyd, R. W., *Nonlinear optics*. Academic Press: Amsterdam; London, 2003.
50. Shen, Y. R., Fundamentals of Sum-Frequency Spectroscopy. **2016**.
51. Lambert, A. G.; Davies, P. B.; Neivandt, D. J., Implementing the Theory of Sum Frequency Generation Vibrational Spectroscopy: A Tutorial Review. *Applied Spectroscopy Reviews* **2005,** *40* (2), 103-145.
52. Lagutchev, A.; Hambir, S. A.; Dlott, D. D., Nonresonant Background Suppression in Broadband Vibrational Sum-Frequency Generation Spectroscopy. *The Journal of Physical Chemistry C* **2007,** *111* (37), 13645-13647.

53. Carter, J. A.; Wang, Z.; Dlott, D. D., Ultrafast Nonlinear Coherent Vibrational Sum-Frequency Spectroscopy Methods To Study Thermal Conductance of Molecules at Interfaces. *Accounts Chem Res* **2009,** *42* (9), 1343-1351.
54. Stiopkin, I. V.; Jayathilake, H. D.; Weeraman, C.; Benderskii, A. V., Temporal effects on spectroscopic line shapes, resolution, and sensitivity of the broad-band sum frequency generation. *The Journal of Chemical Physics* **2010,** *132* (23), 234503.
55. Backus, E. H. G.; Cyran, J. D.; Grechko, M.; Nagata, Y.; Bonn, M., Time-Resolved Sum Frequency Generation Spectroscopy: A Quantitative Comparison Between Intensity and Phase-Resolved Spectroscopy. *J Phys Chem A* **2018,** *122* (9), 2401-2410.
56. Wen, Y. C.; Zha, S.; Liu, X.; Yang, S. S.; Guo, P.; Shi, G. S.; Fang, H. P.; Shen, Y. R.; Tian, C. S., Unveiling Microscopic Structures of Charged Water Interfaces by Surface-Specific Vibrational Spectroscopy. *Physical Review Letters* **2016,** *116* (1), 5.
57. Pezzotti, S.; Galimberti, D. R.; Shen, Y. R.; Gaigeot, M.-P., Structural definition of the BIL and DL: a new universal methodology to rationalize non-linear $\chi(2)(\omega)$ SFG signals at charged interfaces, including $\chi(3)(\omega)$ contributions. *Physical Chemistry Chemical Physics* **2018,** *20* (7), 5190-5199.
58. Yamaguchi, S.; Shiratori, K.; Morita, A.; Tahara, T., Electric quadrupole contribution to the nonresonant background of sum frequency generation at air/liquid interfaces. *The Journal of Chemical Physics* **2011,** *134* (18), 184705.
59. Shiratori, K.; Morita, A., Theory of Quadrupole Contributions from Interface and Bulk in Second-Order Optical Processes. *B Chem Soc Jpn* **2012,** *85* (10), 1061-1076.
60. Kundu, A.; Tanaka, S.; Ishiyama, T.; Ahmed, M.; Inoue, K.-i.; Nihonyanagi, S.; Sawai, H.; Yamaguchi, S.; Morita, A.; Tahara, T., Bend Vibration of Surface Water Investigated by Heterodyne-Detected Sum Frequency Generation and Theoretical Study: Dominant Role of Quadrupole. *The Journal of Physical Chemistry Letters* **2016,** *7* (13), 2597-2601.
61. Gilányi, T.; Varga, I.; Mészáros, R., Specific counterion effect on the adsorption of alkali decyl sulfate surfactants at air/solution interface. *Physical Chemistry Chemical Physics* **2004,** *6* (17), 4338-4346.
62. Biesheuvel, P. M.; van Soestbergen, M., Counterion volume effects in mixed electrical double layers. *J Colloid Interface Sci* **2007,** *316* (2), 490-9.
63. Dang, L. X., Computational Study of Ion Binding to the Liquid Interface of Water. *The Journal of Physical Chemistry B* **2002,** *106* (40), 10388-10394.
64. Levin, Y., Polarizable Ions at Interfaces. *Physical Review Letters* **2009,** *102* (14), 147803.
65. Collins, K. D.; Neilson, G. W.; Enderby, J. E., Ions in water: Characterizing the forces that control chemical processes and biological structure. *Biophysical Chemistry* **2007,** *128* (2), 95-104.
66. Guzmán, E.; Santini, E.; Benedetti, A.; Ravera, F.; Ferrari, M.; Liggieri, L., Surfactant induced complex formation and their effects on the interfacial properties of seawater. *Colloids and Surfaces B: Biointerfaces* **2014,** *123*, 701-709.
67. Mankowich, A. M., The energetics of surfactant adsorption at the air-water interface. *Journal of the American Oil Chemists Society* **1966,** *43* (11), 615-619.
68. Karakashev, S.; Tsekov, R.; Manev, E., Adsorption of Alkali Dodecyl Sulfates on Air/Water Surface. *Langmuir* **2001,** *17* (17), 5403-5405.
69. Sin, J.-S.; Kim, K.-I.; Pak, H.-C.; Sin, C.-S., Effect of orientational ordering of water dipoles on stratification of counterions of different size in multicomponent electrolyte solution near charged surface - a mean field approach. *Electrochimica Acta* **2016,** *207*, 237-246.

70. Kundu, A.; Yamaguchi, S.; Tahara, T., Evaluation of pH at Charged Lipid/Water Interfaces by Heterodyne-Detected Electronic Sum Frequency Generation. *The Journal of Physical Chemistry Letters* **2014,** *5* (4), 762-766.
71. Israelachvili, J. N., Chapter 14 - Electrostatic Forces between Surfaces in Liquids. In *Intermolecular and Surface Forces (Third Edition)*, Israelachvili, J. N., Ed. Academic Press: San Diego, 2011; pp 291-340.
72. Chen, M.; Lu, X.; Liu, X.; Hou, Q.; Zhu, Y.; Zhou, H., Specific Counterion Effects on the Atomistic Structure and Capillary-Waves Fluctuation of the Water/Vapor Interface Covered by Sodium Dodecyl Sulfate. *The Journal of Physical Chemistry C* **2014,** *118* (33), 19205-19213.
73. Wen, Y.-C.; Zha, S.; Tian, C.; Shen, Y. R., Surface pH and Ion Affinity at the Alcohol-Monolayer/Water Interface Studied by Sum-Frequency Spectroscopy. *The Journal of Physical Chemistry C* **2016,** *120* (28), 15224-15229.
74. Gragson, D. E.; McCarty, B. M.; Richmond, G. L., Ordering of interfacial water molecules at the charged air/water interface observed by vibrational sum frequency generation. *Journal of the American Chemical Society* **1997,** *119* (26), 6144-6152.
75. Gragson, D. E.; McCarty, B. M.; Richmond, G. L., Surfactant/water interactions at the air/water interface probed by vibrational sum frequency generation. *J Phys Chem-Us* **1996,** *100* (34), 14272-14275.
76. Raymond, E. A.; Richmond, G. L., Probing the Molecular Structure and Bonding of the Surface of Aqueous Salt Solutions. *The Journal of Physical Chemistry B* **2004,** *108* (16), 5051-5059.
77. Gonella, G.; Lütgebaucks, C.; de Beer, A. G. F.; Roke, S., Second Harmonic and Sum-Frequency Generation from Aqueous Interfaces Is Modulated by Interference. *The Journal of Physical Chemistry C* **2016,** *120* (17), 9165-9173.
78. Schaefer, J.; Gonella, G.; Bonn, M.; Backus, E. H. G., Surface-specific vibrational spectroscopy of the water/silica interface: screening and interference. *Physical Chemistry Chemical Physics* **2017,** *19* (25), 16875-16880.
79. Marcus, Y., Ionic radii in aqueous solutions. *Chemical Reviews* **1988,** *88* (8), 1475-1498.
80. Wen, Y.-C.; Zha, S.; Liu, X.; Yang, S.; Guo, P.; Shi, G.; Fang, H.; Shen, Y. R.; Tian, C., Unveiling Microscopic Structures of Charged Water Interfaces by Surface-Specific Vibrational Spectroscopy. *Physical Review Letters* **2016,** *116* (1), 016101.
81. Giberti, F.; Hassanali, A. A., The excess proton at the air-water interface: The role of instantaneous liquid interfaces. *J Chem Phys* **2017,** *146* (24), 244703.
82. Wenger, D., Acid-Base Behaviour of Short-Chain Fatty Acids on Aqueous Surfaces Using X-Ray Photoelectron Spectroscopy, Nuclear Magnetic Resonance

and Molecular Dynamics. *Master Thesis* **2015**.
83. Liu, D.; Ma, G.; Levering, L. M.; Allen, H. C., Vibrational Spectroscopy of Aqueous Sodium Halide Solutions and Air−Liquid Interfaces: Observation of Increased Interfacial Depth. *The Journal of Physical Chemistry B* **2004,** *108* (7), 2252-2260.
84. Ishiyama, T.; Morita, A., Molecular Dynamics Analysis of Interfacial Structures and Sum Frequency Generation Spectra of Aqueous Hydrogen Halide Solutions. *The Journal of Physical Chemistry A* **2007,** *111* (38), 9277-9285.
85. Ishiyama, T.; Morita, A., Molecular Dynamics Study of Gas−Liquid Aqueous Sodium Halide Interfaces. I. Flexible and Polarizable Molecular Modeling and Interfacial Properties. *The Journal of Physical Chemistry C* **2007,** *111* (2), 721-737.

86. Schaefer, J.; Backus, E. H. G.; Nagata, Y.; Bonn, M., Both Inter- and Intramolecular Coupling of O–H Groups Determine the Vibrational Response of the Water/Air Interface. *The Journal of Physical Chemistry Letters* **2016,** *7* (22), 4591-4595.
87. Hua, W.; Verreault, D.; Allen, H. C., Relative Order of Sulfuric Acid, Bisulfate, Hydronium, and Cations at the Air-Water Interface. *Journal of the American Chemical Society* **2015,** *137* (43), 13920-13926.
88. Pezzotti, S.; Gaigeot, M.-P., Spectroscopic BIL-SFG Invariance Hides the Chaotropic Effect of Protons at the Air-Water Interface. **2018,** *9* (10), 396.
89. Pezzotti, S.; Galimberti, D. R.; Gaigeot, M.-P., 2D H-Bond Network as the Topmost Skin to the Air–Water Interface. *The Journal of Physical Chemistry Letters* **2017,** *8* (13), 3133-3141.
90. Song, S.-H.; Koelsch, P.; Weidner, T.; Wagner, M. S.; Castner, D. G., Sodium Dodecyl Sulfate Adsorption onto Positively Charged Surfaces: Monolayer Formation With Opposing Headgroup Orientations. *Langmuir* **2013,** *29* (41), 12710-12719.
91. Tyrode, E.; Hedberg, J., A Comparative Study of the CD and CH Stretching Spectral Regions of Typical Surfactants Systems Using VSFS: Orientation Analysis of the Terminal CH3 and CD3 Groups. *The Journal of Physical Chemistry C* **2012,** *116* (1), 1080-1091.
92. Backus, E. H. G.; Bonn, D.; Cantin, S.; Roke, S.; Bonn, M., Laser-Heating-Induced Displacement of Surfactants on the Water Surface. *Journal of Physical Chemistry B* **2012,** *116* (9), 2703-2712.
93. Nagata, Y.; Mukamel, S., Vibrational sum-frequency generation spectroscopy at the water/lipid interface: molecular dynamics simulation study. *Journal of the American Chemical Society* **2010,** *132* (18), 6434-6442.
94. Lu, J. R.; Marrocco, A.; Su, T. J.; Thomas, R. K.; Penfold, J., Adsorption of Dodecyl Sulfate Surfactants with Monovalent Metal Counterions at the Air-Water Interface Studied by Neutron Reflection and Surface Tension. *J Colloid Interf Sci* **1993,** *158* (2), 303-316.
95. Agmon, N.; Bakker, H. J.; Campen, R. K.; Henchman, R. H.; Pohl, P.; Roke, S.; Thamer, M.; Hassanali, A., Protons and Hydroxide Ions in Aqueous Systems. *Chem Rev* **2016,** *116* (13), 7642-72.
96. Petersen, P. B.; Saykally, R. J., Is the liquid water surface basic or acidic? Macroscopic vs. molecular-scale investigations. *Chem Phys Lett* **2008,** *458* (4), 255-261.
97. Du, Q.; Superfine, R.; Freysz, E.; Shen, Y. R., Vibrational spectroscopy of water at the vapor/water interface. *Physical Review Letters* **1993,** *70* (15), 2313-2316.
98. Du, Q.; Freysz, E.; Shen, Y. R., Surface Vibrational Spectroscopic Studies of Hydrogen Bonding and Hydrophobicity. *Science* **1994,** *264* (5160), 826.
99. Ji, N.; Ostroverkhov, V.; Tian, C. S.; Shen, Y. R., Characterization of Vibrational Resonances of Water-Vapor Interfaces by Phase-Sensitive Sum-Frequency Spectroscopy. *Physical Review Letters* **2008,** *100* (9), 096102.
100. Bai, C.; Herzfeld, J., Surface Propensities of the Self-Ions of Water. *Acs Central Sci* **2016,** *2* (4), 225-231.
101. Beattie, J. K.; Djerdjev, A. N.; Warr, G. G., The surface of neat water is basic. *Faraday Discuss* **2009,** *141*, 31-39.
102. Saykally, R. J., Two sides of the acid–base story. *Nature Chemistry* **2013,** *5*, 82.
103. Tse, Y.-L. S.; Chen, C.; Lindberg, G. E.; Kumar, R.; Voth, G. A., Propensity of Hydrated Excess Protons and Hydroxide Anions for the Air–Water Interface. *Journal of the American Chemical Society* **2015,** *137* (39), 12610-12616.

104. Imamura, T.; Ishiyama, T.; Morita, A., Molecular Dynamics Analysis of NaOH Aqueous Solution Surface and the Sum Frequency Generation Spectra: Is Surface OH– Detected by SFG Spectroscopy? *The Journal of Physical Chemistry C* **2014,** *118* (50), 29017-29027.
105. Wick, C. D., Comparing hydroxide and hydronium at the instantaneous air-water interface using polarizable multi-state empirical valence bond models. *Comput Theor Chem* **2017,** *1116*, 64-72.
106. Kessler, J.; Elgabarty, H.; Spura, T.; Karhan, K.; Partovi-Azar, P.; Hassanali, A. A.; Kühne, T. D., Structure and Dynamics of the Instantaneous Water/Vapor Interface Revisited by Path-Integral and Ab Initio Molecular Dynamics Simulations. *The Journal of Physical Chemistry B* **2015,** *119* (31), 10079-10086.
107. Dahms, F.; Fingerhut, B. P.; Nibbering, E. T. J.; Pines, E.; Elsaesser, T., Large-amplitude transfer motion of hydrated excess protons mapped by ultrafast 2D IR spectroscopy. *Science* **2017,** *357* (6350), 491.
108. Angelova, M. I.; Bitbol, A.-F.; Seigneuret, M.; Staneva, G.; Kodama, A.; Sakuma, Y.; Kawakatsu, T.; Imai, M.; Puff, N., pH sensing by lipids in membranes: The fundamentals of pH-driven migration, polarization and deformations of lipid bilayer assemblies. *Biochimica et Biophysica Acta (BBA) - Biomembranes* **2018,** *1860* (10), 2042-2063.
109. Rees, N. V.; Compton, R. G., Sustainable energy: a review of formic acid electrochemical fuel cells. *J Solid State Electr* **2011,** *15* (10), 2095-2100.
110. Wan, K.; Yu, Z.-p.; Li, X.-h.; Liu, M.-y.; Yang, G.; Piao, J.-h.; Liang, Z.-x., pH Effect on Electrochemistry of Nitrogen-Doped Carbon Catalyst for Oxygen Reduction Reaction. *Acs Catal* **2015,** *5* (7), 4325-4332.
111. Buch, V.; Milet, A.; Vácha, R.; Jungwirth, P.; Devlin, J. P., Water surface is acidic. **2007,** *104* (18), 7342-7347.
112. Vinaykin, M.; Benderskii, A. V., Vibrational Sum-Frequency Spectrum of the Water Bend at the Air/Water Interface. *The Journal of Physical Chemistry Letters* **2012,** *3* (22), 3348-3352.
113. Nagata, Y.; Hsieh, C. S.; Hasegawa, T.; Voll, J.; Backus, E. H. G.; Bonn, M., Water Bending Mode at the Water-Vapor Interface Probed by Sum-Frequency Generation Spectroscopy: A Combined Molecular Dynamics Simulation and Experimental Study. *Journal of Physical Chemistry Letters* **2013,** *4* (11), 1872-1877.
114. Fournier, J. A.; Carpenter, W. B.; Lewis, N. H. C.; Tokmakoff, A., Broadband 2D IR spectroscopy reveals dominant asymmetric H5O2+ proton hydration structures in acid solutions. *Nature Chemistry* **2018,** *10* (9), 932-937.
115. Knight, C.; Voth, G. A., The Curious Case of the Hydrated Proton. *Accounts Chem Res* **2012,** *45* (1), 101-109.
116. Baer, M. D.; Kuo, I. F. W.; Tobias, D. J.; Mundy, C. J., Toward a Unified Picture of the Water Self-Ions at the Air–Water Interface: A Density Functional Theory Perspective. *The Journal of Physical Chemistry B* **2014,** *118* (28), 8364-8372.
117. Vacha, R.; Buch, V.; Milet, A.; Devlin, P.; Jungwirth, P., Autoionization at the surface of neat water: is the top layer pH neutral, basic, or acidic? *Physical Chemistry Chemical Physics* **2007,** *9* (34), 4736-4747.
118. Lee, H.-S.; Tuckerman, M. E., Ab Initio Molecular Dynamics Studies of the Liquid−Vapor Interface of an HCl Solution. *The Journal of Physical Chemistry A* **2009,** *113* (10), 2144-2151.
119. Duignan, T. T.; Parsons, D. F.; Ninham, B. W., Hydronium and hydroxide at the air–water interface with a continuum solvent model. *Chem Phys Lett* **2015,** *635*, 1-12.

120. Sun, S.; Tang, F.; Imoto, S.; Moberg, D. R.; Ohto, T.; Paesani, F.; Bonn, M.; Backus, E. H. G.; Nagata, Y., Orientational Distribution of Free O-H Groups of Interfacial Water is Exponential. *Physical Review Letters* **2018,** *121* (24), 246101.
121. Petersen, P. B.; Saykally, R. J., Probing the Interfacial Structure of Aqueous Electrolytes with Femtosecond Second Harmonic Generation Spectroscopy. *The Journal of Physical Chemistry B* **2006,** *110* (29), 14060-14073.
122. Petersen, P. B.; Johnson, J. C.; Knutsen, K. P.; Saykally, R. J., Direct experimental validation of the Jones–Ray effect. *Chem Phys Lett* **2004,** *397* (1), 46-50.
123. Petersen, P. B.; Saykally, R. J.; Mucha, M.; Jungwirth, P., Enhanced Concentration of Polarizable Anions at the Liquid Water Surface: SHG Spectroscopy and MD Simulations of Sodium Thiocyanide. *The Journal of Physical Chemistry B* **2005,** *109* (21), 10915-10921.
124. Kreuer, K.-D., Proton Conductivity: Materials and Applications. *Chem Mater* **1996,** *8* (3), 610-641.
125. Cukierman, S., Et tu, Grotthuss! and other unfinished stories. *Biochimica et Biophysica Acta (BBA) - Bioenergetics* **2006,** *1757* (8), 876-885.
126. Wraight, C. A., Chance and design—Proton transfer in water, channels and bioenergetic proteins. *Biochimica et Biophysica Acta (BBA) - Bioenergetics* **2006,** *1757* (8), 886-912.
127. Kulig, W.; Agmon, N., Both Zundel and Eigen Isomers Contribute to the IR Spectrum of the Gas-Phase H9O4+ Cluster. *The Journal of Physical Chemistry B* **2014,** *118* (1), 278-286.
128. Heine, N.; Fagiani, M. R.; Rossi, M.; Wende, T.; Berden, G.; Blum, V.; Asmis, K. R., Isomer-Selective Detection of Hydrogen-Bond Vibrations in the Protonated Water Hexamer. *Journal of the American Chemical Society* **2013,** *135* (22), 8266-8273.
129. Hua, W.; Verreault, D.; Allen, H. C., Surface Electric Fields of Aqueous Solutions of NH4NO3, Mg(NO3)2, NaNO3, and LiNO3: Implications for Atmospheric Aerosol Chemistry. *The Journal of Physical Chemistry C* **2014,** *118* (43), 24941-24949.
130. Baldelli, S.; Schnitzer, C.; Shultz, M. J., The structure of water on HCl solutions studied with sum frequency generation. *Chem Phys Lett* **1999,** *302* (1-2), 157-163.
131. Bonn, M.; Nagata, Y.; Backus, E. H. G., Molecular Structure and Dynamics of Water at the Water–Air Interface Studied with Surface-Specific Vibrational Spectroscopy. *Angewandte Chemie International Edition* **2015,** *54* (19), 5560-5576.
132. Hsieh, C.-S.; Campen, R. K.; Vila Verde, A. C.; Bolhuis, P.; Nienhuys, H.-K.; Bonn, M., Ultrafast Reorientation of Dangling OH Groups at the Air-Water Interface Using Femtosecond Vibrational Spectroscopy. *Physical Review Letters* **2011,** *107* (11), 116102.
133. Zhang, Z.; Piatkowski, L.; Bakker, H. J.; Bonn, M., Ultrafast vibrational energy transfer at the water/air interface revealed by two-dimensional surface vibrational spectroscopy. *Nat Chem* **2011,** *3* (11), 888-893.
134. Hayashi, M.; Shiu, Y. J.; Liang, K. K.; Lin, S. H.; Shen, Y. R., Theory of time-resolved sum-frequency generation and its applications to vibrational dynamics of water. *Journal of Physical Chemistry A* **2007,** *111* (37), 9062-9069.
135. Nihonyanagi, S.; Mondal, J. A.; Yamaguchi, S.; Tahara, T., Structure and Dynamics of Interfacial Water Studied by Heterodyne-Detected Vibrational Sum-Frequency Generation. *Annual Review of Physical Chemistry* **2013,** *64* (1), 579-603.
136. Deiseroth, M.; Bonn, M.; Backus, E. H. G., Electrolytes change the interfacial water structure but not the dynamics. *Manuscript under preparation*.
137. Hsieh, C. S.; Bakker, H. J.; Piatkowski, L.; Bonn, M., Gigahertz Modulation of Femtosecond Time-Resolved Surface Sum-Frequency Generation Due to Acoustic Strain Pulses. *J Phys Chem C* **2014,** *118* (36), 20875-20880.

138. Piatkowski, L.; Zhang, Z.; Backus, E. H.; Bakker, H. J.; Bonn, M., Extreme surface propensity of halide ions in water. *Nat Commun* **2014,** *5*, 4083.
139. Meiboom, S., Nuclear Magnetic Resonance Study of the Proton Transfer in Water. *The Journal of Chemical Physics* **1961,** *34* (2), 375-388.
140. Fischer, S. A.; Dunlap, B. I.; Gunlycke, D., Correlated dynamics in aqueous proton diffusion. *Chem Sci* **2018,** *9* (35), 7126-7132.
141. Pezzotti, S.; Gaigeot, M.-P., Spectroscopic BIL-SFG Invariance Hides the Chaotropic Effect of Protons at the Air-Water Interface. *Atmosphere* **2018,** *9* (10).
142. Vitagliano, V.; Lyons, P. A., Diffusion Coefficients for Aqueous Solutions of Sodium Chloride and Barium Chloride. *Journal of the American Chemical Society* **1956,** *78* (8), 1549-1552.